Pontifícia Universidade Católica
do Rio de Janeiro

Luciana dos Santos Netto dos Reys

Intelligent biomass estimation in pastures using RGB-based vegetation indices from UAV imagery

Dissertação de Mestrado

Dissertation presented to the Programa de Pós–graduação em Engenharia Elétrica of PUC-Rio in partial fulfillment of the requirements for the degree of Mestre em Engenharia Elétrica.

Advisor : Prof. Eduardo Costa da Silva
Co-advisor: Prof. Antonio Candea Leite

Rio de Janeiro
April 2022

Pontifícia Universidade Católica do Rio de Janeiro

Luciana dos Santos Netto dos Reys

Intelligent biomass estimation in pastures using RGB-based vegetation indices from UAV imagery

Thesis presented to the Programa de Pós–graduação em Engenharia Elétrica da PUC-Rio in partial fulfillment of the requirements for the degree of Mestre em Engenharia Elétrica. Approved by the Examination Committee:

Prof. Eduardo Costa da Silva
Advisor
Departamento de Engenharia Elétrica – PUC-Rio

Prof. Antonio Candea Leite
Norwegian University of Life Sciences – NMBU

Prof. Karla Tereza Figueiredo Leite
Universidade do Estado do Rio de Janeiro – UERJ

Prof. Carlos Roberto Hall Barbosa
Programa de Pós-graduação em Metrologia – PUC-Rio

Dr. Bruno José Rodrigues Alves
Embrapa Agrobiologia

Rio de Janeiro, April 28th, 2022

Luciana dos Santos Netto dos Reys

Undergraduated in BSc. Electronics and Computing Engineering by the Federal University of Rio de Janeiro. / Graduada em Engenharia Eletrônica e de Computação pela Universidade Federal do Rio de Janeiro (UFRJ).

Bibliographic data

Reys, Luciana dos Santos Netto dos

Intelligent biomass estimation in pastures using RGB-based vegetation indices from UAV imagery / Luciana dos Santos Netto dos Reys; advisor: Eduardo Costa da Silva; co-advisor: Antonio Candea Leite. – 2022.

142 f: il. color. ; 30 cm

Dissertação (mestrado) - Pontifícia Universidade Católica do Rio de Janeiro, Departamento de Engenharia Elétrica, 2022.

Inclui bibliografia

1. Engenharia Elétrica – Teses. 2. Biomassa de pasto. 3. Modelos de regressão. 4. Inteligência artificial. 5. Redes neurais. 6. Índices de vegetação baseados em RGB. I. Silva, Eduardo Costa da. II. Leite, Antonio Candea. III. Pontifícia Universidade Católica do Rio de Janeiro. Departamento de Engenharia Elétrica. IV. Título.

CDD: 621.3

In dedication to the "Lydias" of my life,
for encouraging me to be who I am today.

Acknowledgments

To my supervisor Professor Eduardo Silva for his availability, support for the development and review of the work.

To my co-supervisor Professor Antonio Leite for the encouragement, conversations and partnership to carry out this work.

To CNPq, for the grants, without which this work could not have been carried out.

To the Embrapa Agrobiology team, for collecting the necessary data and information provided to carry out this work.

To all my professors at PUC-Rio for their teachings and contributions to the development of my knowledge over the years.

To my colleagues at PUC-Rio who were with me during the whole period of classes and projects carried out together.

To my personal friends for all their support, patience and understanding in the most difficult times.

To my parents for encouraging education throughout my life and for giving me all the attention I needed.

To the professors who participated in the examining committee.

To the Department staff for their help in solving the problems.

To all the friends and family that in one way or another encouraged or helped me. Thank you!

This work has received the financial support provided by FONTAGRO, the New Zealand Ministry for Primary Industries, and PROCISUR. The views expressed herein are exclusively those of the author, and do not reflect the points of view of the Sponsoring Institutions, or of the countries they represent. This study was financed in part by the Coordenação de Aperfeiçoamento de Pessoal de Nível Superior - Brasil (CAPES) - Finance Code 001.

Abstract

Reys, Luciana dos Santos Netto dos; Silva, Eduardo Costa da (Advisor); Leite, Antonio Candea (Co-Advisor). **Intelligent biomass estimation in pastures using RGB-based vegetation indices from UAV imagery** . Rio de Janeiro, 2022. 142p. Dissertação de Mestrado – Departamento de Engenharia Elétrica, Pontifícia Universidade Católica do Rio de Janeiro.

The correct management of pastures in agricultural regions plays a fundamental role in the production itself, in the prevention of plant biomass waste and the release of greenhouse gases (GHG). In addition, it is necessary to avoid inappropriate movement of the herd between pastures, as this is a time-consuming process and can be stressful for the animal. The success of this management requires an efficient assessment of the plant resources. The studies developed for this purpose are directly related to the amount estimation of biomass in a specific region of the pasture, because, in practice, it is not carried out accurately, due to the difficulty of measurement throughout the field. This work aims to develop a low-cost biomass estimation methodology, based on regression models that correlate the most relevant input features for the application with the actual density of the plantation, measured in $\mathsf{g/m^2}$. For the features, the height of the forage grass was measured and the vegetation indexes based on RGB were calculated from images of unmanned aerial vehicles (UAV). Linear, nonlinear regression (MNLR), artificial neural networks (ANN) based on multi-layer perceptron (MLP) and the combination of all models generated (stacking ensemble) were the methodologies tested in order to achieve the best correlation. Satisfactory results were achieved using models of neural networks with two layers and using stacking ensemble methodology, reaching a RMSE of 31.76 g/m^2, MAPE of 13.35% and R-Squared of 0.9. Therefore, the proposed methodology may become a promising and affordable solution for plant biomass estimation toward efficient and sustainable herd management.

Keywords

Pasture Biomass; Regression Models; Artificial Intelligence; Neural Networks; RGB-based Vegetation Indices.

Resumo

Reys, Luciana dos Santos Netto dos; Silva, Eduardo Costa da; Leite, Antonio Candea. **Estimador inteligente de biomassa em pastos usando índices de vegetação a partir de imagens capturadas por VANTs**. Rio de Janeiro, 2022. 142p. Dissertação de Mestrado – Departamento de Engenharia Elétrica, Pontifícia Universidade Católica do Rio de Janeiro.

O gerenciamento correto das pastagens em regiões agropecuárias tem papel fundamental na própria produção, na prevenção ao desperdício da biomassa vegetal e a liberação de gases de efeito estufa (GEE). Além disso, é necessário evitar o movimento inapropriado do rebanho entre pastos, pois este é um processo demorado e pode ser estressante para o animal. O sucesso desta gestão requer uma avaliação eficiente dos recursos da plantação. Os estudos desenvolvidos com esta finalidade tem relação direta com a estimativa da quantidade de biomassa em uma região específica da pastagem, pois, na prática, ela não é realizada de forma precisa, devido à dificuldade de medição em toda a área delimitada. Este trabalho tem como objetivo desenvolver uma metodologia de estimativa de biomassa de baixo custo, baseada em modelos de regressão que correlacionem os atributos de entrada mais relevantes para a aplicação com o real peso da plantação, medido em $\mathsf{g/m^2}$. Para os atributos, foi medida a altura da grama forrageira e calculados os índices de vegetação baseados em RGB a partir de imagens de veículos aéreos não tripulados (VANTs). Como metodologia, utilizou-se regressões lineares, não lineares, redes neurais artificiais baseados em perceptrons de múltiplas camadas e a combinação de todos os modelos gerados (stacking ensemble). Foram alcançados resultados satisfatórios utilizando modelos de redes neurais com ainda duas camadas e com a metodologia de empilhamento de modelos, alcançando um RMSE de 31.76 g/m^2, MAPE de 13.35% e R^2 de 0.9. Portanto, a metodologia proposta pode se tornar uma solução promissora e acessível para a estimativa de biomassa vegetal para uma gestão eficiente e sustentável do rebanho.

Palavras-chave

Biomassa de pasto; Modelos de regressão; Inteligência artificial; Redes neurais; Índices de vegetação baseados em RGB.

Table of contents

List of figures

List of tables

List of Abreviations

ANN - Artificial Neural Networks

AU - Animal Unit

B - Blue

BNF - Biological Nitrogen Fixation

CMOS - Complementary metal-oxide-semiconductor

CNN - Convolutional Neural Networks

CO_2 - Carbon dioxide

CSM - Crop Surface Models

DL - Deep Learning

ELM - Extreme Learning Machine

Embrapa - *Empresa Brasileira de Pesquisa Agropecuária* (Brazilian Agricultural Research Corporation)

EVI - Enhanced Vegetation Index

ExG - Excess of Green

ExGR - Excess of Green minus Excess of Red

ExR - Excess of Red

G - Green

GDP - Gross Domestic Product

GHG - Greenhouse Gases

GLI - Green Leaf Index

GSD - Ground Sample Distance

IA - Artificial Intelligence

LiDAR - Light Detection And Ranging

MAPE - Mean Absolute Percentage Error

MLP - Multi-Layer Perceptron

MLR - Multiple Linear Regression

MNLR - Multiple Non-linear Regression

N_2 - Nitrogen

NDVI - Normalized Difference Vegetation Index

NGRDI - Normalized Green-Red Difference Index

NN - Neural Networks

PA - Precision Agriculture

PH - Plant Height

R - Red

RF - Random Forest

RGBVI - Red, Green, Blue Vegetation Index

RMSE - Root Mean Squared Error

RNN - Recurrent Neural Network

SSR - Sum of Squares Regression

SST - Sum of Squares Total

SVR - Support Vector Regression

UAV - Unmanned aerial vehicle

VARI - Visible Atmospherically Resistant Index

VI - Vegetation Index

Winner is not the one who always wins, but
the one who never stops fighting.

Unknown author.

1
Introduction

Agricultural activities such as livestock and cattle raising in open fields have been the essence of food production by humans [1] from the very beginning of civilization and domestication of animals. In this context, agriculture has always been a very relevant sector in Brazil, as it was responsible for populating the countryside together with sugar cane and coffee production [2]. Farming was one of the first economic activities in Brazil, representing more than 20% of the national GDP (Gross Domestic Product) [3]. The development of Brazilian agriculture has also contributed to the mechanization of crops, which consequently, boosted the machinery industry, such as those needed for land preparation, harvesting, slaughtering and others. Climatic and soil conditions are the main factors that favored farming and cattle-raising in the countryside, since there was also a significant perspective of consumption in the domestic market.

A high forage yield is required to attend animal's demand, hence a forage genus which is rainfed and susceptible to seasonal soil water stresses is essential to guarantee the productivity in Brazil. For this reason and due to its high tolerance to low fertility soils, the genus *Brachiaria* comprises 85% of all planted forage area in Brazil [4].

As population grows indefinitely, the urgency for providing more food is inevitable. Therefore, livestock systems evolved drastically during thousands of years, causing an alarming raise in the production of methane and damaging the ozone layer [5]. The optimization of sustainable livestock production became an imperative subject of study to avoid this trend, despite all challenges it may face, such as population growth, climate change, and farmers' lack of awareness. One way to reduce the massive production of methane in herd production is by adding N fertilizers or N_2 fixation into the soil of *Brachiaria* pastures. Although studies have shown that CO_2 emission is significantly reduced and *Brachiaria* can grow vigorously for a few years with Nitrogen fertilizers, the simple addition of nitrogen to the soil can be really expensive and also aggressive [6]. Another methane mitigation method is to apply feed supplements to the herd, which can also be too expensive and time-consuming. On the other hand, the introduction of legumes into the grasses as a forage consortium provides technically viable and cost-effective pasture alternatives. If legumes are planted in the right amount, these plants play the same role as Nitrogen fertilizers, but more natural and organically [7]. There are several different ways and species to implement forage legumes, but an important factor is to keep the rate between *Brachiaria* and legume approximately still during a determined season. In this case, it is important to estimate the total forage of a pasture in order to determine the rate between the types of plant species in a delimited region.

The actual estimate of biomass to feed the herd has always been an issue in agro-industry development. In big farms, the herd shifting between pastures can be laborious and stressing to the animals, as their adaptability to new environments takes time. During the past years, there have been an increased demand for automatic techniques to measure biomass with high accuracy in a more practical and easier way [8]. The optimal management of the herd in pastures can lead to the correct maintenance of population and productivity of the species, contributing to compliance with the proper amount of nutrients to the animals [9].

1.1 Motivation

There are some known methods of measuring biomass in the field. The most usual are the ruler and the plate meter (Figure 1.1). The ruler is used to measure the average height of the plant in some spots in the field and a simple calculation is made to estimate the total biomass. On the other hand, the plate meter works by measuring the density of the pasture in the area covered by the plate with a specific weight. Since most farmers evaluate the amount of biomass using these methods in just few small delimited areas, the estimation of the total biomass becomes inaccurate as it is laborious and extremely time consuming to be done across the entire field.

(a) Ruler

(b) Plate Meter

Figure 1.1: Methods of measuring the height of the pasture, using a ruler or a plate meter.

Taking this into account, agronomy urges to introduce in the field a low-cost technique to assist farmers to measure the biomass accurately and without exposing themselves weekly into varied spots across the field.

As stated by [10], an unmanned aerial vehicle (UAV) is a system capable of sustained flight with or without direct human control and able to perform a specific task. These aircraft are popularly known as drones and have become increasingly popular in recent decades, as technologies used for their assembly and remote control are more user-friendly [11]. Besides, equipment and software costs reduction made drones more accessible and hence increased considerably their market share.

Applications vary between military use, surveillance, meteorological investigations [12], or even, personal purposes, which considerably widen up their use and lowered their cost. In addition, the application of these aerial vehicles in agriculture is a branch that has gained strength in the last decade, due to the growing need to optimize production resources (Figure 1.2). The automation of crops ensures greater productivity and assertiveness to agribusiness, as the incorporation of technology allows farmers to make quicker and more reliable decisions [13]. The work in the crops was normally a manual task, often considered laborious and low-accurate, contributing to the raising of Precision Agriculture (PA) [14], which has been contributing to improve the quality and productivity of plant and animal production, with cost reduction and less environmental impact.

Figure 1.2: Drones doing tasks in the field.

In this context, considering that drones are able to collect several forms of data and therefore provide strategic information to farmers [13], they can play an important role in acquiring data for biomass estimation.

Also, the accurate determination of the dry mass of the grass is essential to properly calculate the total available forage and, consequently, the number of animals that should occupy a given region of the pasture, formally known as “Stocking Rate” [15]. This calculation assists in the management of pasture and in estimating the demand for forage. It is often expressed in AUs/unit area (AU means Animal Unit and represents 450 kg of live weight).

In addition, a pasture can be a mixture of grass and legumes in order to transfer fixed nitrogen (N) to associated grasses. This process, called Biological Nitrogen Fixation (BNF), aims to increase productivity and/or minimize effects of nutrient limitations, low soil moisture, soil acidity, pests and diseases [16]. The optimal rate between legumes and grass lies between 2% and 26% of legumes in the pasture [16], so that, besides estimating the overall biomass, monitoring the amount of legumes in each field is also important to evaluate soil’s health and hence livestock agriculture production.

1.2 State of the Art

Considering the methods used to reach the expected results, numerous studies have worked with regression models to estimate biomass of grass forage [17, 18, 19, 20, 21, 22, 23] or other types of crops, as wheat [24] and forests [8, 25]. Regression models are also used in agriculture business to estimate the amount of nitrogen accumulated in the crop [26, 27].

These studies have used linear and nonlinear regression models [19, 21, 22, 26], machine learning models as Random Forest (RF) [18, 20], Support Vector Regression (SVR) and Extreme Learning Machine (ELM) [24], neural networks, as Multi-Layer Perceptron (MLP) [25, 28], and deep learning methods, as Convolutional Neural Networks (CNNs) [17]. These estimation models use different types of data as inputs, such as from optical or reflectance sensors [21, 28], processed data from satellites (remote sensing) [19, 20] or imagery from unmanned aerial vehicles (UAVs) or drones [17, 24].

Considering papers with estimation of pasture biomass as the main goal, it is possible to compare the results obtained by [17, 18, 22] with our work. Our work aims at minimizing the RMSE (root mean squared error), but, R-Squared will be used for comparison purposes, as it is the only metric shown in all related works identified in literature.

The work described in [17] presents a study of biomass estimation using RGB-based images captured by a drone, reaching a R-Squared of 0.88. However, the methodology used is based on CNN (convolutional neural networks). The main disadvantage for this method is the necessity of a large amount of data to build the training data set, which is not the case for our study.

The author in [22] compared the estimation of biomass between RGB-based VIs and NDVI (Normalized Difference Vegetation Index) from the N-Sensor measurements, which use non-visible bands in their formulation. The authors developed a linear regression model that reached a R-Squared of 0.65, using NDVI as input. The linear regression models using VARI and NGRDI also presented good results (0.63 and 0.62, respectively), so they were further investigated in our work. The results obtained in [22] did not reach satisfactory R-Squared, as the models were not so complex, but it represents an indication that other works should explore more the RGB-based VIs, instead of only NDVI, as NDVI cameras are more expensive and simple RGB cameras can reach similar results, depending on the application environment.

Another interesting work [18] used UAV imagery to compose the data set. Their photogrammetry and image processing were more complex as it used cameras with higher quality and hyperspectral images. The model was computed using a Random Forest from Machine Learning methodologies of regression. With all of these high cost technological resources, it reached a high R-Squared of 0.9.

Several solutions can be adopted to accomplish a more accurate estimation of the total forage available for the animals, with the use of multiple sensors, multi-spectral cameras and high-performance neural networks. However, this work aims to reach the same result with the simplest solutions.

1.3 Goals

In this work, we aim to develop a biomass estimation methodology based on images acquired by a simple RGB camera embedded on the DJI Spark drone, a low-cost unmanned aerial vehicle (UAV). The obtained images are pre-processed to extract some relevant features for the local biomass determination, such as their pixel channels, vegetation indices and the light intensity using the picture histogram. More specifically, beyond the Red, Green and Blue Channels themselves, the RGB images were also used to compute the following RGB-based Vegetation Indices (VIs): RGBVI (Red, Green and Blue Vegetation Index) [29], GLI (Green Leaf Index) [30], VARI (Visible Atmospherically Resistant Index) [31], NGRDI (Normalized Green-Red Difference Index) [32], ExG (Excess of Green) [33] and ExGR (Excess of Green minus Excess of Red) [34].

Each spot captured by the drone's camera had its plant height measured by a ruler, aiming at using this feature as an input of the developed regression models. Moreover, the drone flight altitude of each image captured was also stored to be used as input of the models. In order to deliver more relevant data to the models, aiming at improving their results, two other features were also acquired due to their potential importance for the regression models. They were the intensity of green light on image's histogram and solar radiation, measured externally by a weather station.

The fresh matter was destructively collected in the experimental field and measured in $\mathsf{g/m^2}$ to compose the data set. In this work, only Green Biomass (legumes and grass) was analyzed and tested. The inputs and outputs will be further discussed in Chapter 2.

Once the data set is acquired, different regression algorithms were implemented and optimized aiming at identifying their best configurations for this problem, by analyzing the performance results of each configuration.

As a baseline, linear and non-linear regression algorithms were used to establish a correlation between biomass and inputs based on the RGB-channels, vegetation indices and other relevant features. Furthermore, a regression method based on artificial neural networks (ANNs) was also developed, aiming at higher accuracy. Moreover, a stacking method was proposed to improve the achieved performance metrics by using the best configurations of the linear, nonlinear and ANN regressions. Besides, we evaluated how different sets of input combinations affect the ANN accuracy, in order to identify the most relevant inputs to biomass estimation.

Therefore, this work focuses on the development of an intelligent biomass estimator, based on the comparison of regression models, including a supervised neural network, using the back-propagation method based on MLP.

1.4 Text Structure

This document is structured as follows. This Chapter presented a brief introduction to the study, the motivation of estimating biomass in crop fields, the state of the art considering the regression methods and the goals of this work.

In Chapter 2, we present the materials that were relevant to our problem, which contemplates the data acquisition regarding the images captured by the drone and the measured matter in the field. It also presents the methods used to analyze and test different inputs for the developed regression models.

In Chapter 3, we present the theoretic formulation and the implemented algorithms used to process the regression and obtain the results.

In Chapter 4 we show the obtained results and the evaluation of each one. Then, a comparative section discusses the best results and advantages of each proposed method.

Finally, in Chapter 5 we present our conclusion, based on the results presented in Chapter 4, and suggest future works, that can represent a relevant progress to this project.

2
Materials and methods

In this chapter, we present the main aspects of the materials and methods used in this work. Firstly, we describe the process of data acquisition and how the information was treated to build the data set for the problem. Then, the section of the analyzed inputs explains the combined methods that were studied and used in this work to obtain several options of possible relevant inputs to the developed algorithms, described in Chapter 3.

2.1
Data Acquisition

The study area used in this work is located at Embrapa Agrobiologia, the Brazilian Agricultural Research Corporation, in Seropédica, Rio de Janeiro, Brazil (Figure 2.1). At the test field (Figure 2.1 c), there are two different species of forage: *Brachiaria* grass (*Brachiaria brizantha cv Marandu*) and the Legume (*Macrotyloma axillare cv Java*).

(a) Rio de Janeiro

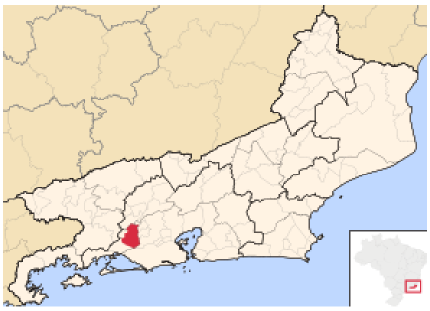

(b) Seropédica, RJ

(c) Test field

Figure 2.1: Location of the study area for biomass estimation.

Once a month, in the period of 10 months consecutively, agronomists and engineers of Embrapa destructively collected the fresh matter in spots on the experimental field and measured the weight of the mass to compose the data set used in this work.

In each day of measurement, around 12 spots were chosen randomly in the forage and marked on the ground with a red plastic frame of one square meter, as shown in Fig. 2.2.

(a) 5 m of altitude

(b) 10 m of altitude

(c) 15 m of altitude

(d) 20 m of altitude

(e) 30 m of altitude

(f) 50 m of altitude

Figure 2.2: Top view of the forage captured by the UAV at different heights: (a) 5 m; (b) 10 m; (c) 15 m; (d) 20 m; (e) 30 m; and (f) 50 m.

For each spot marked on the ground, the controller positioned the drone above the red square area, with its camera pointing to the ground, and took pictures from 5 to 50 meters high, aiming at analyzing the trade off between a reasonable resolution and a safe flight height. Notice that this procedure generates different pictures representing the same amount of biomass. We built the data set taking pictures at different heights aiming at contributing to develop a model more robust to drone's specific fighting altitude. Furthermore, in farms with uneven terrains, although the drone is flying in a direct line, different heights from the ground will be seen by its camera, as illustrated on Fig. 2.3. Some drones can adjust the difference of height automatically, but this method also enables the farmer to fly with the drone at any suitable height within this range.

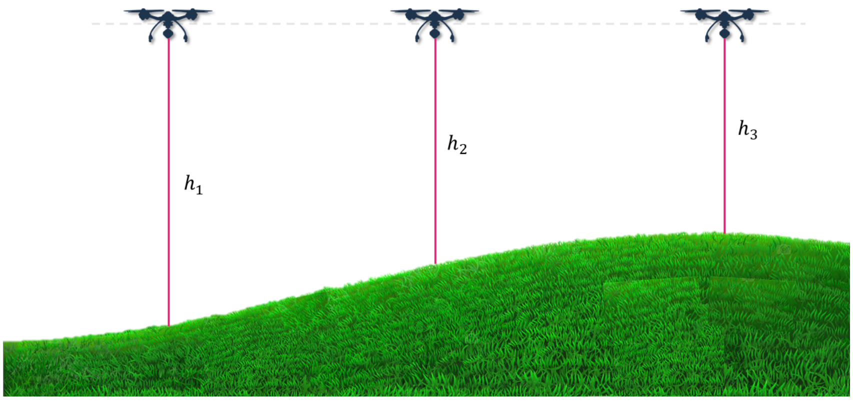

Figure 2.3: Drone flying over a hill, where $h_1 > h_2 > h_3$.

Although images captured at 5m height lead to the best resolution, this is not a suitable height as it requires more flight time to cover the entire field and it is not pleasant for the herd, if they are in the field at the same moment that images are captured. Also, some farms have high voltage lines crossing the fields, establishing another safety issue for the drone flight. Depending on its voltage, these lines can reach 30 meters of height [35].

Therefore, in this work, the images were captured in the experimental field with a DJI Spark drone using an embedded RGB camera with 12 MP resolution (3968×2976 pixels), in the following heights: (i) 5 m; (ii) 10 m; (iii) 15 m; (iv) 20 m; (v) 30 m; and (vi) 50 m, as shown in Figure 2.4.

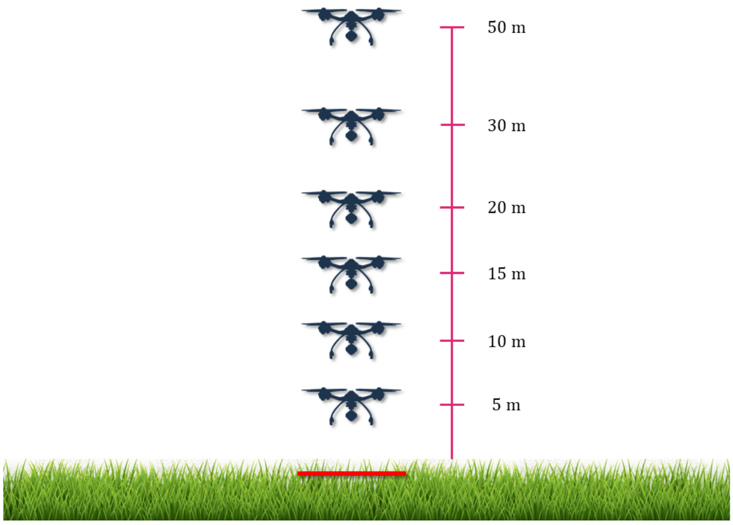

Figure 2.4: Front view of the drone flying at different heights.

To obtain the desired images, the following process was repeated at each spot:

1. Drone is positioned on the ground;
2. Drone flies at 5 m high;
3. Controller takes a picture;
4. Drone flies at 10 m high;
5. Controller takes a picture;
6. Drone flies at 15 m high;
7. Controller takes a picture;
8. Drone flies at 20 m high;
9. Controller takes a picture;
10. Drone flies at 30 m high;
11. Controller takes a picture;
12. Drone flies at 50 m high;
13. Controller takes a picture;
14. Biomass is collected from the red square area on the ground;
15. The procedure is repeated at another random spot in the field.

The higher achieved altitude was 50 meters as the picture resolution decreases as the drone flies higher. A simple calculation in order to analyze the resolution for each picture taken at different heights is the GSD (Ground Sample Distance), a parameter that represents the size of the image pixels. Using the principle of similar triangles, GSD makes a ratio between the size of the pixel in the image and the focal distance of the camera, and multiplies it by the distance from the ground, as illustrated in Figure 2.5 and shown in Equation 2-1.

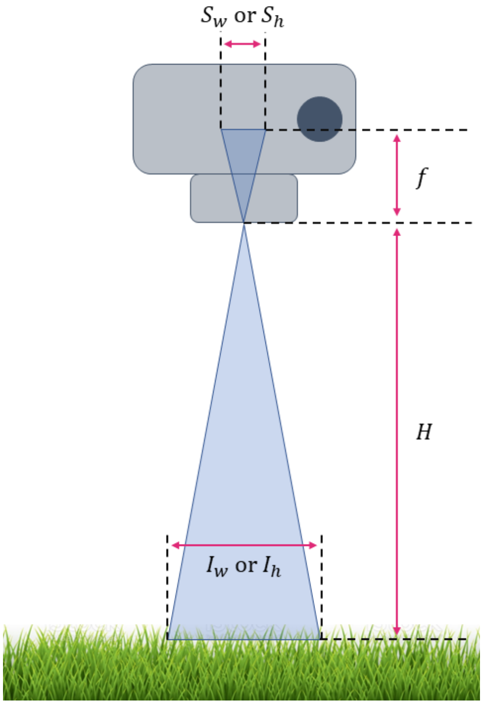

Figure 2.5: Similarity of triangles to calculate GSD parameter.

$$GSD_h = \frac{H * S_h}{f * I_h}$$

$$GSD_w = \frac{H * S_w}{f * I_w}\,, \tag{2-1}$$

where H is the flight height in cm, f is the focal length of the camera in mm, S_h is the sensor height in mm, S_w is the sensor width in mm, I_h is the image height and I_w is the image width, both in pixels. GSD_h and GSD_w refer to the height and the width parameters of GSD, respectively, in cm/px.

As stated by DJI® [36], the focal length of the DJI Spark drone camera is 25 mm and its sensor is a 1/2.3″ CMOS, with 6.16×4.55 mm. Therefore, the GSD for this camera is given by:

$$GSD_h = \frac{H * 4.55}{25 * 2976} = 6.11559 \times 10^{-5}\, H$$
$$GSD_w = \frac{H * 6.16}{25 * 3968} = 6.20968 \times 10^{-5}\, H \qquad (2\text{-}2)$$

The pixel's projection are not always perfectly squared, so the worst case scenario (greatest value between GSD_h and GSD_w) will be used to estimate image resolution. By Eq. 2-2, it is possible to see that we will use GSD_w, in our case.

The corresponding GSD values, in cm/px, for each height are described in Table 2.1 below:

Table 2.1: GSD_w results.

5 m	10 m	15 m	20 m	30 m	50 m
0.031	0.062	0.093	0.124	0.186	0.310

Even at 50 meters, the GSD of our system (0.31 cm/px) achieved a good ratio compared to other similar works, as 0.5 cm/px used by [17].

All measurements were performed once a month during 10 months, always between 9 am and 11 am, more precisely: (i) 17 November 2020; (ii) 19 January 2021; (iii) 8 February 2021; (iv) 23 March 2021; (v) 6 April 2021; (vi) 7 May 2021; (vii) 8 June 2021; (viii) 5 July 2021; (iv) 8 August 2021; and (x) 3 September 2021.

The flight altitudes used to capture images at each month were as follows: (i) November 2020 and January 2021, images were taken at two different heights (5 and 10 meters); (ii) March, April and May 2021, images were taken at six different heights (5, 10, 15, 20, 30 and 50 meters); (iii) June, July, August and September 2021, images were taken at five different heights (5, 10, 15, 20 and 30 meters). In the first two months, only two heights of images were acquired by the drone because it was, by the time, a test period of the resources and the possibilities. After the first evaluations, we observed that the minimum resolution allowed the drone to go higher and that would be safer considering the voltage lines and the stress of the animals. Also, this could mean more data to the regression models and a robustness for the variation of flights in the input. Pictures at 50 meters of height were not captured at the last 4 months because the obtained results until then showed that the image resolution at this height was not satisfactory.

The number of images captured in each month is shown in Tab. 2.2, summing-up 570 images in total.

Table 2.2: Number of Images Captured by the UAV.

Month	Spots	Different heights	Number of images
November 2020	12	2	24
January 2021	12	2	24
February 2021	12	6	72
March 2021	13	6	78
April 2021	12	6	72
May 2021	10	6	60
June 2021	12	5	60
July 2021	12	5	60
August 2021	12	5	60
September 2021	12	5	60
Total	119		570

After capturing all images, the areas marked with the red square were cropped to obtain the desired picture that represents the measured biomass, as exemplified by Figure 2.6.

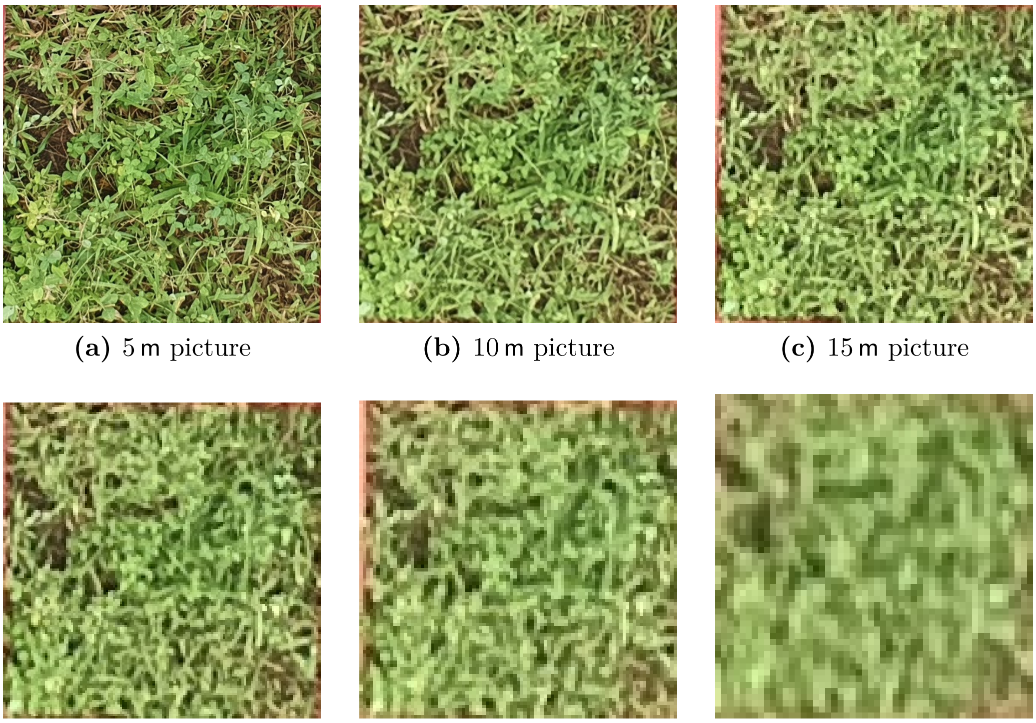

(a) 5 m picture **(b)** 10 m picture **(c)** 15 m picture

(d) 20 m picture **(e)** 30 m picture **(f)** 50 m picture

Figure 2.6: Processed images at different heights: (a) 5 m; (b) 10 m; (c) 15 m; (d) 20 m; (e) 30 m; and (f) 50 m.

Another representation of the images is show in Fig. 2.7, respecting the proportion and the resolution after cropping them.

The biomass measurements considered for this work are the sum of both *Brachiaria* and Legume weights. Besides, without loss of generality, the weight

(a) 5 m picture

(b) 10 m picture

(c) 15 m picture

(d) 20 m picture

(e) 30 m picture

(f) 50 m picture

Figure 2.7: Processed images at different heights respecting its proportion: (a) 5 m; (b) 10 m; (c) 15 m; (d) 20 m; (e) 30 m; and (f) 50 m.

of straw was not considered in the total biomass measurements. This will be further stressed on Section 2.3.

2.2 Analyzed Inputs

It was observed that, for different months and intensities of light, the amount of biomass had a better R-Squared when direct sunlight was exposed in the field. Rainy and cloudy days made the color of the images less vivid and so more difficult to properly estimate biomass. Hence, histogram of green light intensity was used to determine weights for pictures with higher brightness and contrast.

Two other factors were also used to help with the biomass estimation. The first one is the height of the vegetation, that was measured in each spot where biomass was collected. The height information can deliver the sense of third dimension as the weight of the biomass is related with its volume. So, it is an important factor to be considered to estimate the correct amount of biomass [29]. The second one is related to an external sensor of solar radiation, measured every hour at the weather station nearby the crop field (approximately 700 m from the field). The value of the radiation was also used and tested in the models to determine the vivacity and intensity of light.

Moreover, other external factors like temperature, humidity and precipitation level could also aid to estimate local biomass, as stated in [37]. However, they would only play an important role if they were measured at least one week earlier to the collection of pasture material, as it takes time for the rain and the environment temperature to affect the growing pasture. These measurements were obtained by consulting the weather station located nearby, but the herd were consuming the pasture during the period between the measurement and the pasture collection. So, the only possible moment to collect information would be during the pasture extraction, using images. In addition to the fact that using other sensors in the field could not deliver a relevant data for the regression, it would increase project's cost. Consequently, the installation of external sensors in the field was not considered in this work.

Nonetheless, this section presents the system inputs that can contribute to the biomass estimation of the mixed pasture analysis, including the Red, Green and Blue Channels of pixels (RGB), different RGB-based vegetation indices (VI), plant height (PH) measurements, altitude of the drone flight, intensity of the green light and solar radiation.

2.2.1
Red, Green and Blue Channels (RGB)

All images in this work are composed by three matrices of color channels that altogether form the colored image, as the example shown in Fig. 2.8. These channels are the primary colors: red, green and blue.

Figure 2.8: Example of Original Picture.

The arrays are matrices with the size of the squared cropped image used in the input, so that the size varies for different distances from the camera to the ground. The red square used to mark the spots on the ground has 1 m^2 and so the related image have approximately the dimension of 1 m^2 divided by the respective GSD values defined in Tab. 2.1, for each drone height. Figure 2.9 shows the representation of Fig. 2.8 by the arrays in red, green and blue channels, respectively. Notice that each separate channel forms a gray scale image. Each pixel varies the intensity of gray to define the image. The range is in between 0-255, where 0 represents the black color and 255 the white.

(a) Array of Red Channel **(b)** Array of Green Channel **(c)** Array of Blue Channel

Figure 2.9: Representation of the image using arrays of channels separately: (a) Red,; (b) Green; and (c) Blue.

The next step taken to create a value as an input was the calculation of the mean value of the selected image's pixels. Each array will generate a value, representing the mean intensity of the red (R), green (G) and blue (B) channels of each image of the data set. These values will be used in the regression to correlate with the biomass.

Therefore, since the data set has 570 images, 570 values were produced to each color channel. Tab. 2.3 shows the upper and lower bounds, average, standard deviation and a ratio between standard deviation and average value, for each color channel.

Table 2.3: Upper and Lower Bounds of the Dataset.

Data	Min.	Max.	Avg.	Std. Dev.	Ratio
R	61.858	165.196	126.152	17.898	0.142
G	82.911	166.302	138.66	16.316	0.118
B	43.666	111.742	81.781	12.408	0.152

2.2.2 Vegetation Indices (VI)

Considering the red, green and blue arrays explained in the section above, it is possible to define some equations using their values in order to emphasize a desired characteristic present in the images. These equations, called Vegetation Indices (VI), are largely used in Agricultural Research.

The most used VIs nowadays are the NDVI (Normalized Difference Vegetation Index) and the EVI (Enhanced Vegetation Index). The NDVI quantifies the growth of vegetation. It can range between -1 and +1. The higher the NDVI value is, the greater is crop's force of growth [38]. On the other hand, the EVI was designed to optimize the presence of vegetation, increasing the sensitivity in regions with high concentrations of biomass. It is also used to improve the vegetation monitoring by coupling the canopy bottom signal and reducing the influence of the atmosphere [39].

However, both of these Vegetation Indices use infrared values in their formulation, which is a non visible spectrum and can not be reached by a normal RGB camera, as the one used in this project. Only hyper or multi spectral cameras can inform the infrared and other spectrum arrays, but they are considerably more expensive, so that they were not used in the present work, since it focuses in the development of a low cost system.

Since these Vegetation Indices are not possible to access with RGB cameras, other VIs were tested in this work, considering only R, G and B data. Please, see Tab. 2.4 for the description of the analyzed vegetation indices and their associated references. All of them analyze and reinforce the importance of the green information in the image.

Table 2.4: Vegetation Indices Equations.

VI	Name	Equation	Reference
RGBVI	Red, Green and Blue Vegetation Index	$\frac{G^2 - R\,B}{G^2 + R\,B}$	[29]
GLI	Green Leaf Index	$\frac{2G - R - B}{2G + R + B}$	[30]
VARI	Visible Atmospherically Resistant Index	$\frac{G - R}{G + R - B}$	[31]
NGRDI	Normalized Green-Red Difference Index	$\frac{G - R}{G + R}$	[32]
ExG	Excess of Green	$2g - r - b$	[33]
ExGR	Excess of Green minus Excess of Red	$2g - 0.4r$	[34]

where

$$r = \frac{R^*}{\Delta}\,, \qquad g = \frac{G^*}{\Delta}\,, \qquad b = \frac{B^*}{\Delta}\,,$$

with $\Delta = (R^* + G^* + B^*)$ and

$$R^* = R/255\,, \qquad G^* = G/255\,, \qquad B^* = B/255\,.$$

A vegetation index (VI) was associated to each image, by calculating the VI of each pixel inside the red square located in the field and then computing the average value of these pixels. The obtained VIs were used as inputs of the regression models developed. In this case, there were six different possible inputs to analyze: RGBVI, GLI, VARI, NGRDI, ExG and ExGR.

Therefore, since the data set has 570 images, 570 values were produced to each VI. Tab. 2.5 shows the upper and lower bounds, average, standard deviation, and a ratio between standard deviation and average value, for each VI analyzed.

Table 2.5: Upper and Lower Bounds of the Vegetation Indices.

Data	Min.	Max.	Avg.	Std. Dev.	Ratio	Count
RGBVI	0.04	0.595	0.347	0.134	0.386	570
GLI	−0.006	0.336	0.166	0.078	0.471	570
VARI	−0.163	0.292	0.074	0.101	1.368	570
NGRDI	−0.124	0.236	0.057	0.075	1.321	570
ExG	0	0.535	0.244	0.121	0.494	570
ExR	0.227	0.385	0.296	0.029	0.098	570
ExGR	−0.384	0.286	−0.052	0.133	−2.565	570

2.2.3 Plant Height (PH)

Another important information of the forage for biomass estimation is the plant height. It gives the third dimension information that can not be captured by a top view image. Commonly, it is measured using the method of multi-temporal crop surface models (CSMs) derived from 3D point clouds [29].

In this work, the plant height was measured by inferring the average height of plants within the red square area and this information will be used as an input for the evaluated regression algorithms. It was manually measured with a ruler in the delimited area and also used as a neural network input. It is important to mention that the ruler was used to measure the plant height data used to build the data set used in this work, but the idea is to take these measurements by embedding an optical sensor to the drone in the final system to determine the plant height and avoid the laborious work in the field.

Table 2.6 shows the upper and lower bounds, average, standard deviation, a ratio between standard deviation and average value, and total count of data. Notice that, we do not have the measurements of PH in the first month (November 2020), so that we have only 107 PH measurements, rather than 119 (Tab. 2.2).

Table 2.6: Upper and Lower Bounds of Plant Height, measured in cm.

Data	Min.	Max.	Avg.	Std. Dev.	Ratio	Count
PH	12	43.2	27.138	5.861	0.216	107

2.2.4 Altitude of Drone Flight (DF)

Images closer to the ground have higher resolution delivering more valuable information to the network. The altitude of the drone can be easily accessed by the embedded electronics, so that this information was also used as input aiming at compensating distortions associated with lower image resolutions at higher altitudes.

Considering that our data set is composed by images captured at 6 different heights, the DF input assumes the following discrete values: 5 m, 10 m, 15 m, 20 m, 30 m and 50 m.

2.2.5 Green Intensity (GI)

An important component of an image is its histogram. It informs the intensity of each channel separately and makes it possible to analyze if the majority of pixels is nearer 0 (black) or 255 (white). Figure 2.10 shows the complete histogram of the image shown in Fig. 2.8, as an example.

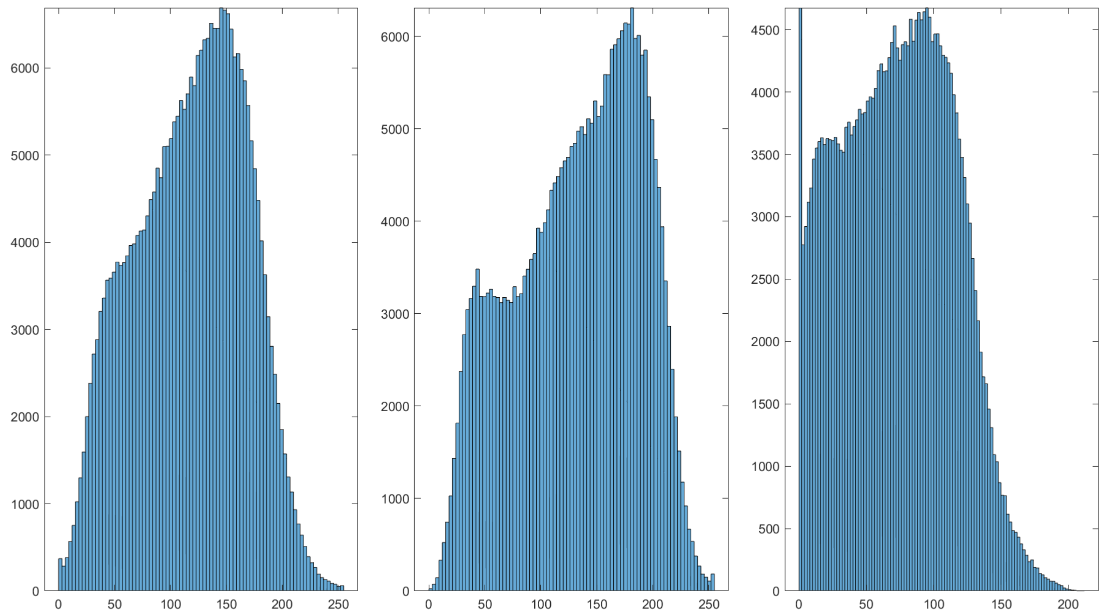

(a) Histogram of Red **(b)** Histogram of Green **(c)** Histogram of Blue

Figure 2.10: Histogram of the image shown in Fig. 2.8.

It was observed experimentally that images with direct light have better R-Squared with biomass estimation than indirect light. So, in order to separate and give weights to images in sunny days (direct light) and in cloudy/rainy days (indirect light), the Green Histogram was used. It was observed that the maximum peaks of the pixel frequency in green histogram under direct light occur for lower pixel intensities than in indirect light. In order to give this information to the developed regression models, it was created the GI input which is directly proportional to the pixel intensity (PI) of the maximum pixel frequency (PF) in green histogram, as stated in Eq. (2-3). It is possible to observe in Fig. 2.12 the difference in the histogram when modifying the original image from one of direct light to another with indirect light.

$$GI_{input} = PI(max(PF)) \tag{2-3}$$

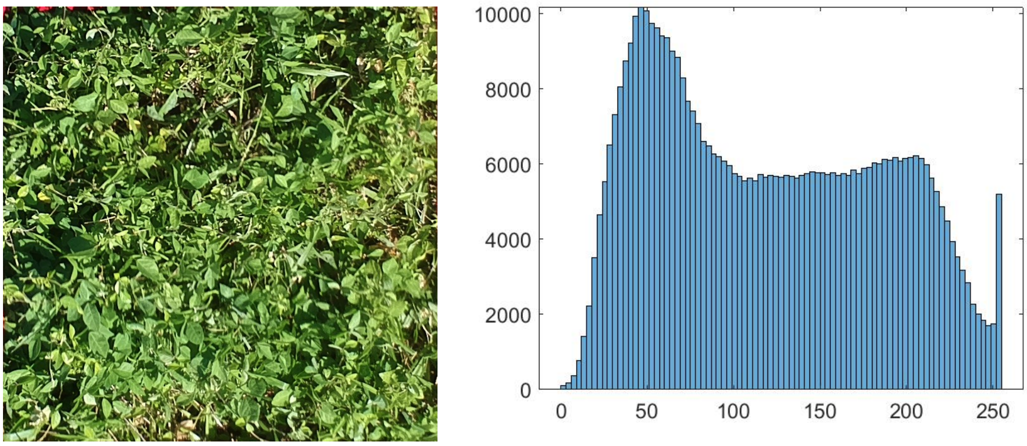

(a) Original Direct Light Image **(b)** Green Histogram of Direct Light Image

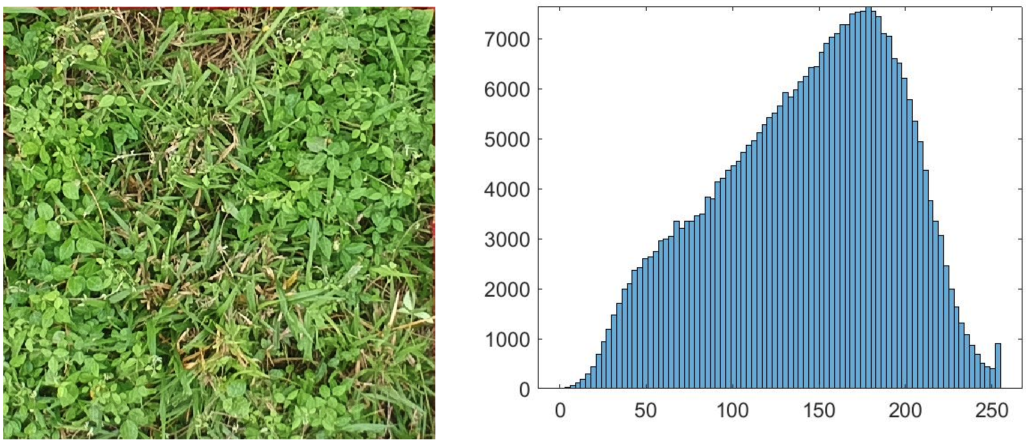

(c) Original Indirect Light Image **(d)** Green Histogram of Indirect Light Image

Figure 2.12: Comparison between indirect and direct light images.

Tab. 2.7 shows the upper and lower bounds, average, standard deviation, a ratio between standard deviation and average value, and total count of data for the GI.

Table 2.7: Upper and Lower Bounds of Green Channel Intensity.

Data	Min.	Max.	Avg.	Std. Dev.	Ratio	Count
GI	18	205	134.861	41.167	0.305	570

2.2.6
Solar Radiation (SR)

In order to contribute with the aspects observed in subsection above, measurements of the Solar Radiation were captured by a pyranometer, assembled in a weather station located nearby the measurement field. Pyranometers are sensors that combine direct and diffuse components of the solar irradiance, widely used by meteorologists, climatologists, atmospheric scientists, and renewable energy researchers [40].

The solar radiation data is hourly measured in the station mainly between 9 am and 6 pm, depending on sunlight. The values used were the ones captured at approximately 10 am at the dates where the data set images were captured. The unity used for SR is $\mathsf{kJ/m^2}$.

Table 2.8 shows the upper and lower bounds, average, standard deviation, a ratio between standard deviation and average value, and total count of data.

Table 2.8: Upper and Lower Bounds of Solar Radiation.

Data	Min.	Max.	Avg.	Std. Dev.	Ratio	Count
SR	8	524.13	143.235	170.695	1.192	119

2.3
Analyzed Outputs

The outputs in this work refer to the measured biomass, measured by agronomists at Embrapa Agrobiologia. The process of destructive collection in the experimental field was carefully done with appropriate tools and revision of data.

The spots were randomly positioned in the field, each month, and plant was cropped above 15 cm from the ground, because the material below this height is not consumed by the herd. All collected plant in the squared area were maintained separated between Grass (*Brachiaria brizantha*), Legume (*Macrotyloma axillare*) and Straw in order to have separate information about each of them. The weight of the fresh matter was measured with a scale and annotated in g/m^2. However, the weight of the fresh matter does not represent the reality as the plants, mainly the Legume, retain water in its composition. Thus, it should not be considered as the final data.

Therefore, in sequence, the process of drying the matter is executed by placing the fresh material in air-forced drying oven at 65ºC and the final dry matter weight is also annotated. All information that could be used in the project is listed in Tab. 2.9.

Table 2.9: List of possible outputs.

	Fresh Matter	**Dry Matter**
Original data	Legume Grass Straw	Legume Grass Straw
Variations	Green Biomass (Grass + Legume) Total Biomass (Grass + Legume + Straw) % Legume % Grass	Green Biomass (Grass + Legume) Total Biomass (Grass + Legume + Straw) % Legume % Grass

Table 2.10 shows the upper and lower bounds, average, standard deviation, a ratio between standard deviation and average value, and total count of data.

Table 2.10: Analyzed Output Data (in g/m^2).

Data	**Min.**	**Max.**	**Avg.**	**Std. Dev.**	**Ratio**	**Count**
Legume	0	256.368	96.229	57.326	0.596	119
Grass	13.156	474.142	110.35	85.375	0.774	119
Straw	0.001	236.989	81.815	62.341	0.762	119
Green Bio	36.301	581.604	206.579	108.289	0.524	119
Total Bio	41.467	723.988	288.394	139.725	0.484	119
% Legume	0	83.925	36.951	20.37	0.551	119
% Grass	10.442	73.342	35.99	13.802	0.384	119

For this work, all regression data used the dry matter of the Green Biomass as an output. Figure 2.13 shows the histogram of the Green Biomass data set built for this work. Note that the majority (89%) of the measured biomass lies in between 50 and 350 g/m^2. This happens because when the pasture is too high, it loses quality. Thus, the number of animals in the pasture is regulated so that the pasture is neither too low (overgrazing) nor too high.

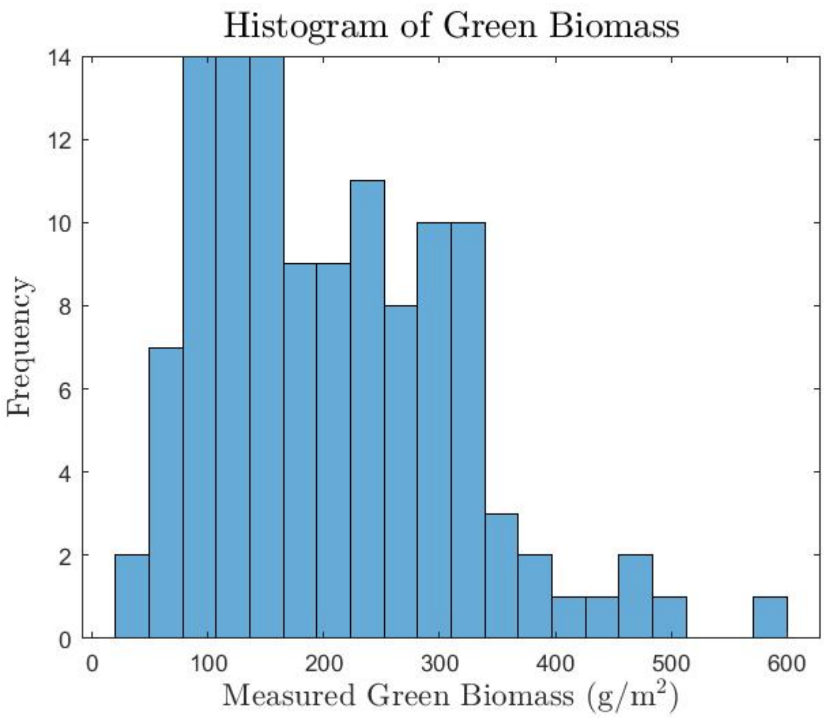

Figure 2.13: Histogram of Green Biomass.

3
Methodology

In this chapter, all developed algorithms for biomass estimation are presented with the formulation necessary to generate the results. All regression algorithms were optimized aiming at minimizing their root mean square errors. The data set used to training the regression models was pre-processed and the algorithms were developed using natural functions from Statistics and Machine Learning Toolbox or Neural Networks Toolbox (`NNToolbox`) in MATLAB R2020b (The MathWorks, Inc.). The hardware setup is composed by an Intel(R) Core(TM) i7-1065G7 CPU @ 1.30 GHz and 8 GB of RAM. The process established for the work is represented in Fig. 3.1.

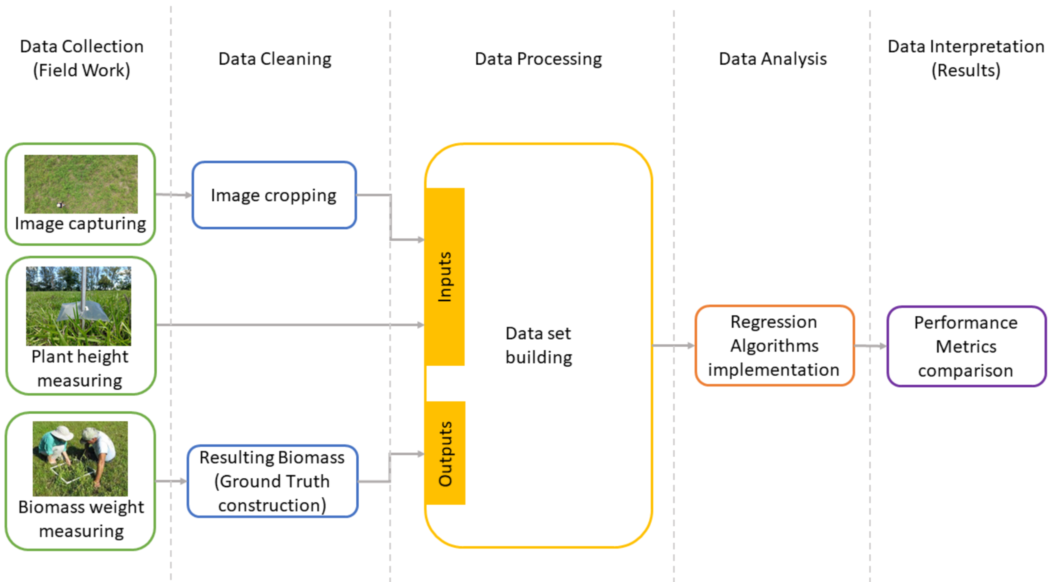

Figure 3.1: Block Diagram of the work process.

There are three different types of data measured in the field: (i) the images captured by the drone at different flight altitudes and different spots of measurement; (ii) the value of dry biomass at each spot (ground truth); (iii) the average plant height at each spot.

After acquiring the images, all of them were cropped so that only the area inside the red square marker, that indicates the desired spot on the field, is used to generate all the analyzed inputs. In the algorithms, it was possible to choose which inputs to test, among the ones listed in 2.2. They sum 13 different inputs, that could be used alone or combined with others.

The ground truth set of data was constructed from the collected dry matter, described in 2.3. More specifically, in this work, all tests and results were achieved by using the dry matter of Green Biomass (Grass + Legume) as output for the developed regression models. Moreover, a selection process of which images of the data set would be effectively used to train the regression models was implemented, aiming at testing if images with poor resolution (higher flight altitudes) could be degrading the results when used.

Considering the complexity of the work, Fig. 3.2 shows a block diagram representing everything that was developed to reach the desirable results.

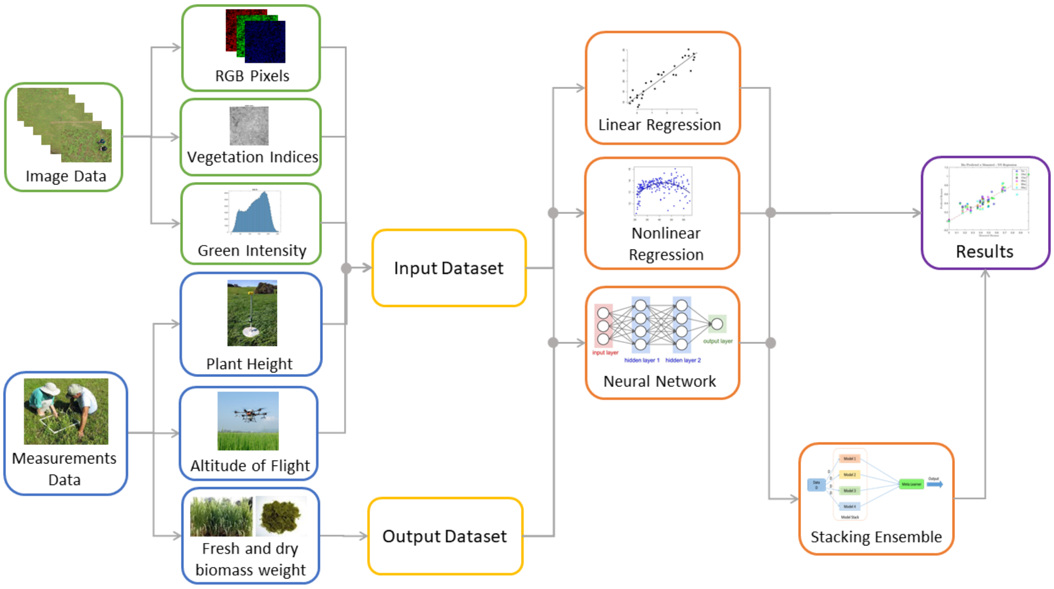

Figure 3.2: Complete Work Diagram.

After acquiring, cleaning and processing the data, it was submitted firstly to three different regression methodologies: (i) linear regression; (ii) nonlinear regression; (iii) MLP regression. Their models were developed in algorithms, using Matlab, and they were evaluated separately. Then they were analyzed for their best results, considering the inputs used. These best results were submitted to another model, based on stacking ensemble methodology, which is developed using a new neural network and the vectors of estimated biomass of each previous regression as inputs. They will be further explained and discussed in this section.

Later in section, we briefly present the performance metrics used in this work for comparison and analysis purposes.

3.1
Linear Regression Algorithm

Here, we implement a simple linear regression model, using all captured data, aiming to evaluate the natural correlation of the inputs (independent variables) with the measured biomass (dependent variable). If more than one input was used, it is considered a MLR (Multiple Linear Regression). In the algorithm, 80% of the data set was randomly chosen for training and the remaining 20% for testing. The algorithm was executed 30 times and the best results were annotated, in order to analyze how the performance metrics would respond to variations in the model coefficients induced by different training and test sets.

The linear regression is described by the following Eq. (3-1):

$$y_L = \beta_0 + \beta_1\, x_1 + \beta_2\, x_2 + \beta_3\, x_3 \ldots\,, \tag{3-1}$$

where $\beta_0, \beta_1, \beta_2, \beta_3, \cdots$ are the linear coefficients, y_L is the biomass estimated by the linear regression and $x_1, x_2, x_3, \cdots$ are the chosen inputs. All values are assumed to be positive parameters.

3.2 Nonlinear Regression Algorithm

In this scenario, a nonlinear regression model is implemented, using minimum squared errors technique as performance metrics, aiming to evaluate which is the better correlation of the inputs with the measured biomass. As stated by [29], the relationships between the biomass and VIs or Plant Height (PH) are often nonlinear. So, a multiple nonlinear regression (MNLR) model is proposed, using a quadratic regression model, with up to 5 different input variables and their corresponding number of coefficients, as shown in equation (3-2).

$$\#\alpha_n = \frac{1}{2}\, n\,(n+1) \tag{3-2}$$

where $\#\alpha_n$ is the number of coefficients and n is the number of inputs used.

The developed nonlinear regression models are described by the following equations (3-3), (3-4), (3-5), (3-6) and (3-7), according to the number of input variables (n) chosen in the algorithm:

- $n = 1$:

$$y_{NL} = \alpha_0 + \alpha_1\, x_1^2 + \alpha_2\, x_1\,, \tag{3-3}$$

- $n = 2$:

$$\begin{aligned} y_{NL} = \;& \alpha_0 + \alpha_1\, x_1^2 + \alpha_2\, x_2^2 + \alpha_3\, x_1\, x_2 + \\ & \alpha_4\, x_1 + \alpha_5\, x_2\,, \end{aligned} \tag{3-4}$$

- $n = 3$:

$$\begin{aligned} y_{NL} = \; & \alpha_0 + \alpha_1 \, x_1^2 + + \alpha_2 \, x_2^2 + \alpha_3 \, x_3^2 + \alpha_4 \, x_1 \, x_2 + \\ & \alpha_5 \, x_1 \, x_3 + \alpha_6 \, x_2 \, x_3 + \alpha_7 \, x_1 + \alpha_8 \, x_2 + \alpha_9 \, x_3 \, , \end{aligned} \tag{3-5}$$

- $n = 4$:

$$\begin{aligned} y_{NL} = \; & \alpha_0 + \alpha_1 \, x_1^2 + + \alpha_2 \, x_2^2 + \alpha_3 \, x_3^2 + \alpha_4 \, x_4^2 + \alpha_5 \, x_1 \, x_2 + \\ & \alpha_6 \, x_1 \, x_3 + \alpha_7 \, x_1 \, x_4 + \alpha_8 \, x_2 \, x_3 + \alpha_9 \, x_2 \, x_4 + \alpha_{10} \, x_3 \, x_4 + \\ & \alpha_{11} \, x_1 + \alpha_{12} \, x_2 + \alpha_{13} \, x_3 + \alpha_{14} \, x_4 \, , \end{aligned} \tag{3-6}$$

- $n = 5$:

$$\begin{aligned} y_{NL} = \; & \alpha_0 + \alpha_1 \, x_1^2 + \alpha_2 \, x_2^2 + \alpha_3 \, x_3^2 + \alpha_4 \, x_4^2 + \alpha_5 \, x_5^2 + \\ & \alpha_6 \, x_1 \, x_2 + \alpha_7 \, x_1 \, x_3 + \alpha_8 \, x_1 \, x_4 + \alpha_9 \, x_1 \, x_5 + \\ & \alpha_{10} \, x_2 \, x_3 + \alpha_{11} \, x_2 \, x_4 + \alpha_{12} \, x_2 \, x_5 + \\ & \alpha_{13} \, x_3 \, x_4 + \alpha_{14} \, x_3 \, x_5 + \alpha_{15} \, x_4 \, x_5 + \\ & \alpha_{16} \, x_1 + \alpha_{17} \, x_2 + \alpha_{18} \, x_3 + \alpha_{19} \, x_4 + \alpha_{20} \, x_5 \, , \end{aligned} \tag{3-7}$$

where $\alpha_0, \alpha_1, \alpha_2, \alpha_3, \cdots$ are the MNLR coefficients, y_{NL} is the resulting biomass and $x_1, x_2, x_3, \cdots$ are the chosen inputs. All values are assumed to be positive parameters.

The upper bound of input variables was set to 5 different possible inputs to limit the total variables in the model and compare results with other regression methods that could overfit using more input variables, considering the total amount of data.

As developed for the Linear Regression, training and test sets were defined randomly: 80% for training and 20% for testing. Furthermore, each evaluated regression model was executed 30 times and the best results were annotated, to analyze how the performance metrics would respond to variations in the model coefficients induced by different training and test sets.

3.3 MLP Regression Algorithm

A coherent next step to increase complexity on the model and find a more efficient parameter learning procedure than regressions with established forms of equations is to develop an Artificial Neural Network (ANN).

Artificial Neural Networks are part of Artificial Intelligence (IA) methodologies that simulate the working of neurons in the human brain, using computational nodes as the neurons and connections between them as synapses. The main function of the neuron is to receive the information by a synapse, make a decision and pass it forward as it conveys. The simulation of this synaptic decision is computed with weights on the connections between the nodes in the ANN.

Another important aspect of the human brain is its capacity of learning. It receives backward information stimulated by the rest of the human body or by external environment in the form of electrical impulses and redefine the synaptic decision, which can be of excitation or inhibition. This is called the error-correction learning rule. In this case, the ANN allows the error back-propagation algorithm in order to simulate the capacity of learning from the human brain. It works in two ways: first, in a forward pass, the inputs are applied into the nodes throughout the net, layer by layer, and the weights are computed until the final response reached by the network. Then, the real response, called target or ground truth, is used to calculate the difference between these two responses and produce the error signal. In a backward pass, the error travels back throughout the network in the sense of returning to the first layer, adjusting all the weights in the way it passes in order to modify the final response towards the desired target. Hence, the error is back propagated against the direction of the connections every time there is a forward pass and the network is learning with it [41]. This process is repeated in a determined number of times, called epochs, or until it reaches the minimum tolerance of error.

Even though synapses are simple units of interactions between the neurons, the human brains are efficient structures because they have a large number of neurons and synapses. It is estimated the order of 10 billion neurons and 60 trillion synapses or connections in a human brain [41]. It means that, as long as the number of nodes and connections increases, more complex decisions can be done by the neural network as the ability of learning is enhanced. This is the definition of Deep Learning and used in methods as Convolutional Neural Networks (CNN), Recurrent Neural Networks (RNN) and others. They will not be used in this work as the total amount of data in our data set is not compatible with these methods, so this work will be restricted to a Shallow Learning of an Artificial Neural Network.

Perceptron is the name of the first model for learning in a supervised manner, proposed by Rosenblatt in 1958 [41]. It is composed by a single neuron and it was able to perform tasks that were linearly separable. It means that it can only separate patterns that lie in different sides of a hyperplane. Yet, supervised learning consists in models of neural networks which already have a target to be followed. Considering these concepts and expanding Rosenblatt's Perceptron theory to the proposed work, the generalization of a single layer perceptron is the Multi-Layer Feedforward Network, commonly referred as Multi-Layer Perceptron (MLP). It allows to create hidden layers on the network and to introduce nonlinearities in the model, increasing the complexity without the necessity of determining the whole equation and coefficients manually. As more layers are included in the model, the resulting region for each pattern becomes increasingly complex.

The ability to learn the complex relationship between features and target from the neural network is also due to the presence of activation functions in each layer. Rosenblatt's single neuron solve linearly separable patterns for classification and it is activated by a nonlinear function, differentiable, in order to maintain the characteristics of the inputs and separate the patterns into different classes. This principle is used in all kinds of neural networks until today. There are several researches looking for optimized activation functions to boost network performance [42]. Usually, logarithmic or hyperbolic tangent functions are used as activation functions in most neural networks but it actually depends on the problem to be solved. Moreover, in general, a linear function is used to activate the output layer for regression analysis.

In this work, we developed an artificial neural network, based on a Multi-Layer Perceptron (MLP) regression algorithm with backpropagation error. Aiming at optimizing the performance metrics of the developed MLPs, some hyperparameters of the neural network for each type of input evaluated were adjusted in the tests, as highlighted in Tab. 3.1. On the other hand, the fixed hyperparameters used in the designed neural network are listed in Tab. 3.2.

Table 3.1: Varied Hyperparameters.

Hyperparameters	**Variation**
Epochs	5000 - 10000 - 50000
Early Stop	500 - 1000 - 5000
Neurons per layer	4 - 6 - 8 - 10 - 12 - 14 - 16 - 18 - 20

Table 3.2: Fixed Hyperparameters.

Hyperparameters	**Value**
Number of Hidden Layers	2
Activation Function (hidden layers)	log
Activation Function (output layer)	linear

The back propagation algorithm used in this work is the gradient descent with momentum ($\alpha = 0.97$) and adaptive rate ($\eta = 0.01$). The tolerance of the gradient was set to 1×10^{-6} to reach better results. The data set is randomly divided into three parts to avoid overfitting and model selection bias: 70% for training set, 20% for validation set and 10% for testing set. Besides, all data used as inputs/outputs were linearly normalized between 0 and 1, so that all values are in the same range, avoiding biasing. This normalization was applied even for the VIs, that already vary mostly in this range. When data set is ready, the first step is to train several networks doing a Layer Sweep, where all possible combination of number of neuron per layers are used. They were set from 4 to 20 neurons for both layers, in steps of 2. Besides, the number of epochs and early stops were varied for each combination. They were set to three different combinations: (i) Epochs: 5000, Early Stop: 500; (i) Epochs: 10000, Early Stop: 1000; (i) Epochs: 50000, Early Stop: 5000. This was implemented so that we could analyze generalization for each input combination. These configurations sums up to 243 trainings. The results were stored and then analyzed.

In a second step, the three best configurations for each type of combination of input were trained again for 30 times in a row. Then, the model delivers the final performance results for this method.

3.4
Stacking Ensemble Algorithm

The Stacking Ensemble method consists in combining several models altogether to make a prediction. Just as classification problem, it can also be used in a regression, which is the case of our work. Researches in this type of approach have been increasing in the past years as good results have been achieved. Robustness and accuracy are the main benefits reported when using a Stack Ensemble method compared to single models. Although most of works define techniques related to classification problems and they are often not applicable to regression, there are many options to apply this method to regression problems [43].

Therefore, this work implements Stacking Ensemble Method as a fourth model, aiming to increase the performance and achieve better results. It combines the first 3 methods (Linear Regression, Nonlinear Regression and MLP ANN), using their outputs as the input vector, as shown in Fig. 3.3.

In this work, the implementation of Stacking Ensemble consisted in a new neural network, using only 3 inputs: the best results for the previous methods, considering the lowest RMSE value reached by each one of them. The method used here was the same for the MLP Regression, described in 3.3. The fixed hyperparameters were the same as Tab. 3.2 and the varied one as Tab. 3.1. First a Layer Sweep was implemented using the three predefined inputs. Then, the best 3 configurations were submitted to 30 runs in order to

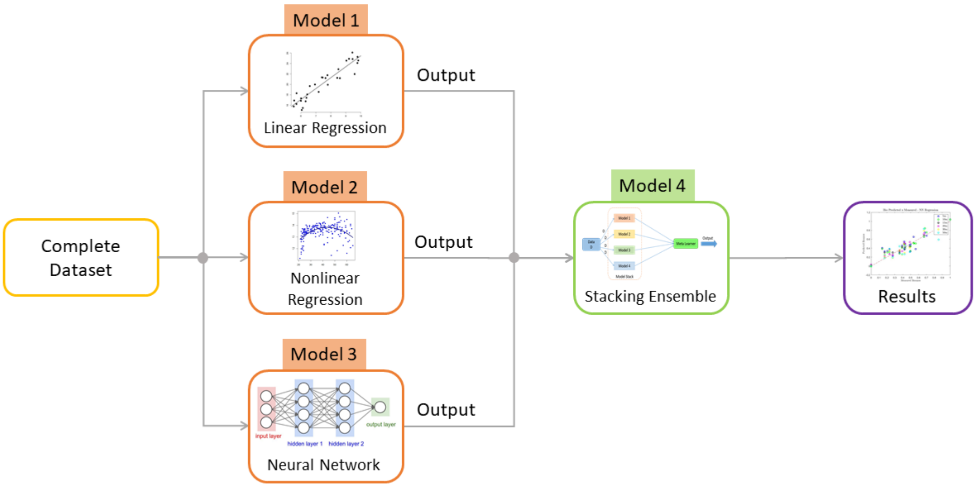

Figure 3.3: Block Diagram of the Stacking Ensemble Method.

guarantee the reliability of the final metrics, statistically speaking.

In this case, Stacking Ensemble can be interpreted as a potential improvement for the MLP results, since it is expected that the Artificial Neural Network reaches better results than simple regressions methods, considering it fits more complex correlations between inputs and the output.

3.5 Performance Metrics

The performance of the regression algorithms is evaluated by the Coefficient of Determination (R-Squared) and two different types of error metrics: root-mean-square error (RMSE) and mean-absolute percentage error (MAPE). All results were considered as the best ones when the lowest RMSE values were achieved.

$$\text{RMSE} = \sqrt{\frac{1}{N}\sum_{n=1}^{N}(y_n - \hat{y}_n)^2}\,, \tag{3-8}$$

$$\text{MAPE} = \frac{1}{N}\sum_{n=1}^{N}\frac{y_n - \hat{y}_n}{\hat{y}}\,, \tag{3-9}$$

$$R^2 = 1 - \frac{\text{SSR}}{\text{SST}}\,, \tag{3-10}$$

where $\text{SSR} = \sum_{n=1}^{N} y - \hat{y}^2$, $\text{SST} = \sum_{n=1}^{N} y - \overline{\hat{y}}^2$, $\hat{y}$ is the measured biomass (ground truth), $\overline{\hat{y}}$ the mean value of measured biomass, y the predicted biomass and N the size of the data set.

4
Results and Discussion

In this section, we describe experimental results for biomass estimation obtained after running each algorithm 30 times. According to the central limit theorem, if the sample size is 30, the studentized sampling distribution approximates the standard normal distribution and assumptions about the population distribution are meaningless since the sampling distribution is considered normal [44]. Also, it presents a comparison of the results achieved by the different regression models analyzed. The outputs are the total biomass, within the 1 m^2 red square present on each image.

First, we present the linear regression results, then nonlinear regression, MLP regression and finally the stacked ensemble algorithm. For each methodology, two subsections are presented, showing first the results where the inputs are tested separately in order to analyze the influence of the 13 different inputs in the output. To facilitate the performance comparison, we generate graphs with the target (measured biomass) in the horizontal axis and the achieved output (predicted biomass) in the vertical axis. All graphs presented in the work are based on the test set defined randomly in the algorithm.

Afterwards, in the second subsection, we combined some inputs which could boost the relationship between the inputs and the target. It is foreseen that the plant height can have a significant effect on the determination of a biomass from vegetation indices [29]. Hence, it was combined with all the inputs to check the validity of this hypothesis. The other inputs, that are neither vegetation indices nor the channels of pixels, were combined with best results of separate vegetation indices to enhance the result's accuracy. Moreover, configurations with all channels (R, G and B) as inputs were tested to see if they altogether can perform better than separately. Finally, combinations between the vegetation indices where also evaluated aiming at achieving higher R-Squared and lower RMSE and MAPE.

4.1
Linear Regression

In this section, it will be presented all the results and their related discussion for the tested inputs. Firstly they will be evaluated separately, in order to analyze the influence of each of them in the estimated biomass. This will give a perception of the most promising inputs that could be tested together, aiming at higher performance.

Then, in another subsection, they will be tested in different combinations after analyzing the performance of each of them separately. In both subsections, it will be presented a table summarizing the data analysis of the RMSE in each of the 30 runs, as average value, standard deviation, lower and upper bounds. The second table presents the best RMSE found among the 30 runs and their corresponding MAPE and R-Squared. Furthermore, the plots associated to the best RMSE for each analyzed input will be shown in the related images.

4.1.1 Separate inputs

The influence of each one of the inputs, described in Chapter 2, in the estimated outputs can be an important factor to choose how to combine them aiming to increase performance. Hence, they are tested separately in this subsection, first analyzing the VIs and channels and then, the features.

4.1.1.1 RGB-based

Table 4.1 shows the results of the RMSE analysis for the VIs and channels as separate and unique inputs.

Table 4.1: Analysis of RMSE performance for the RGB-based as separate inputs using Linear Regression

Input	Avg RMSE (g/m^2)	Std Dev RMSE (g/m^2)	Min RMSE (g/m^2)	Max RMSE (g/m^2)
R	102.46	6.57	90.09	119.36
G	111.70	6.78	101.37	126.99
B	103.32	7.93	86.01	118.67
RGBVI	97.61	4.98	83.96	107.09
GLI	95.83	7.13	85.76	110.07
VARI	93.31	8.34	78.41	106.23
NGRDI	93.33	8.17	79.74	108.71
ExG	97.45	5.21	90.80	108.23
ExGR	94.02	7.48	79.96	112.84

The best linear fitting performance metrics for each of the VIs is shown in Table 4.2, together with their respective MAPE and R-Squared. On the other hand, Fig. 4.1 shows the plots associated to the best RMSE obtained for each input, among the thirty results generated for each one of them.

The RMSE was chosen as the main performance metrics, as the least mean square (LMS) algorithm was used to set the coefficients of the linear regression model, aiming at minimizing the mean squared error.

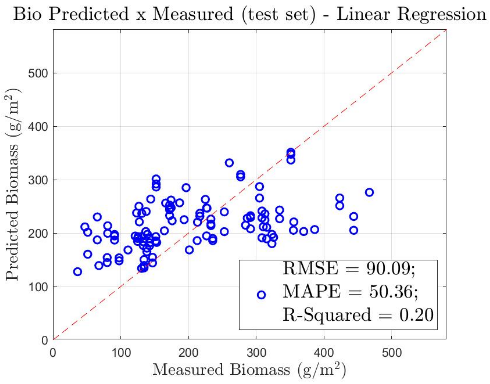

(a) Red

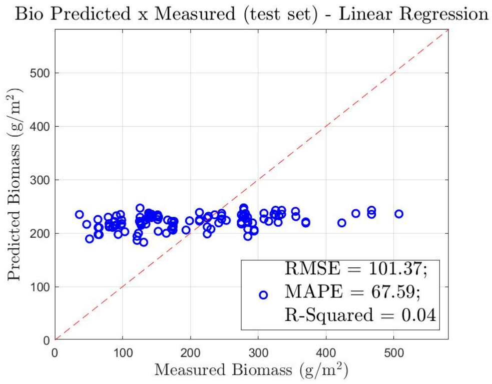

(b) Green

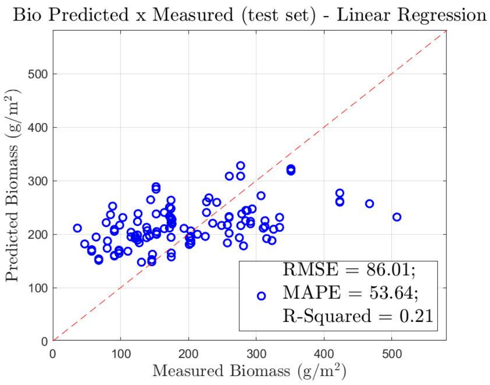

(c) Blue

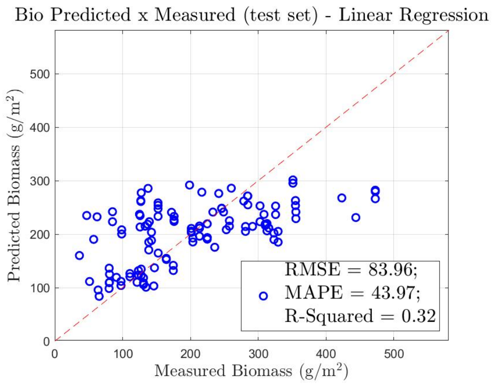

(d) RGBVI

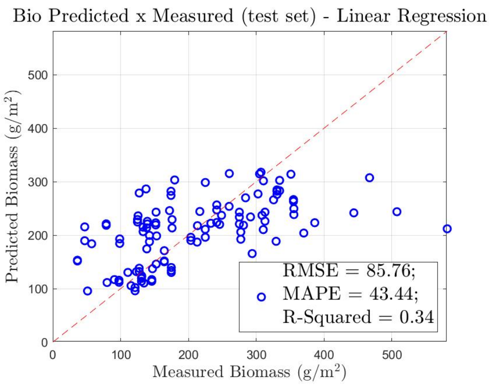

(e) GLI

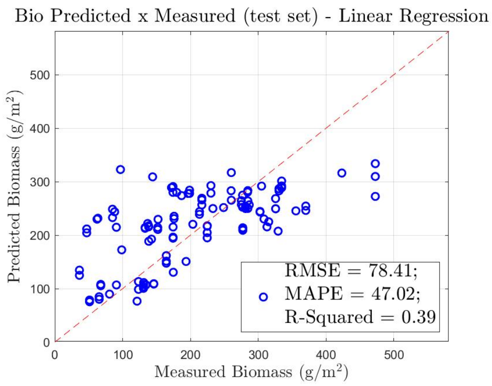

(f) VARI

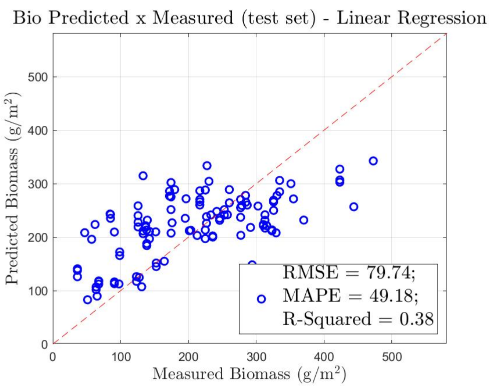

(g) NGRDI

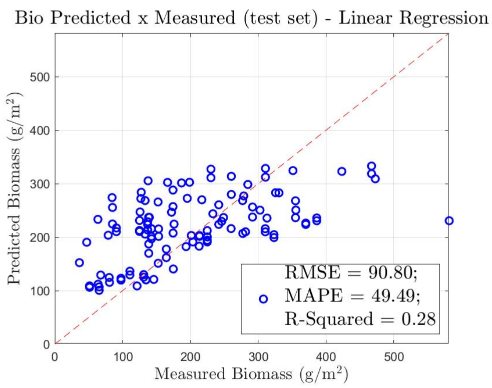

(h) ExG

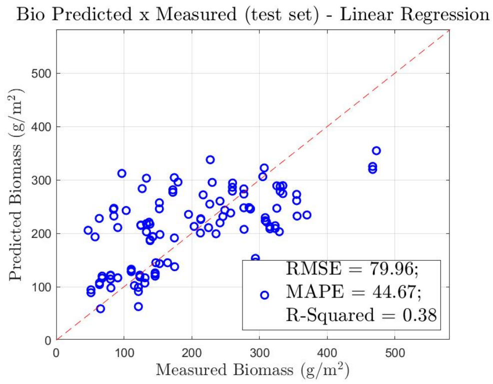

(i) ExGR

Figure 4.1: Best Linear Regression Performance for the RGB-based as Separate Inputs: (a) Red, (b) Green, (c) Blue, (d) RGBVI, (e) GLI, (f) VARI, (g) NGRDI, (h) ExG, (i) ExGR.

Table 4.2: Results for the RGB-based as separate inputs using Linear Regression

Input	Best RMSE (g/m^2)	MAPE (%)	R^2
R	90.09	50.36	0.20
G	101.37	56.68	0.05
B	86.00	53.64	0.21
RGBVI	83.96	43.97	0.32
GLI	85.76	43.44	0.34
VARI	78.41	47.02	0.39
NGRDI	79.74	49.18	0.38
ExG	90.80	49.49	0.28
ExGR	79.96	44.67	0.37

Although GLI vegetation index presents the best MAPE, it is possible to observe that the performance achieved by the VARI have the higher R-Squared and the lower RMSE in Linear Regression, when running the algorithm for each one of the RGB-based inputs separately. NGRDI and ExGR can also be considered among the best results as they have the second and third lowest RMSE. It is noticeable that the R, G and B inputs have high RMSE values and do not correlate so well with the output. They will be further analyzed when combined to observe if the results can be improved.

4.1.1.2 Features

Table 4.3 shows the RMSE analysis of the features used as inputs alone.

Table 4.3: Analysis of RMSE performance for the features as separate inputs, using Linear Regression

Input	Avg RMSE (g/m^2)	Std Dev RMSE (g/m^2)	Min RMSE (g/m^2)	Max RMSE (g/m^2)
PH	111.05	6.87	99.63	127.19
DF	110.43	6.52	96.08	125.91
GI	110.58	4.92	100.41	122.52
SR	111.31	6.70	97.05	121.16

Figure 4.2 shows the plots associated to the best RMSE obtained for each feature input, among the thirty results generated for each one of them. Also, the best linear fitting performance metrics for each of the features is shown in Table 4.4, together with their respective MAPE and R-Squared.

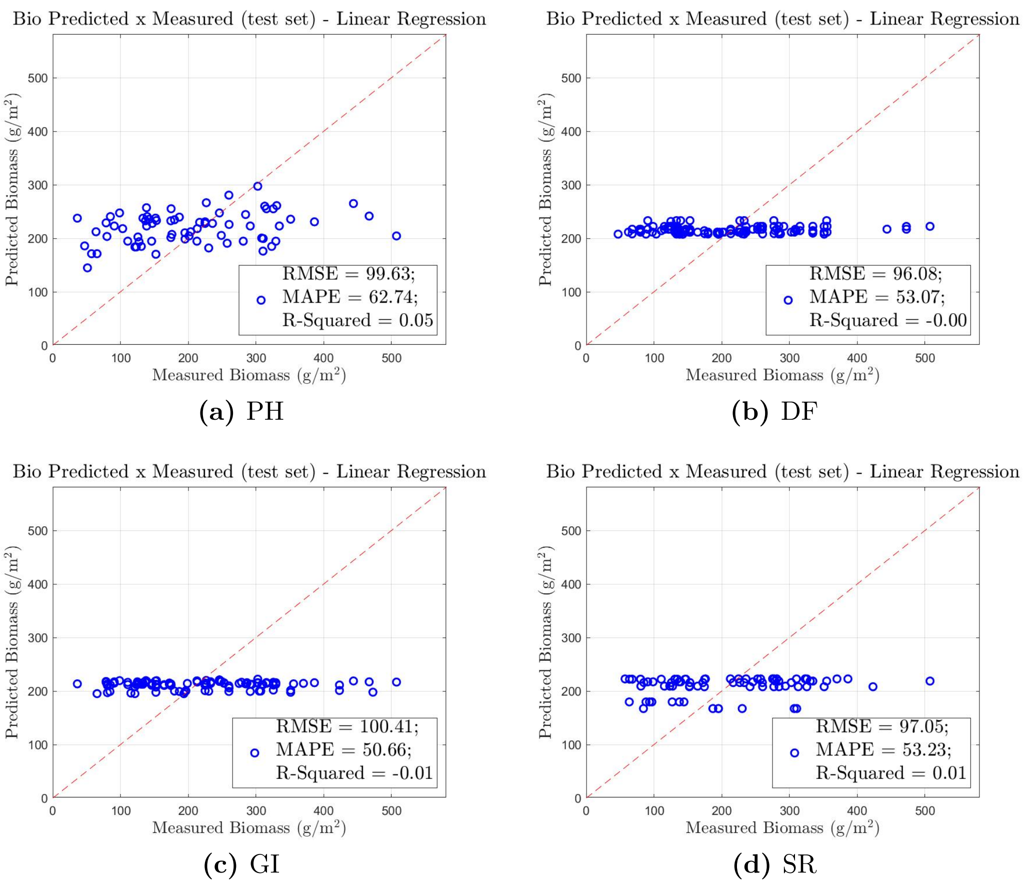

(a) PH **(b)** DF **(c)** GI **(d)** SR

Figure 4.2: Best Linear Regression Performance for the features as Separate Inputs: (a) PH, (b) DF, (c) GI and (d) SR.

Table 4.4: Results for the features as separate inputs using Linear Regression

Input	Best RMSE (g/m^2)	MAPE (%)	R^2
PH	99.63	62.74	0.05
DF	96.08	53.07	-0.01
GI	100.41	50.66	-0.01
SR	97.05	53.23	0.01

As expected, it is noticeable that DF, GI and SR alone do not have any significant relationship with the output whatsoever. These features will only be relevant when combined with the channels or the VIs. The plant height itself does not have a good direct correlation with the output, but it can also be a promising feature to combine with others.

4.1.2 Combined inputs

In this subsection, combinations of R, G and B will be made to test how the model responds to each one of them. Moreover, the inputs generated from the channels of the pixel's image and the VIs will be combined with the plant height (PH), altitude of drone's flight (DF), intensity of green light (GI) and solar radiation (SR). They will be tested here as a boosting factor for the model's performance and to further comparison with the neural network that will receive these parameters as inputs for the same purpose.

4.1.2.1 Combinations of R, G and B

Notice that R (red), G (green) and B (blue) don't correlate so well with the outputs, when tested separately. Hereafter, they will be combined among themselves and tested to observe which association is better to be used from now on. The RMSE analysis is shown in Tab. 4.5. The metric results are shown in Tab. 4.6 and in Fig. 4.3.

Table 4.5: Analysis of RMSE performance for different combinations of the RGB channels

Input	Avg RMSE (g/m^2)	Std Dev RMSE (g/m^2)	Min RMSE (g/m^2)	Max RMSE (g/m^2)
R and G	92.15	5.29	81.59	102.07
R and B	106.72	6.59	91.88	118.55
G and B	96.26	7.24	80.69	111.07
R, G and B	92.25	7.29	79.90	105.32

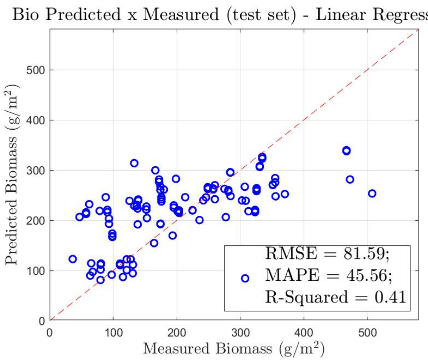

(a) R and G

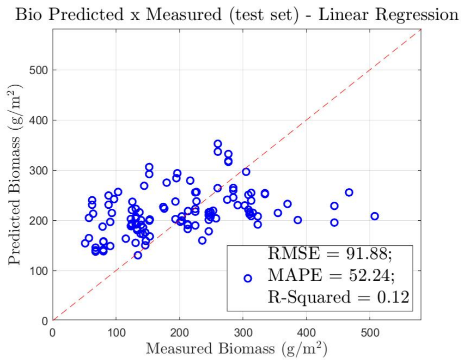

(b) R and B

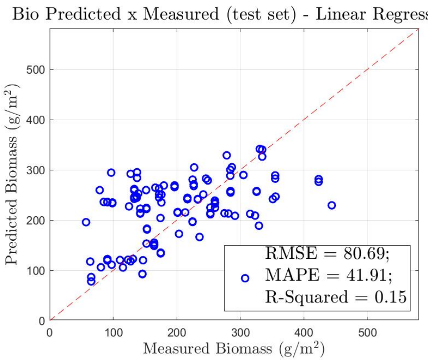

(c) G and B

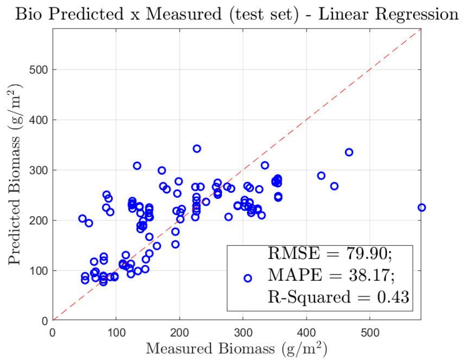

(d) R, G and B

Figure 4.3: Best Linear Regression Performance for Combined Inputs between R, G and B: (a) R and G, (b) R and B, (c) G and B, and (d) R, G and B

Table 4.6: Results for combined R, G and B using Linear Regression

Input	Best RMSE (g/m^2)	MAPE (%)	R^2
R and G	81.59	45.56	0.41
R and B	91.88	52.23	0.12
G and B	80.69	41.91	0.15
R, G and B	79.90	38.17	0.43

The best combination of R, G and B occurs when the three are used as inputs of the linear regression altogether. Notice that case reaches even higher R-Squared than VARI (0.39). The inputs R and G also show a good RMSE and R-Squared, when compared to the other combinations. This is probably due to the importance of the contrast between the red and the green colors in the image and how it can reflect in the measured biomass. The red color can be inferred as a representation of the straw biomass whereas the green represents the grass and legume, which are the biomass we are trying to estimate in this work. In addition, this is also observed when NGRDI does not present the blue color in its equation (see Tab. 2.4).

4.1.2.2 RGB-based and PH

Table 4.7 shows the analysis of RMSE data in the 30 runs executed for each one of the inputs combined with the plant height. The table shows the average value, standard deviation, lower and upper bounds.

Table 4.7: Analysis of RMSE performance using Linear Regression, for combinations of the RGB channels and VIs with PH.

Input	Avg RMSE (g/m^2)	Std Dev RMSE (g/m^2)	Min RMSE (g/m^2)	Max RMSE (g/m^2)
R and PH	102.26	6.89	89.41	117.06
G and PH	109.01	7.81	93.88	121.98
B and PH	103.13	7.26	89.16	120.91
R, G and PH	89.33	8.35	72.64	103.96
R, B and PH	99.68	11.30	80.43	125.44
G, B and PH	92.32	4.68	83.47	104.75
R, G, B and PH	85.25	7.34	68.96	96.82
RGBVI and PH	94.36	8.52	78.71	117.52
GLI and PH	93.00	5.82	79.89	102.37
VARI and PH	89.75	6.69	72.00	99.83
NGRDI and PH	91.69	7.44	71.34	104.74
ExG and PH	92.83	6.99	76.41	105.42
ExGR and PH	92.38	7.29	76.70	105.83

Figure 4.4 shows the plots of the predicted biomass as a function of the measured biomass, considering as inputs combinations of the RGB channels and VIs with the plant height (PH) feature. The curves plot in Fig. 4.4 represent the best RMSE obtained for each input combination, among the 30 runs performed for each of them. Table 4.8 shows the comparative results of the performance metrics for each case.

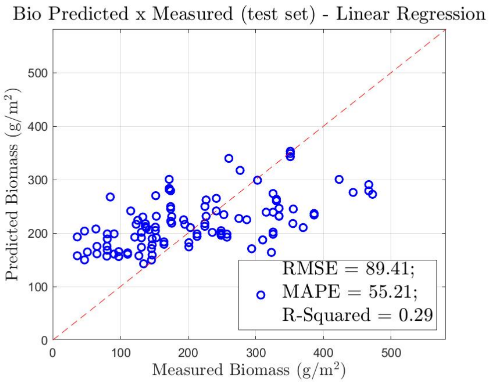

(a) Red and PH

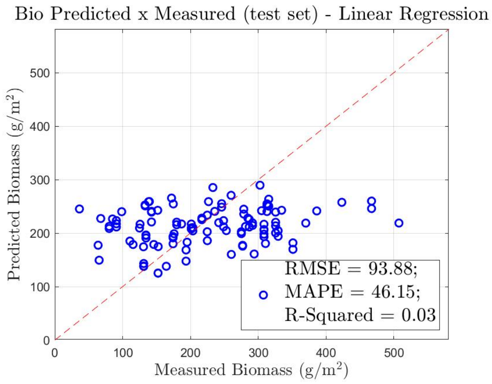

(b) Green and PH

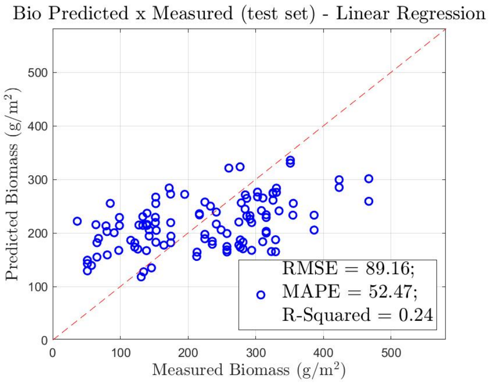

(c) Blue and PH

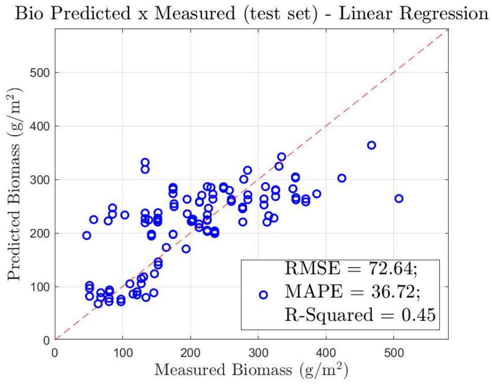

(d) R, G and PH

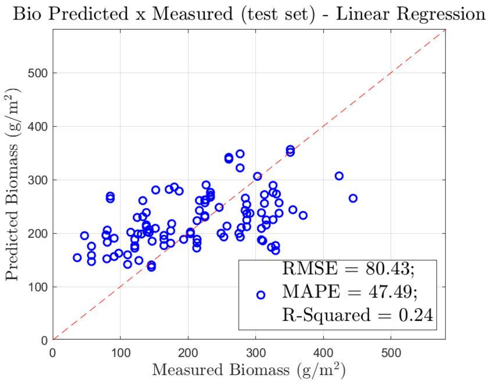

(e) R, B and PH

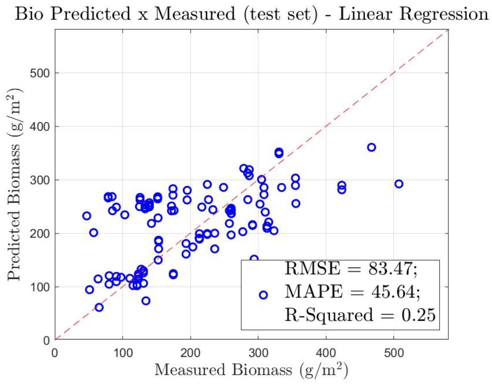

(f) G, B and PH

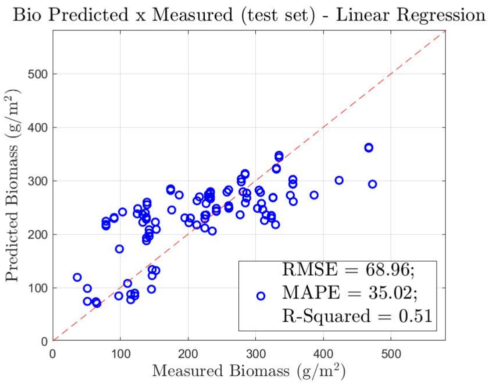

(g) R, G, B and PH

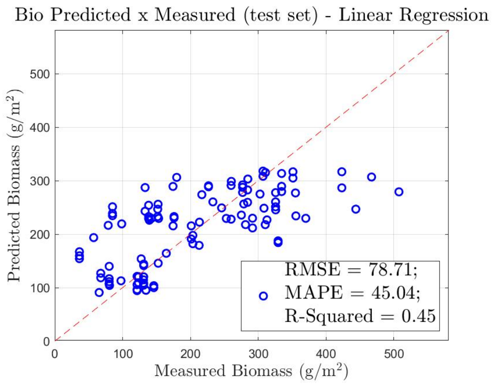

(h) RGBVI and PH

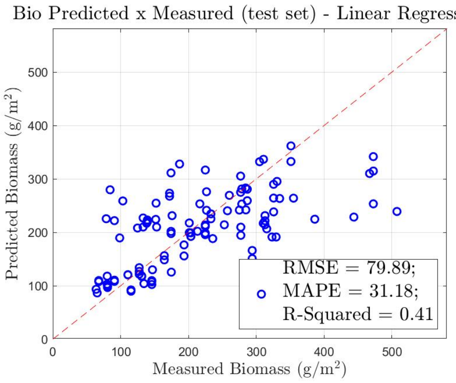

(i) GLI and PH

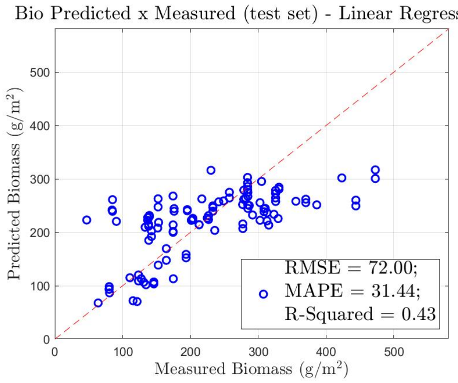

(j) VARI and PH

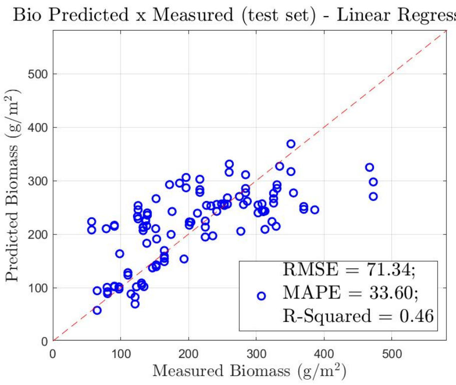

(k) NGRDI and PH

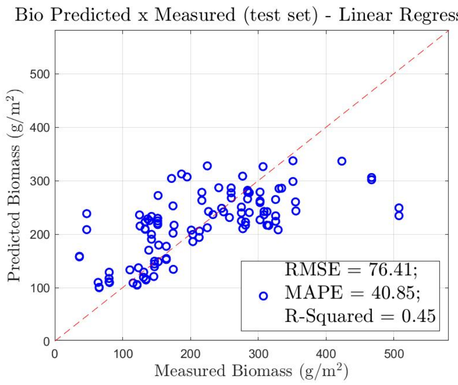

(l) ExG and PH

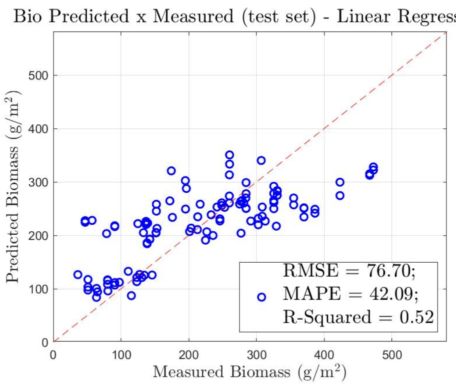

(m) ExGR and PH

Figure 4.4: Best Linear Regression Performance using as inputs combinations of the RGB channels and VIs with the plant height (PH): (a) R and PH, (b) G and PH, (c) B and PH, (d) R, G and PH, (e) R, B and PH, (f) G, B and PH, (g) R, G, B and PH, (h) RGBVI and PH, (i) GLI and PH, (j) VARI and PH, (k) NGRDI and PH, (l) ExG and PH, and (m) ExGR and PH.

Table 4.8: Results of different performance metrics for the developed Linear Regression models, using as inputs combinations of the RGB channels and VIs with the plant height (PH).

Input	Best RMSE (g/m^2)	MAPE (%)	R^2
R and PH	89.41	55.21	0.29
G and PH	93.88	46.15	0.03
B and PH	89.16	52.47	0.24
R, G and PH	72.64	36.72	0.45
R, B and PH	80.43	47.49	0.24
G, B and PH	83.47	45.64	0.25
R, G, B and PH	68.96	35.02	0.51
RGBVI and PH	78.71	45.04	0.45
GLI and PH	79.89	31.18	0.41
VARI and PH	72.00	31.44	0.43
NGRDI and PH	71.34	33.60	0.46
ExG and PH	76.41	40.85	0.45
ExGR and PH	76.70	42.09	0.52

It is possible to observe in Tab. 4.8 that the RMSE achieved by combining PH with the R, G and B channels alone, or even combinations between two of these channels, is higher than the one achieved by combining the VIs with PH. However, the best RMSE value was achieved by using all RGB channels as inputs together with PH. On the other hand, the best R-Squared metric was obtained using ExGR and PH as inputs. Nevertheless, notice that it is only slightly higher than the one found with R, G and B and plant height, both being over 0.5.

Moreover, the linear regression with GLI and PH as inputs presents the lower MAPE of all. It is important to note that R, G and B together, NGRDI and VARI have been presenting the best results until now (lower RMSEs). When simulated along with PH, they reach better performance, but it is still not satisfactory to estimate biomass accurately.

4.1.2.3
RGB-based and DF

The next tests were done combining RGB channels and VIs with the altitude of the drone flight. First, the RMSE analysis is shown in Tab. 4.9. The plots of the best results among the 30 runs performed for each inputs combination can be seen on Fig. 4.5 and the comparative results of the performance metrics for each case are shown in Tab. 4.10.

Table 4.9: Analysis of RMSE performance using Linear Regression, for combinations of the RGB channels and VIs with DF.

Input	Avg RMSE (g/m^2)	Std Dev RMSE (g/m^2)	Min RMSE (g/m^2)	Max RMSE (g/m^2)
R and DF	101.78	9.00	75.88	117.35
G and DF	111.96	5.43	98.03	122.80
B and DF	103.48	6.67	88.47	118.19
R, G and DF	92.17	7.22	77.32	106.62
R, B and DF	101.01	6.30	89.98	115.45
G, B and DF	97.19	5.18	88.28	109.22
R, G, B and DF	90.49	6.09	80.58	100.49
RGBVI and DF	97.51	6.60	85.96	112.38
GLI and DF	95.83	7.66	80.14	113.00
VARI and DF	90.62	7.45	72.89	106.09
NGRDI and DF	93.77	8.29	81.22	113.48
ExG and DF	94.70	7.92	79.47	111.86
ExGR and DF	97.76	7.37	83.60	108.49

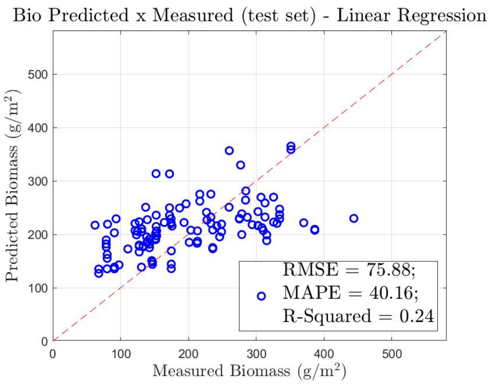

(a) Red and DF

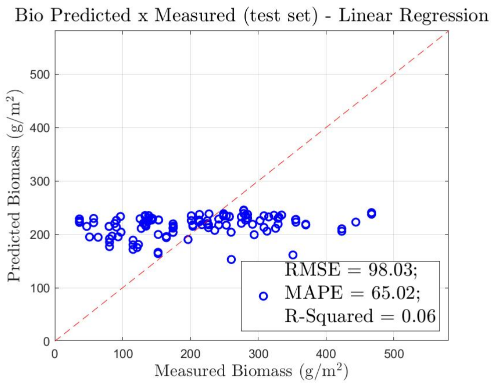

(b) Green and DF

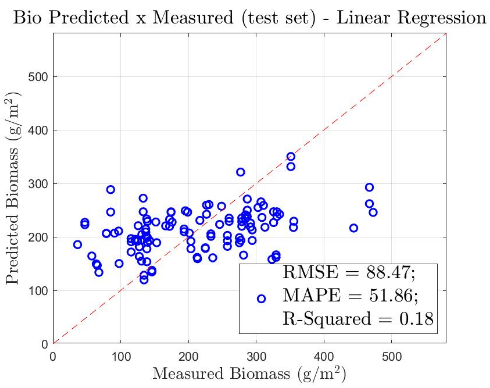

(c) Blue and DF

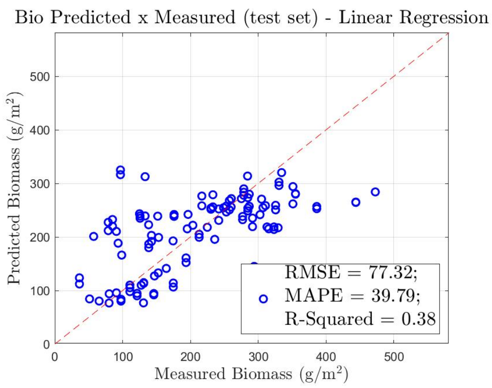

(d) R, G and DF

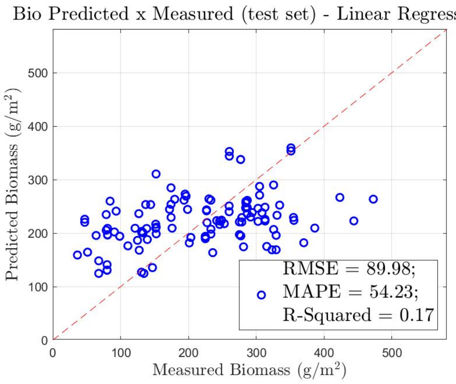

(e) R, B and DF

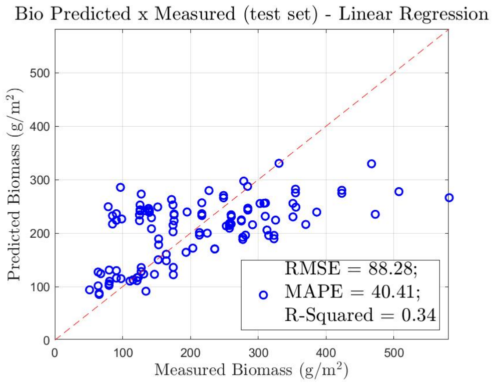

(f) G, B and DF

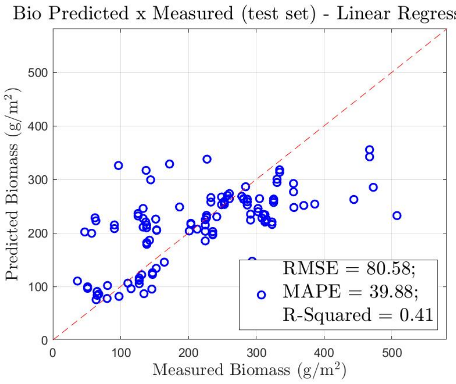

(g) R, G, B and DF

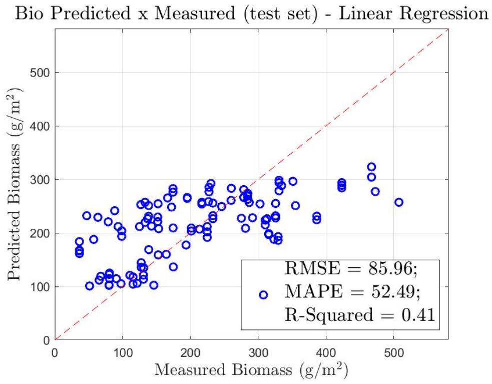

(h) RGBVI and DF

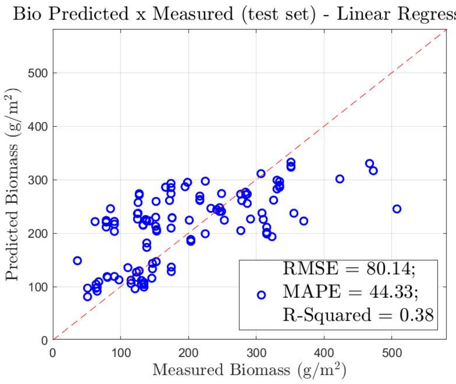

(i) GLI and DF

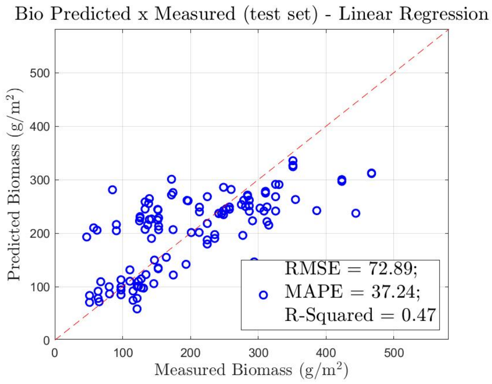

(j) VARI and DF

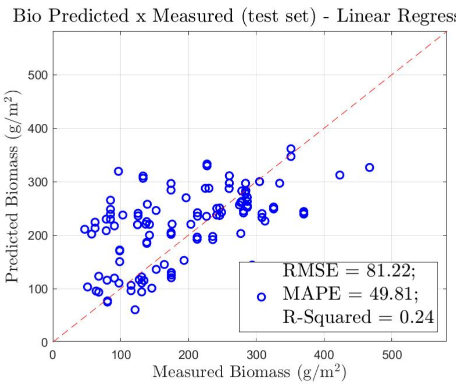

(k) NGRDI and DF

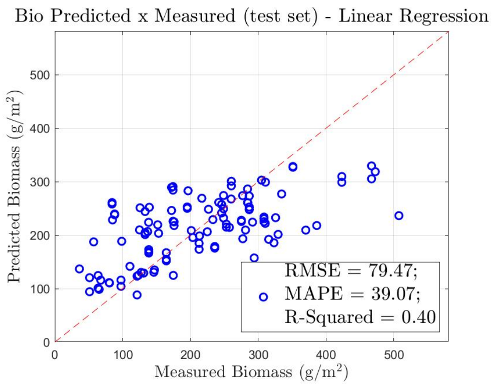

(l) ExG and DF

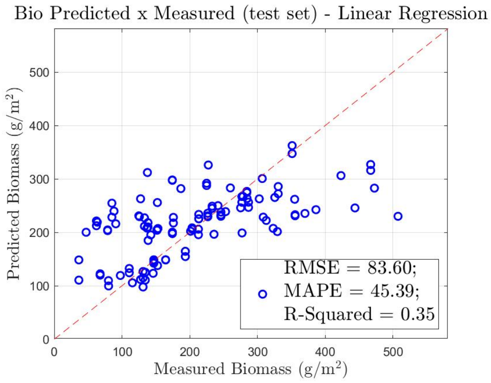

(m) ExGR and DF

Figure 4.5: Best Linear Regression Performance using as inputs combinations of the RGB channels and VIs with the altitude of the drone flight (DF): (a) R and DF, (b) G and DF, (c) B and DF, (d) R, G and DF, (e) R, B and DF, (f) G, B and DF, (g) R, G, B and DF, (h) RGBVI and DF, (i) GLI and DF, (j) VARI and DF, (k) NGRDI and DF, (l) ExG and DF, and (m) ExGR and DF.

Table 4.10: Results of different performance metrics for the developed Linear Regression models, using as inputs combinations of the RGB channels and VIs with the altitude of the drone flight (DF).

Input	Best RMSE (g/m^2)	MAPE (%)	R^2
R and DF	75.88	40.16	0.24
G and DF	98.03	65.02	0.06
B and DF	88.47	51.86	0.18
R, G and DF	77.32	39.79	0.38
R, B and DF	89.98	54.23	0.17
G, B and DF	88.28	40.41	0.34
R, G, B and DF	80.58	39.88	0.41
RGBVI and DF	85.96	52.49	0.41
GLI and DF	80.14	44.33	0.38
VARI and DF	72.89	37.24	0.47
NGRDI and DF	81.22	49.81	0.24
ExG and DF	79.47	39.07	0.40
ExGR and DF	83.60	45.39	0.35

In this test, the best results in terms of RMSE, MAPE and R-Squared were obtained using VARI and DF as inputs. However, comparing these results with the previous ones, that evaluated combinations of the RGB channels and VIs with the PH, it is noticeable that the PH contributes more significantly to the enhancement of the performance metrics than the DF. Notice that the performance of all inputs combinations presented in Tab. 4.10 are worst than the ones shown in Tab. 4.8.

4.1.2.4
RGB-based and GI

The next tests were done combining the RGB channels and the VIs with intensity of green on the histogram (GI). The RMSE analysis is shown in Tab. 4.11.

Table 4.11: Analysis of RMSE performance using Linear Regression, for combinations of the RGB channels and VIs with GI.

Input	Avg RMSE (g/m^2)	Std Dev RMSE (g/m^2)	Min RMSE (g/m^2)	Max RMSE (g/m^2)
R and GI	101.05	8.51	81.23	118.64
G and GI	108.16	5.47	97.90	118.99
B and GI	102.31	6.96	88.09	115.56
R, G and GI	90.46	7.22	72.73	104.17
R, B and GI	101.56	7.44	84.73	116.31
G, B and GI	98.86	6.23	85.08	112.31
R, G, B and GI	92.29	7.14	79.00	106.40
RGBVI and GI	95.65	7.03	82.75	109.29
GLI and GI	95.30	7.34	79.06	109.27
VARI and GI	92.83	10.07	75.97	117.63
NGRDI and GI	93.61	8.29	77.59	110.55
ExG and GI	96.48	7.16	82.15	113.06
ExGR and GI	91.92	9.54	71.01	111.66

The plots of the best results among the 30 runs performed for each input combination can be seen on Fig. 4.6 and the comparative results of the performance metrics for each case are shown in Tab. 4.12.

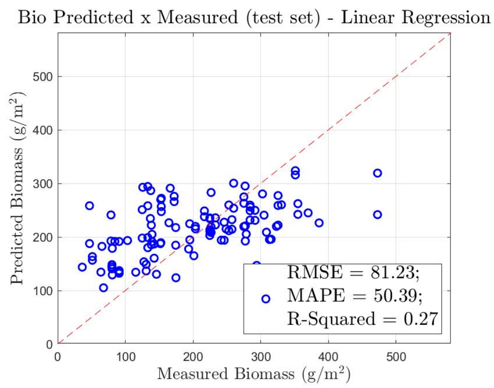

(a) Red and GI

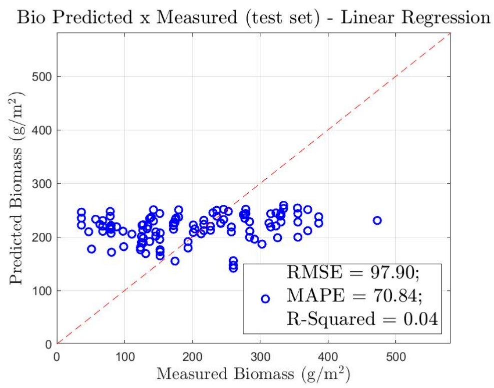

(b) Green and GI

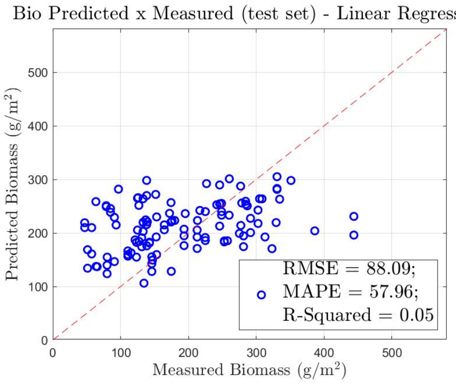

(c) Blue and GI

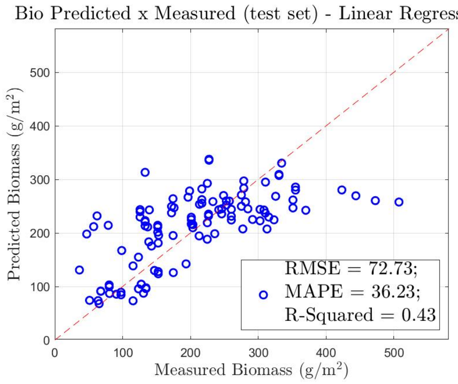

(d) R, G and GI

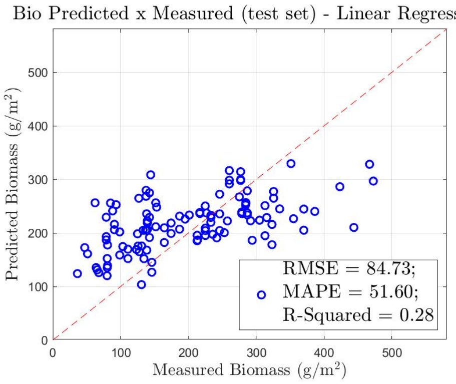

(e) R, B and GI

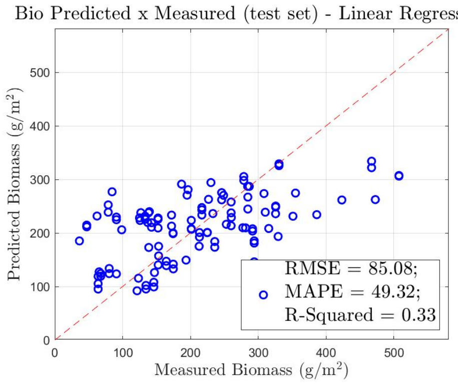

(f) G, B and GI

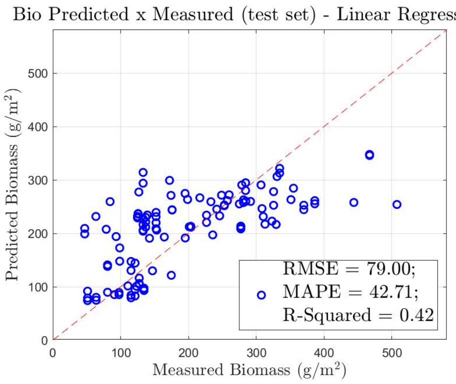

(g) R, G, B and GI

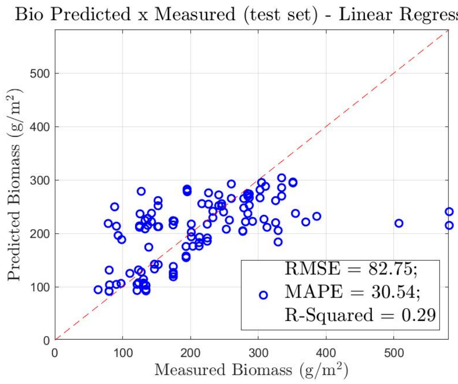

(h) RGBVI and GI

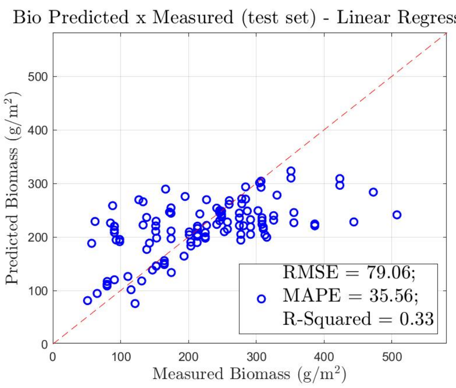

(i) GLI and GI

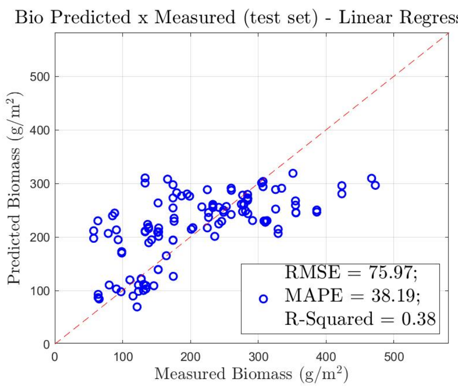

(j) VARI and GI

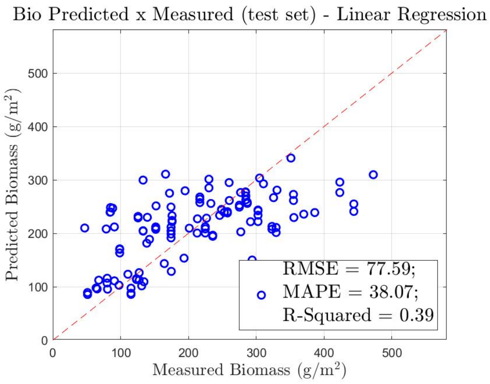

(k) NGRDI and GI

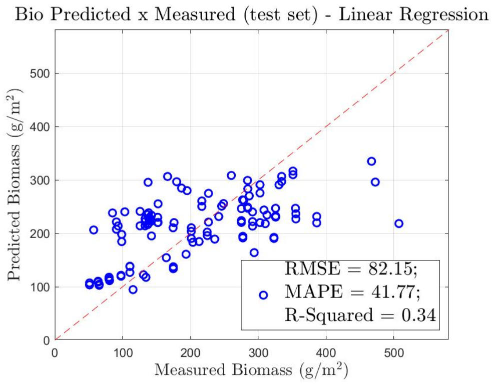

(l) ExG and GI

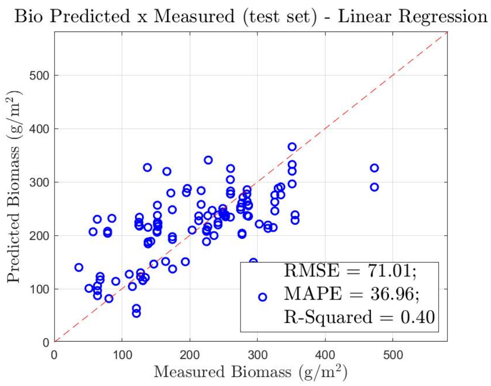

(m) ExGR and GI

Figure 4.6: Best Linear Regression Performance using as inputs combinations of the RGB channels and VIs with the green intensity (GI): (a) R and GI, (b) G and GI, (c) B and GI, (d) R, G and GI, (e) R, B and GI, (f) G, B and GI, (g) R, G, B and GI, (h) RGBVI and GI, (i) GLI and GI, (j) VARI and GI, (k) NGRDI and GI, (l) ExG and GI, and (m) ExGR and GI.

The obtained results show different combination of inputs leading to the best performances, depending on the considered performance metrics. The combination of the GI with ExGR showed the best RMSE, with RGBVI the best MAPE and with R and G the best R-Squared. In this test, the best input combinations are more diverse than the ones found before. Moreover, it is noticeable that they do not reach RMSE values as low as the ones found with the inputs combined with the plant height. Surprisingly, the best MAPE obtained here is better than all others, obtained in the previous tests. However, it is important to highlight that our algorithm search for the coefficients that minimize the RMSE, so that it does not ensure the minimization of MAPE or maximization of R-Squared. Probably, the randomly chosen test set that computed the performance metrics of model with RGBVI and GI as inputs have higher biomass values than the one used for the model with ExGR and GI as inputs, for example. Hence, this could have contributed to the lower

Table 4.12: Results of different performance metrics for the developed Linear Regression models, using as inputs combinations of the RGB channels and VIs with the green intensity (GI).

Input	Best RMSE (g/m^2)	MAPE (%)	R^2
R and GI	81.23	50.39	0.27
G and GI	97.90	70.84	0.04
B and GI	88.09	57.96	0.05
R, G and GI	72.73	36.23	0.43
R, B and GI	84.73	51.60	0.28
G, B and GI	85.08	49.32	0.33
R, G, B and GI	79.00	42.71	0.42
RGBVI and GI	82.75	30.54	0.29
GLI and GI	79.06	35.56	0.33
VARI and GI	75.97	38.19	0.38
NGRDI and GI	77.59	38.07	0.39
ExG and GI	82.15	41.77	0.34
ExGR and GI	71.01	36.96	0.40

MAPE values obtained with the RGBVI and GI inputs in spite of the lower RMSE of the model implemented with ExGR and GI as inputs.

4.1.2.5
RGB-based and SR

The next tests were done combining the RGB channels and the VIs with solar radiation (SR). The analysis of RMSE is shown in Tab. 4.13. The plots of the best results among the 30 runs performed for each inputs combination can be seen on Fig. 4.7 and the comparative results of the performance metrics for each case are shown in Tab. 4.14.

Table 4.13: Analysis of RMSE performance using Linear Regression, for combinations of the RGB channels and VIs with SR.

Input	Avg RMSE (g/m^2)	Std Dev RMSE (g/m^2)	Min RMSE (g/m^2)	Max RMSE (g/m^2)
R and SR	102.34	5.66	89.45	114.05
G and SR	110.84	7.30	97.82	130.29
B and SR	97.98	5.85	87.37	110.40
R, G and SR	88.57	7.65	72.47	100.41
R, B and SR	98.63	6.14	85.01	109.00
G, B and SR	91.87	5.75	78.27	101.65
R, G, B and SR	85.27	6.09	74.58	100.31
RGBVI and SR	90.75	5.38	79.06	101.26
GLI and SR	85.10	6.82	70.75	96.24
VARI and SR	86.27	7.06	73.95	99.74
NGRDI and SR	87.40	8.33	71.25	100.33
ExG and SR	89.71	5.54	77.58	99.22
ExGR and SR	88.87	6.39	76.42	106.31

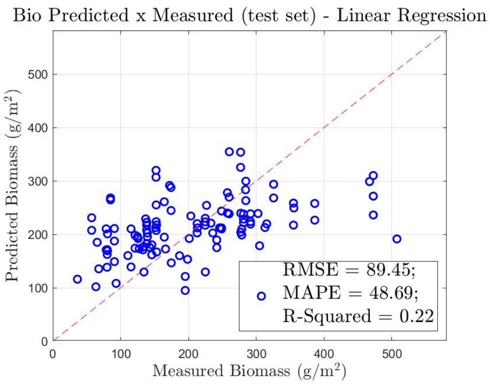

(a) Red and SR

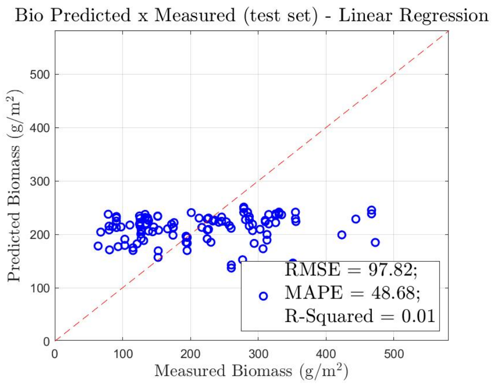

(b) Green and SR

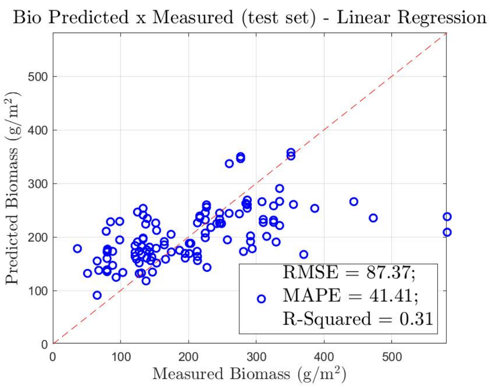

(c) Blue and SR

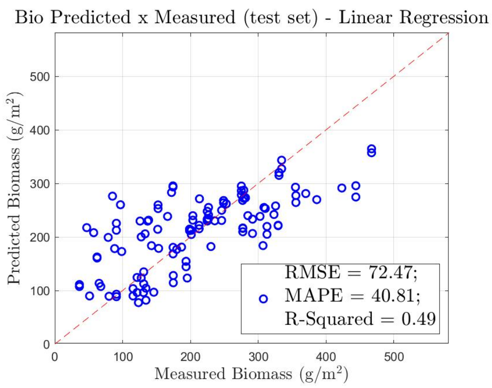

(d) R, G and SR

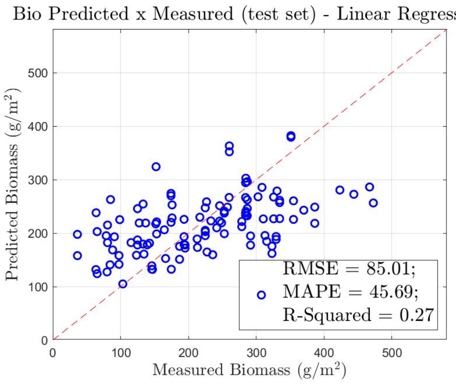

(e) R, B and SR

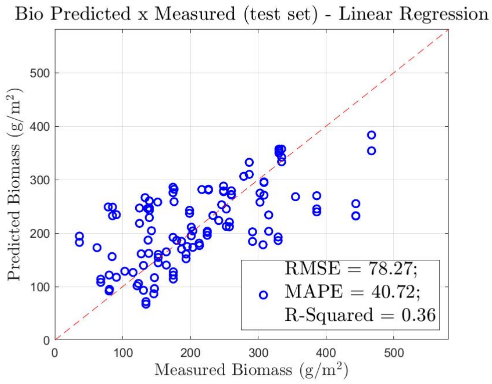

(f) G, B and SR

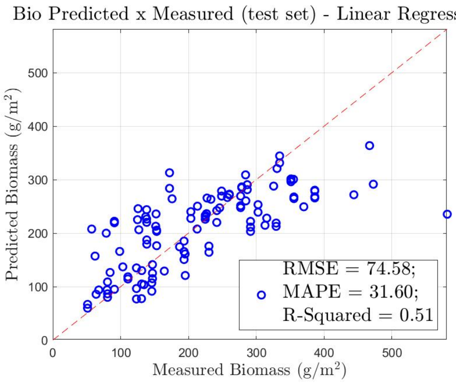

(g) R, G, B and SR

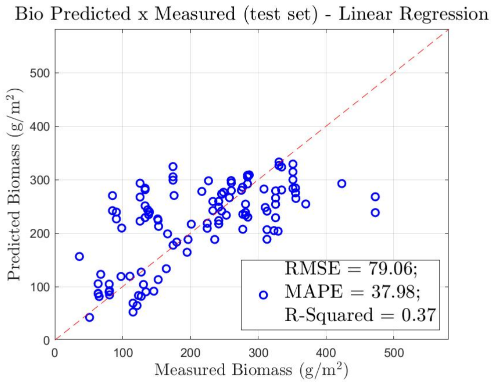

(h) RGBVI and SR

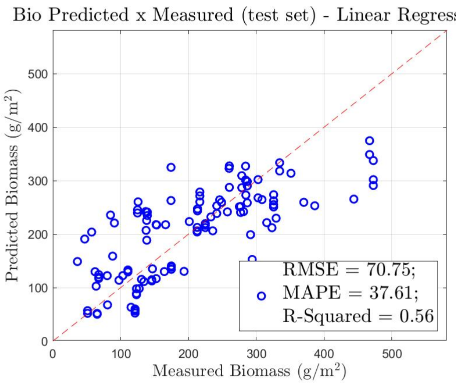

(i) GLI and SR

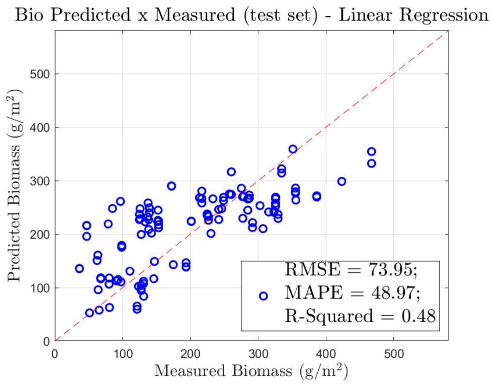

(j) VARI and SR

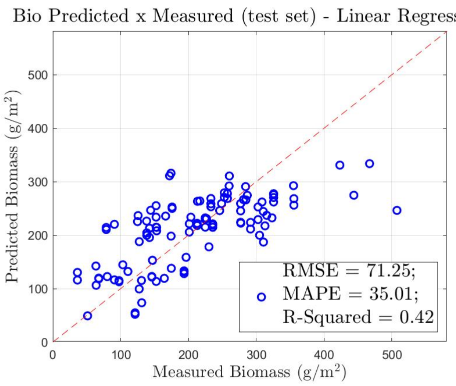

(k) NGRDI and SR

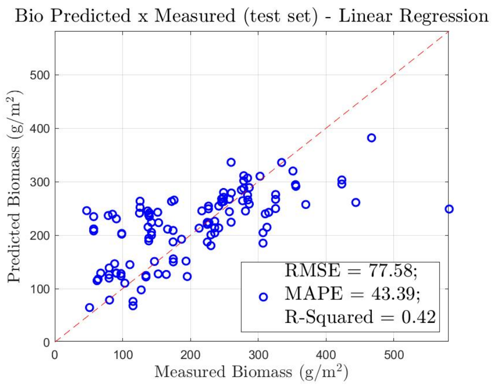

(l) ExG and SR

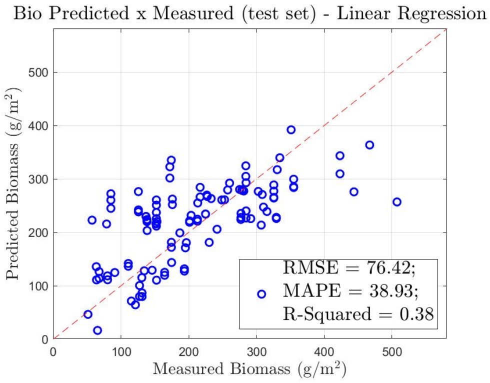

(m) ExGR and SR

Figure 4.7: Best Linear Regression Performance using as inputs combinations of the RGB channels and VIs with the solar radiation (SR): (a) R and SR, (b) G and SR, (c) B and SR, (d) R, G and SR, (e) R, B and SR, (f) G, B and SR, (g) R, G, B and SR, (h) RGBVI and SR, (i) GLI and SR, (j) VARI and SR, (k) NGRDI and SR, (l) ExG and SR, and (m) ExGR and SR.

Table 4.14: Results of different performance metrics for the developed Linear Regression models, using as inputs combinations of the RGB channels and VIs with the solar radiation (SR).

Input	Best RMSE (g/m^2)	MAPE (%)	R^2
R and SR	89.45	48.69	0.22
G and SR	97.82	48.68	0.01
B and SR	87.37	41.41	0.31
R, G and SR	72.47	40.81	0.49
R, B and SR	85.01	45.69	0.27
G, B and SR	78.27	40.72	0.36
R, G, B and SR	74.58	31.60	0.51
RGBVI and SR	79.06	37.98	0.37
GLI and SR	70.75	37.61	0.56
VARI and SR	73.95	48.97	0.48
NGRDI and SR	71.25	35.01	0.42
ExG and SR	77.58	43.39	0.42
ExGR and SR	76.42	38.93	0.38

Among the analyzed combinations of the SR with RGB channels and VIs, the best RMSE and R-Squared were achieved using SR and GLI as inputs of the linear regression model. Furthermore, it is noteworthy that this input configuration leads to the highest R-Squared among all cases previously evaluated in this subsection. On the other hand, the minimum MAPE was obtained using R, G, B and SR as inputs. In addition, the results obtained for all the VIs and also for the R, G and B channels together showed, in general, smaller errors and higher R-Squared than the other input's configurations previously evaluated. This is an important factor to observe in future tests, as solar radiation is a promising feature to improve results when combined with RGB-based inputs.

4.1.3
Comparative Results

Gathering the three best results obtained for each one of the tested input's combinations, except for the combination of the channels that had only one result collected, we built Tab. 4.15. The cases considered as best results are those with the lowest RMSEs in each one of the tables presented in this section, which are: (i) Separate Inputs for the RGB-based; (ii) Separate Inputs for the features; (iii) Combination of channels; (iv) Combined Inputs between VIs and channels with PH; (v) Combined Inputs between VIs and channels with DF; (vi) Combined Inputs between VIs and channels with GI; and (vii) Combined Inputs between VIs and channels with SR. The marked results on the table show the three best RMSE values in blue and the best associated MAPE and R-Squared in red.

Table 4.15: Best results for Linear Regression.

Input	Best RMSE (g/m^2)	MAPE (%)	R^2
VARI	78.41	47.02	0.39
NGRDI	79.74	49.18	0.38
ExGR	79.96	44.67	0.37
DF	96.08	53.07	-0.01
R, G and B	79.90	38.17	0.43
R, G, B and PH	68.96	35.02	0.51
VARI and PH	72.00	31.44	0.43
NGRDI and PH	71.34	33.60	0.46
R and DF	75.88	40.16	0.24
R, G and DF	77.32	39.79	0.38
VARI and DF	72.89	37.24	0.47
R, G and GI	72.73	36.23	0.43
VARI and GI	75.97	38.19	0.38
ExGR and GI	71.01	36.96	0.40
R, G and SR	72.47	40.81	0.49
GLI and SR	70.75	37.61	0.56
NGRDI and SR	71.25	35.01	0.42

The obtained results indicate that, among the RGB channels combinations and the VIs, the best performances were achieved with R, G and B together, VARI, NGRDI and ExGR. When comparing with other features combined with the RGB channels and VIs, the ones that contributes the most to performance enhancements are plant height and solar radiation. Indeed, they reach the best results in this section.

It is possible to assume by now that these inputs are more capable of delivering better results than others. This will be further stressed in the next sections, that deal with the development of the Nonlinear Regression and the Neural Network Regression. In MLP, the second-hand inputs (PH, DF, GI and SR) will be tested with more combinations, as these features can contribute to the network accuracy.

Finally, note that the results achieved by the linear regression are not satisfactory regarding the metrics of evaluation. The best RMSE (68.96 $\mathsf{g/m^2}$) and the best R^2 (0.56) doesn't guarantee a good relationship between the input and output, so this regression can not be considered as a reliable method to estimate biomass on a pasture for this work.

4.2 Nonlinear Regression

This section presents the best fitting plots and performance metrics achieved by the MNLR regression models, after running the algorithm 30 times for each tested configuration. First, the inputs were analyzed separately to evaluate the influence of each one of them in the output, and then, they were combined aiming at boosting the performance metrics, similarly to what was done for the Linear Regression. As a comparison analysis, a table depicting the average, standard deviation, lower and upper bounds of RMSE is presented for each input or input combination analyzed. The corresponding MAPE and R-Squared associated to the minimum RMSE achieved for each analyzed input configuration are shown in a second table. Graphs with the target (measured biomass) in the horizontal axis and the achieved output (predicted biomass) in the vertical axis are also presented for the case that lead to the minimum RMSE, among the 30 runs performed for each input configuration.

4.2.1 Separate inputs

This subsection presents the analysis of the nonlinear regression models tested with separate inputs, firstly with the RGB-based ones and then with features. As the inputs in this subsection were computed separately, the equation used to perform the MNLR regression is Eq. (3-3).

4.2.1.1 RGB-based

Figure 4.8 shows the fitting plot of the measured biomass by the predicted biomass, associated to the best RMSE achieved for each input configuration. Moreover, Tab. 4.16 shows the RMSE analysis and Tab. 4.17 the respective performance metrics.

Table 4.16: Analysis of RMSE performance for the RGB-based as separate inputs using Nonlinear Regression.

Input	Avg RMSE (g/m^2)	Std Dev RMSE (g/m^2)	Min RMSE (g/m^2)	Max RMSE (g/m^2)
R	105.40	9.08	85.20	125.11
G	107.31	6.59	93.78	120.28
B	105.74	7.41	89.31	123.63
RGBVI	97.39	6.89	82.11	108.78
GLI	93.97	6.51	81.94	107.36
VARI	92.42	7.99	79.77	109.57
NGRDI	94.10	6.51	80.81	109.72
ExG	95.92	7.32	83.36	108.77
ExGR	94.18	6.99	79.68	105.60

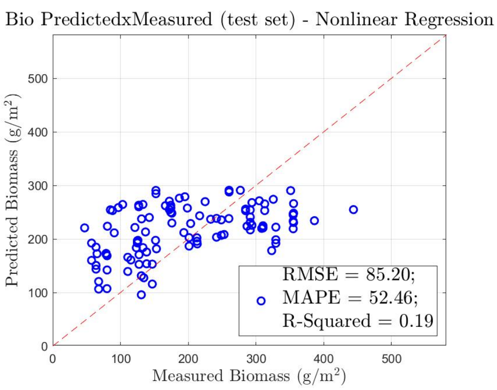

(a) Red

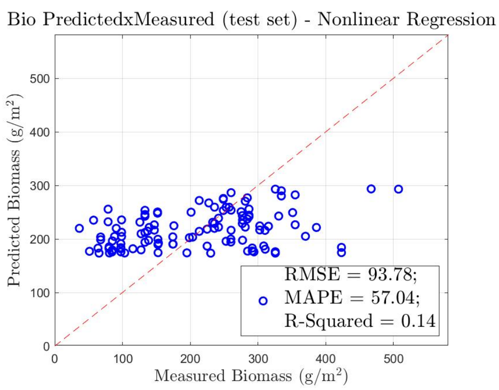

(b) Green

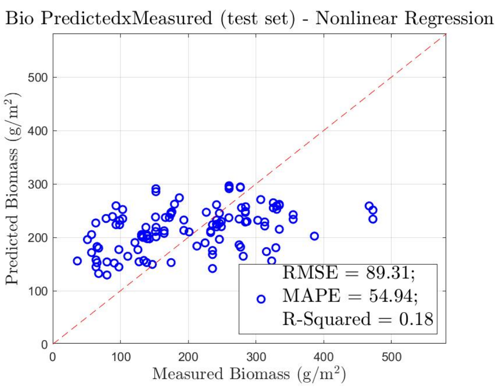

(c) Blue

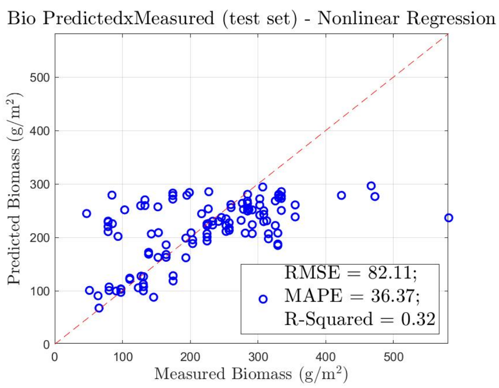

(d) RGBVI

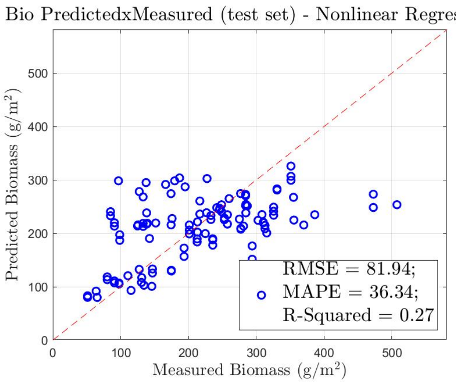

(e) GLI

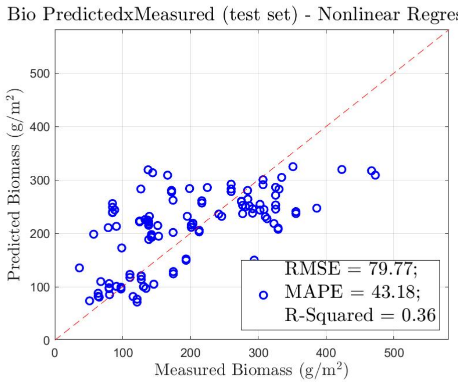

(f) VARI

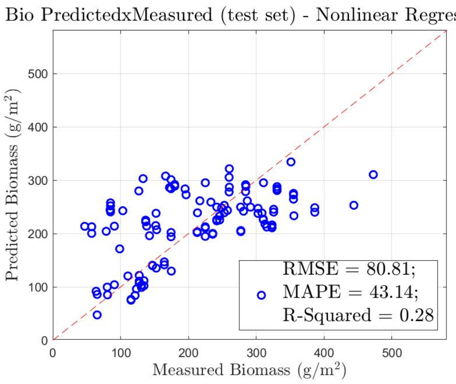

(g) NGRDI

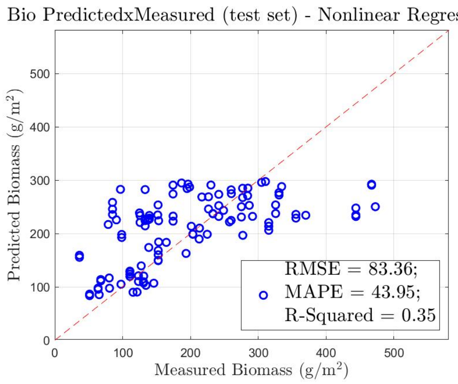

(h) ExG

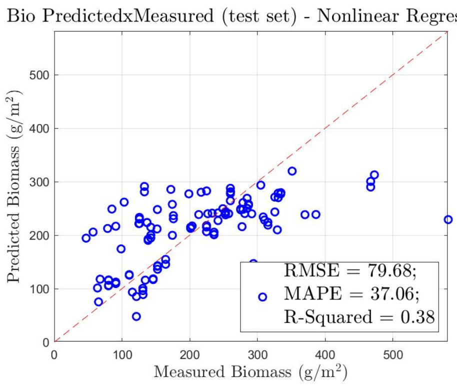

(i) ExGR

Figure 4.8: Best Nonlinear Regression Performance for the RGB-based as Separate Inputs: (a) Red, (b) Green, (c) Blue, (d) RGBVI, (e) GLI, (f) VARI, (g) NGRDI, (h) ExG, (i) ExGR, (j) PH, (k) DF, (l) GI and (m) SR

Table 4.17: Results for the RGB-based as separate inputs using Nonlinear Regression.

Input	Best RMSE (g/m^2)	MAPE (%)	R^2
R	85.20	52.46	0.19
G	93.78	57.04	0.14
B	89.31	54.94	0.18
RGBVI	82.11	36.37	0.32
GLI	81.94	36.34	0.27
VARI	79.77	43.18	0.36
NGRDI	80.81	43.14	0.28
ExG	83.36	43.95	0.35
ExGR	79.68	37.06	0.38

Notice that, by observing Tab. 4.17, with the nonlinear regression, the best result considering the lower RMSE is found using VARI as an input. The same evaluation was done in the Linear Regression when tested the RGB-based inputs separately. GLI and ExGR show the best MAPE and R-Squared, respectively. However, none of them reach acceptable performance metrics alone, as the higher R-Squared, found with ExGR input, is only 0.38 and the best linear regression reached a R-Squared of 0.56.

4.2.1.2
Features

Figure 4.9 shows the fitting plot of the measured biomass by the predicted biomass, associated to the best RMSE achieved for each input configuration. Moreover, Tab. 4.18 shows the RMSE analysis and Tab. 4.19 the respective performance metrics.

Table 4.18: Analysis of RMSE performance for the features as separate inputs, using Nonlinear Regression.

Input	Avg RMSE (g/m^2)	Std Dev RMSE (g/m^2)	Min RMSE (g/m^2)	Max RMSE (g/m^2)
PH	110.61	6.13	101.26	126.28
DF	113.47	8.12	99.16	134.41
GI	112.10	6.05	96.47	122.78
SR	111.76	5.71	99.23	120.66

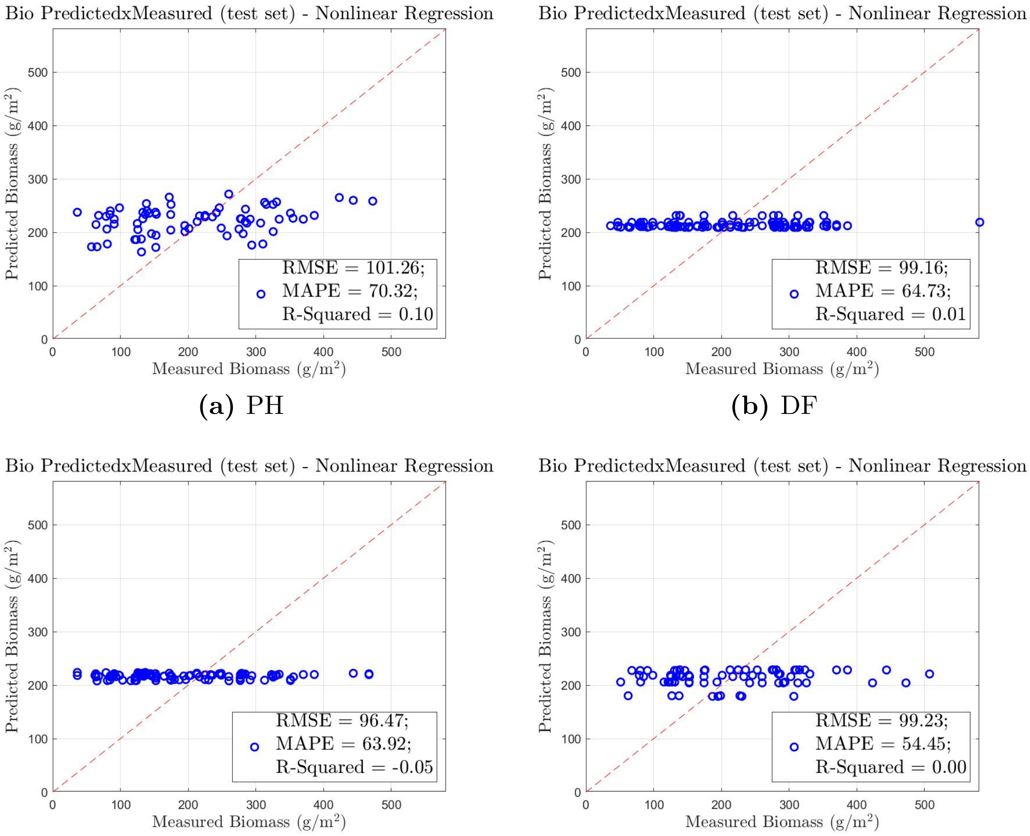

(a) PH **(b)** DF **(c)** GI **(d)** SR

Figure 4.9: Best Nonlinear Regression Performance for the features as Separate Inputs: (a) PH, (b) DF, (c) GI and (d) SR

Table 4.19: Results for the features as separate inputs, using Nonlinear Regression.

Input	Best RMSE (g/m^2)	MAPE (%)	R^2
PH	101.26	70.32	0.10
DF	99.16	64.73	0.01
GI	96.47	63.92	-0.05
SR	99.23	54.45	0.00

For the nonlinear regression's results with the features as unique inputs, we can observe that they do not correlate well with the output, even after increasing the degree of the equation, when comparing with linear regression. They will be further analyzed in MLP Regression as it can generalize sufficiently for these inputs.

4.2.2
Combined inputs

As done in the development process of the linear regression model, combinations of the R, G and B channels as inputs will be tested to investigate if they reach better metrics. Moreover, in this subsection, different combinations of the inputs based on RGB and features were made in order to analyze the response of the nonlinear regression model, when increasing the number of coefficients and independent variables in the equation.

4.2.2.1
Combinations of R, G and B

Once again, it is noticeable that R (red), G (green) and B (blue) don't correlate so well with the outputs, when tested separately. Hereafter, they will be combined among themselves and tested to observe these associations from now on. The RMSE analysis is shown in Tab. 4.20. The metric results are shown in Tab. 4.21 and in Fig. 4.10.

Table 4.20: Analysis of RMSE performance for different combinations of the RGB channels, using Nonlinear Regression.

Input	Avg RMSE (g/m^2)	Std Dev RMSE (g/m^2)	Min RMSE (g/m^2)	Max RMSE (g/m^2)
R, G	90.47	5.86	81.47	105.48
R, B	101.70	9.44	81.27	120.82
G, B	94.52	6.56	83.84	112.85
R, G, B	89.26	6.81	79.28	105.99

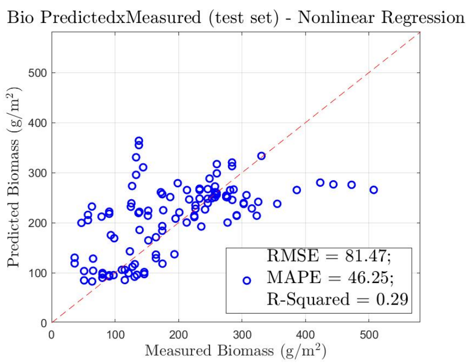

(a) R and G

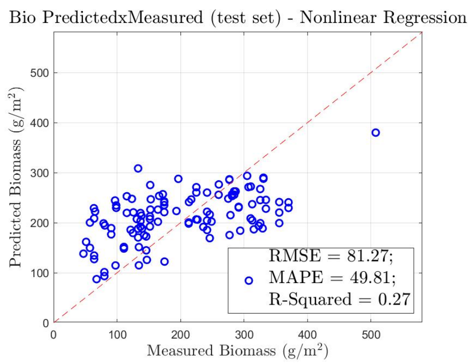

(b) R and B

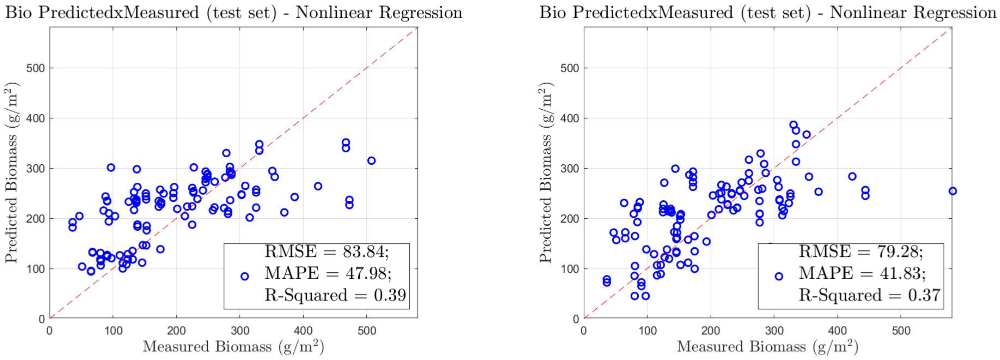

(c) G and B **(d)** R, G and B

Figure 4.10: Best Nonlinear Regression Performance for Combined Inputs between R, G and B: (a) R and G, (b) R and B, (c) G and B, and (d) R, G and B

Table 4.21: Results for combined R, G and B using Nonlinear Regression

Input	Best RMSE (g/m^2)	MAPE (%)	R^2
R and G	81.47	46.25	0.29
R and B	81.27	49.81	0.27
G and B	83.84	47.98	0.39
R, G and B	79.28	41.83	0.37

As observed for the linear regression model, the results of the nonlinear regression also indicate that the RMSE can be reduced by combining the RGB channels. In particular, among the analyzed cases, the best RMSE is achieved by using all RGB channels as inputs of the nonlinear model. On the other hand, comparing this study with the equivalent test performed for the linear model (Tab. 4.20), it can be noticed that the nonlinear model did not considerably improve the performance metrics, since for some of the same input configurations the linear model presented a better performance. Therefore, the dependency of the estimated biomass (output) with the RGB channels (inputs) do not seem to significantly benefits from a more complex nonlinear model. Moreover, nonlinear regression does not achieve R-Squared as high as the linear regression.

The next subsections presents the results of MNLR when using two or more features as inputs, aiming to analyze if the performance metrics can be improved by adding more information to the model's input.

4.2.2.2
RGB-based and PH

Table 4.22 shows the analysis of RMSE data in the 30 runs executed for each one of the inputs combined with the plant height. The table shows the average value, standard deviation, lower and upper bounds.

Table 4.22: Analysis of RMSE performance using Nonlinear Regression, for combinations of the RGB channels and VIs with PH.

Input	Avg RMSE (g/m^2)	Std Dev RMSE (g/m^2)	Min RMSE (g/m^2)	Max RMSE (g/m^2)
R and PH	100.37	7.83	84.30	110.90
G and PH	101.92	7.19	88.48	113.21
B and PH	101.37	8.16	88.83	120.30
R, G and PH	83.04	6.31	67.27	94.55
R, B and PH	94.98	8.29	79.41	108.78
G, B and PH	85.46	6.90	72.74	101.95
R, G, B and PH	81.50	5.68	73.99	95.04
RGBVI and PH	92.53	8.10	71.73	105.11
GLI and PH	93.14	6.60	79.13	107.87
VARI and PH	86.11	6.66	73.93	102.97
NGRDI and PH	88.46	7.51	74.14	101.48
ExG and PH	90.21	8.06	75.87	106.55
ExGR and PH	89.97	7.87	73.75	103.04

Figure 4.11 shows the plots of the predicted biomass as a function of the measured biomass, considering as inputs combinations of the RGB channels and VIs with the plant height (PH) feature. The curves plot in Fig. 4.11 represent the best RMSE obtained for each input combination, among the 30 runs performed for each of them. On the other hand, Tab. 4.23 shows the MAPE and S-Squared associated to the best RMSE obtained for each input combination.

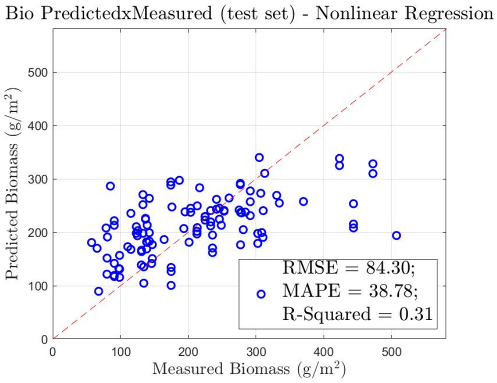

(a) Red and PH

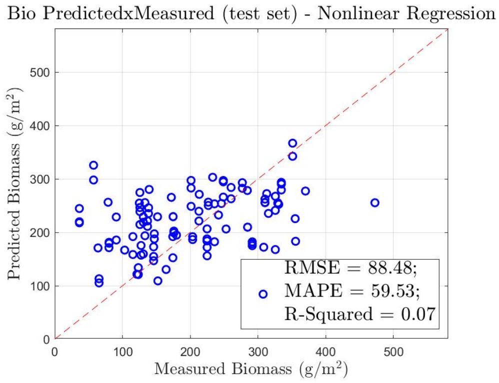

(b) Green and PH

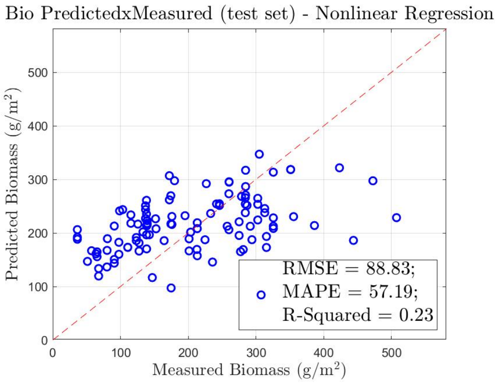

(c) Blue and PH

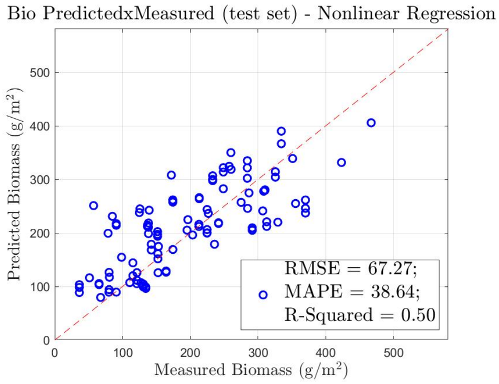

(d) R, G and PH

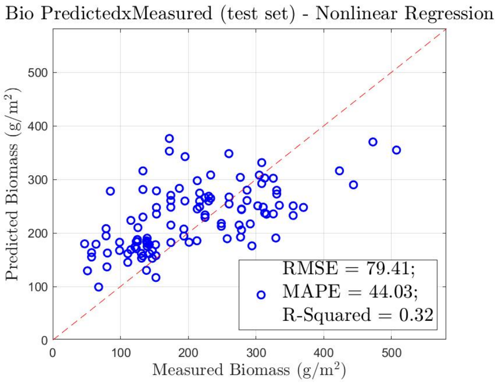

(e) R, B and PH

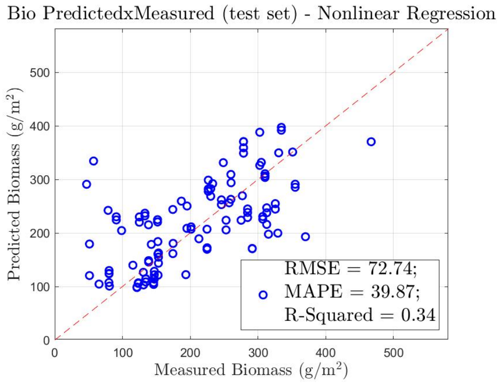

(f) G, B and PH

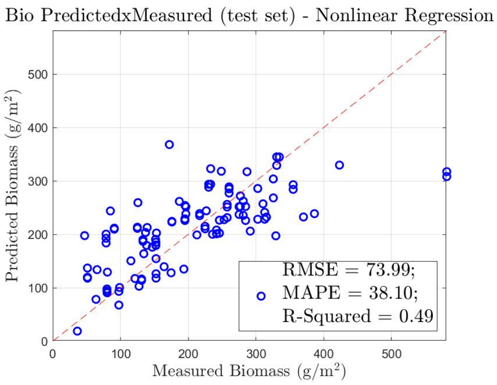

(g) R, G, B and PH

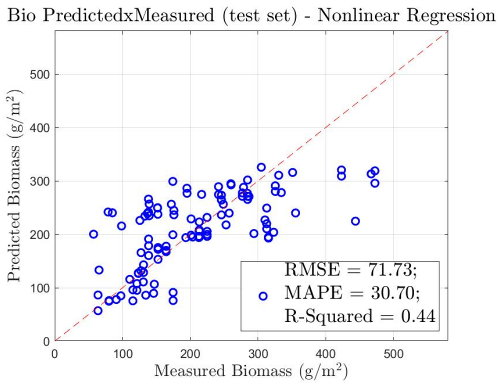

(h) RGBVI and PH

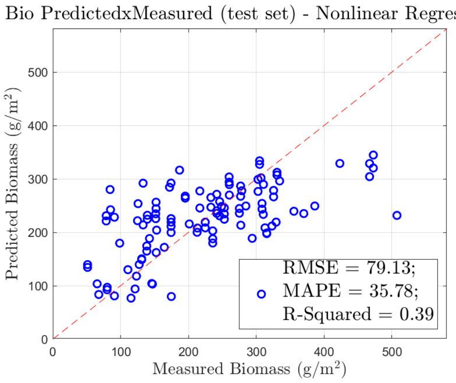

(i) GLI and PH

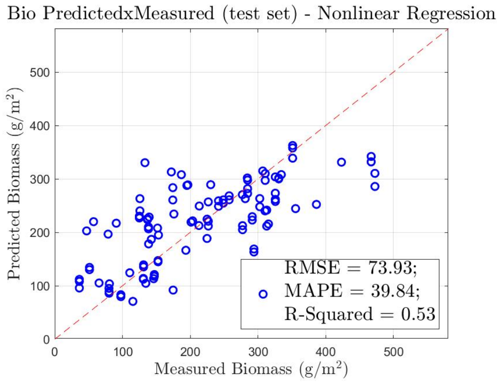

(j) VARI and PH

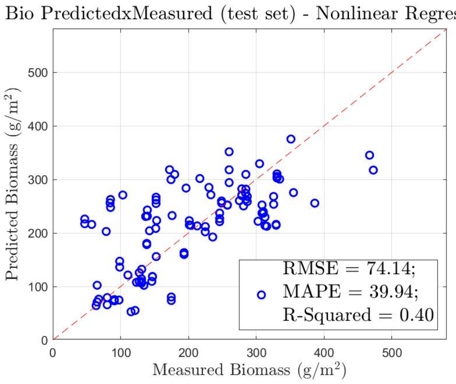

(k) NGRDI and PH

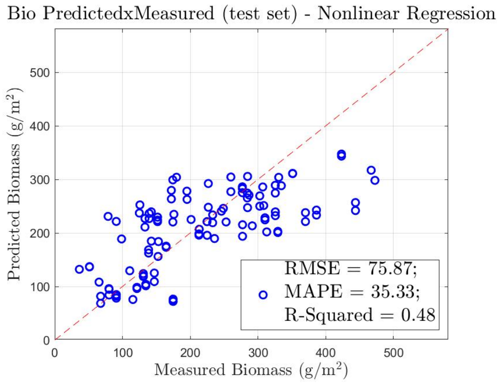

(l) ExG and PH

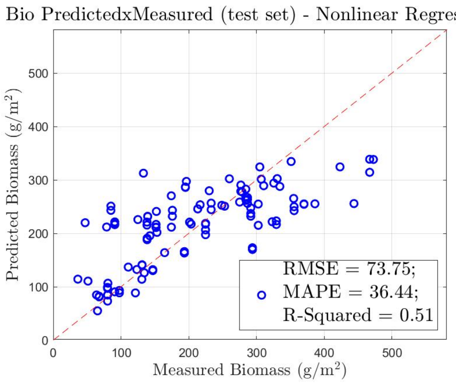

(m) ExGR and PH

Figure 4.11: Best Nonlinear Regression Performance using as inputs combinations of the RGB channels and VIs with the plant height (PH): (a) R and PH, (b) G and PH, (c) B and PH, (d) R, G and PH, (e) R, B and PH, (f) G, B and PH, (g) R, G, B and PH, (h) RGBVI and PH, (i) GLI and PH, (j) VARI and PH, (k) NGRDI and PH, (l) ExG and PH, and (m) ExGR and PH.

Table 4.23: Results of different performance metrics for the developed Nonlinear Regression models, using as inputs combinations of the RGB channels and VIs with the plant height (PH).

Input	Best RMSE (g/m^2)	MAPE (%)	R^2
R and PH	84.30	38.78	0.31
G and PH	88.48	59.53	0.07
B and PH	88.83	57.19	0.23
R, G and PH	67.27	38.64	0.50
R, B and PH	79.41	44.03	0.32
G, B and PH	72.74	39.87	0.34
R, G, B and PH	73.99	38.10	0.49
RGBVI and PH	71.73	30.70	0.44
GLI and PH	79.13	35.78	0.39
VARI and PH	73.93	39.84	0.53
NGRDI and PH	74.14	39.94	0.40
ExG and PH	75.87	35.33	0.48
ExGR and PH	73.75	36.44	0.51

Notice that the performance metrics shown in Tab. 4.23 indicate that the best RMSE result is found using R and G as inputs along with the PH, as highlighted in Fig. 4.11. The hypothesis for this fact was stressed in 4.1.2.1 and it can be applicable for both results. Nonetheless, surprisingly, the third best RMSE result was found for the G and B input along with PH, which contradicts the referred hypothesis. In this case, the analysis with PH indicates that blue color can have an important influence in the result as well. Among the VIs, RGBVI and VARI, which include blue color in their definitions, presented the lowest MAPEs and the highest R-Squared, respectively.

4.2.2.3
RGB-based and DF

The next test was done by combining RGB channels and VIs with the altitude of the drone flight (DF). First, the RMSE analysis is shown in Tab. 4.24. The plots of the best results among the 30 runs performed for each inputs combination can be seen on Fig. 4.12 and the comparative results of the performance metrics for each case are shown in Tab. 4.25.

Table 4.24: Analysis of RMSE performance using Nonlinear Regression, for combinations of the RGB channels and VIs with DF.

Input	Avg RMSE (g/m^2)	Std Dev RMSE (g/m^2)	Min RMSE (g/m^2)	Max RMSE (g/m^2)
R and DF	102.69	8.99	81.73	126.44
G and DF	109.02	7.17	92.59	128.03
B and DF	104.05	7.70	86.89	121.80
R, G and DF	91.01	8.19	77.62	108.91
R, B and DF	99.55	7.39	83.47	114.28
G, B and DF	95.19	6.97	81.84	110.93
R, G, B and DF	88.41	4.72	79.09	97.89
RGBVI and DF	94.11	9.26	74.01	113.06
GLI and DF	91.70	7.20	76.06	109.59
VARI and DF	92.29	10.58	75.73	118.98
NGRDI and DF	89.10	7.63	77.61	102.22
ExG and DF	93.01	8.31	75.04	109.45
ExGR and DF	92.15	6.99	75.06	106.59

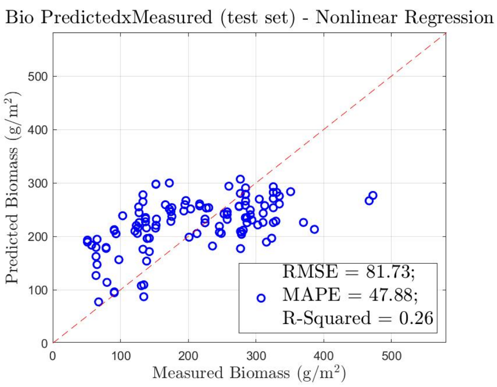

(a) Red and DF

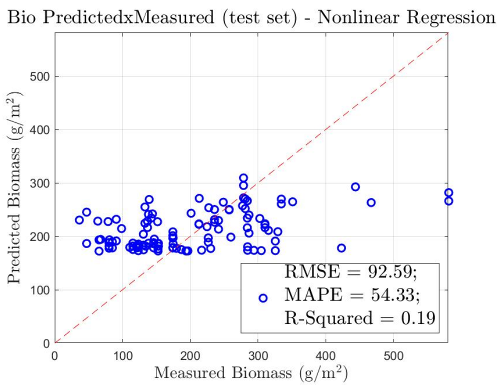

(b) Green and DF

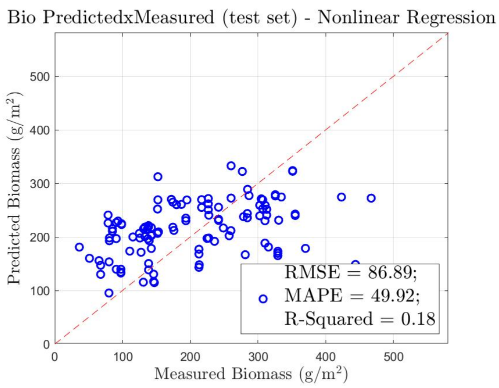

(c) Blue and DF

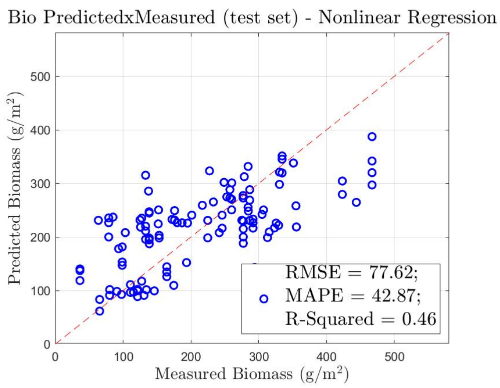

(d) R, G and DF

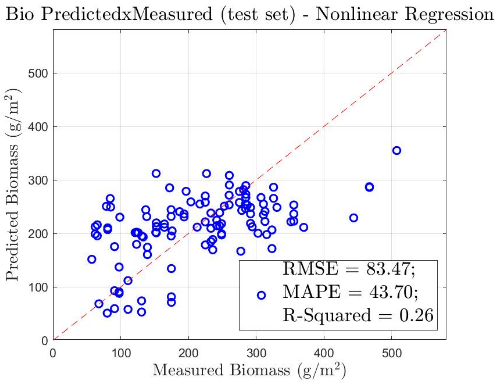

(e) R, B and DF

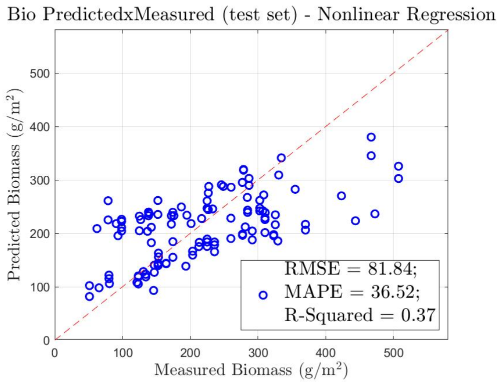

(f) G, B and DF

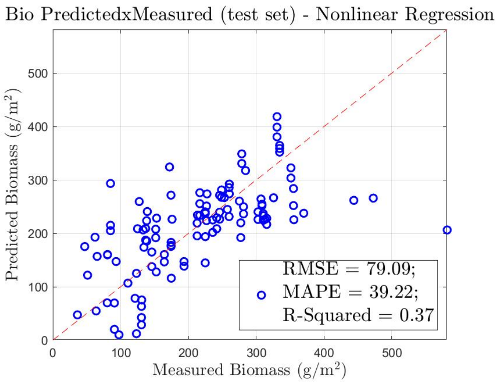

(g) R, G, B and DF

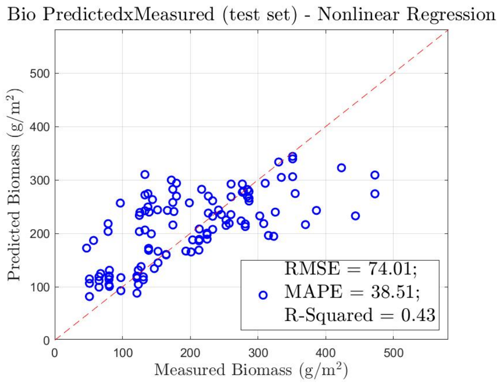

(h) RGBVI and DF

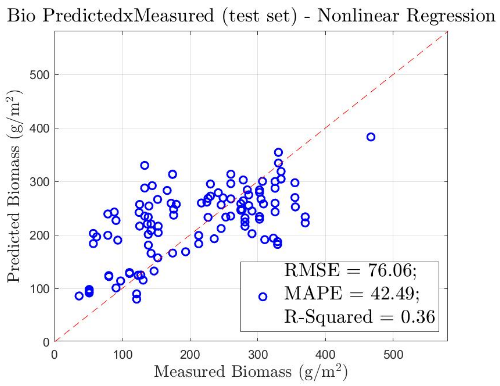

(i) GLI and DF

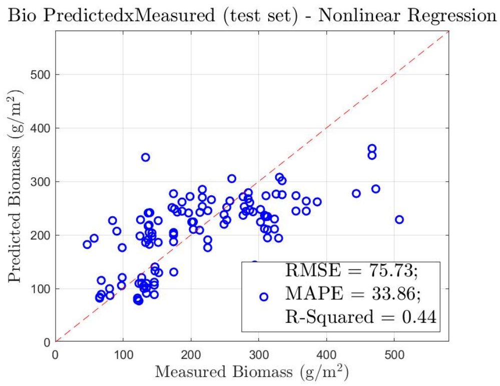

(j) VARI and DF

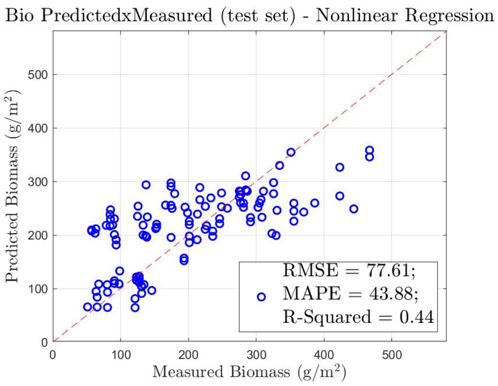

(k) NGRDI and DF

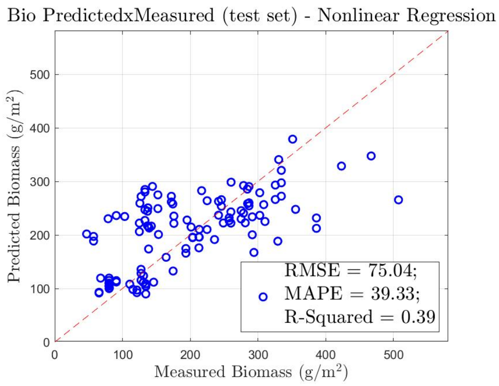

(l) ExG and DF

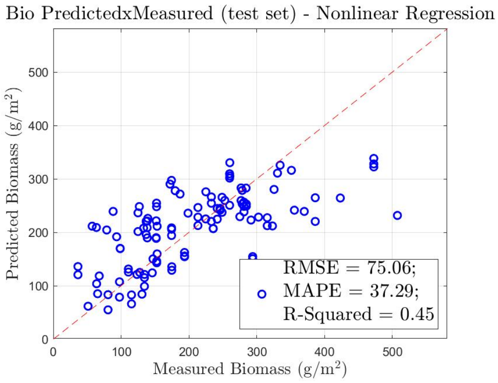

(m) ExGR and DF

Figure 4.12: Best Nonlinear Regression Performance using as inputs combinations of the RGB channels and VIs with the altitude of the drone flight (DF): (a) R and DF, (b) G and DF, (c) B and DF, (d) R, G and DF, (e) R, B and DF, (f) G, B and DF, (g) R, G, B and DF, (h) RGBVI and DF, (i) GLI and DF, (j) VARI and DF, (k) NGRDI and DF, (l) ExG and DF, and (m) ExGR and DF.

Table 4.25: Results of different performance metrics for the developed Nonlinear Regression models, using as inputs combinations of the RGB channels and VIs with the altitude of the drone flight (DF).

Input	Best RMSE (g/m^2)	MAPE (%)	R^2
R and DF	81.73	47.88	0.26
G and DF	92.59	54.33	0.19
B and DF	86.89	49.92	0.18
R, G and DF	77.62	42.87	0.46
R, B and DF	83.47	43.70	0.26
G, B and DF	81.84	36.52	0.37
R, G, B and DF	79.09	39.22	0.37
RGBVI and DF	74.01	38.51	0.43
GLI and DF	76.06	42.49	0.36
VARI and DF	75.73	33.86	0.44
NGRDI and DF	77.61	43.88	0.44
ExG and DF	75.04	39.33	0.39
ExGR and DF	75.06	37.29	0.45

Analyzing the results obtained from combinations with the altitude of the drone flight, RGBVI have the lowest RMSE, VARI the lowest MAPE and R and G the highest R-Squared. However, it is noteworthy that the RMSE obtained by using RGBVI and DF as inputs is not so low as RMSE previously achieved for other input's combinations.

4.2.2.4
RGB-based and GI

The next tests were done combining the RGB channels and the VIs with intensity of green on the histogram (GI). The RMSE analysis is shown in Tab. 4.26. The plots of the best results among the 30 runs performed for each input's combination can be seen on Fig. 4.13 and the comparative results of the performance metrics for each case are shown in Tab. 4.27.

Table 4.26: Analysis of RMSE performance using Nonlinear Regression, for combinations of the RGB channels and VIs with GI.

Input	Avg RMSE (g/m^2)	Std Dev RMSE (g/m^2)	Min RMSE (g/m^2)	Max RMSE (g/m^2)
R and GI	99.49	8.82	78.51	115.33
G and GI	106.00	7.07	81.85	117.85
B and GI	101.17	7.31	87.79	116.21
R, G and GI	87.89	5.59	79.08	104.49
R, B and GI	98.22	7.75	84.90	114.52
G, B and GI	91.58	5.22	77.96	101.66
R, G, B and GI	87.75	8.21	72.51	106.14
RGBVI and GI	97.82	8.22	83.79	110.39
GLI and GI	94.13	9.45	75.96	114.53
VARI and GI	90.22	8.48	76.04	106.31
NGRDI and GI	91.61	6.74	79.96	108.26
ExG and GI	93.92	7.42	72.38	107.34
ExGR and GI	92.14	8.05	74.62	108.31

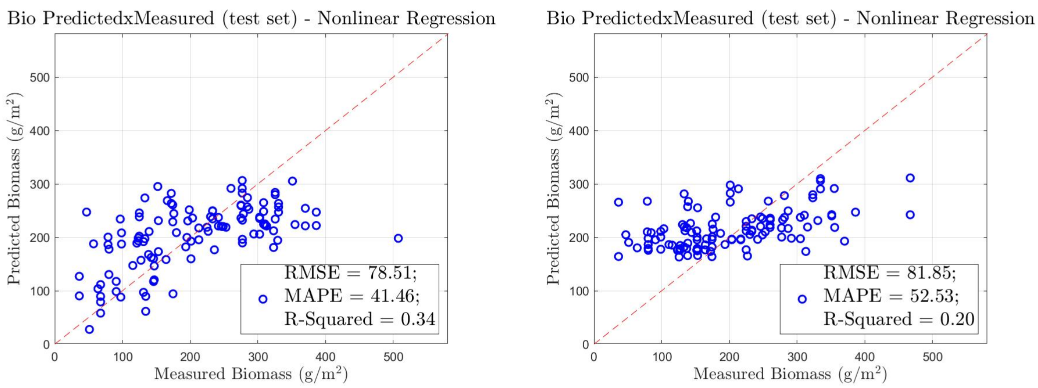

(a) Red and GI **(b)** Green and GI

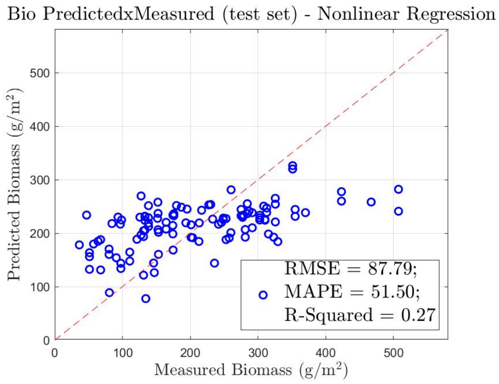

(c) Blue and GI

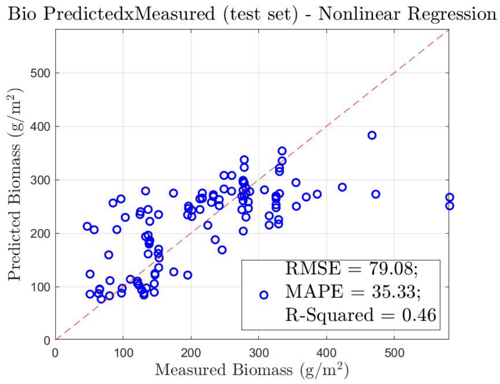

(d) R, G and GI

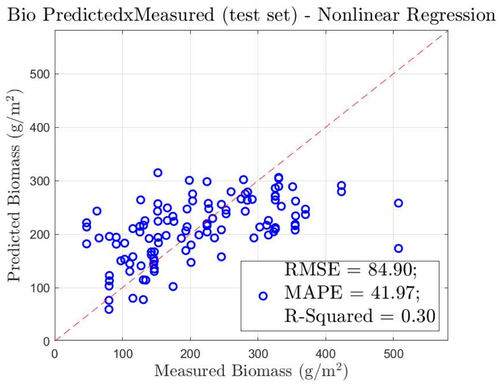

(e) R, B and GI

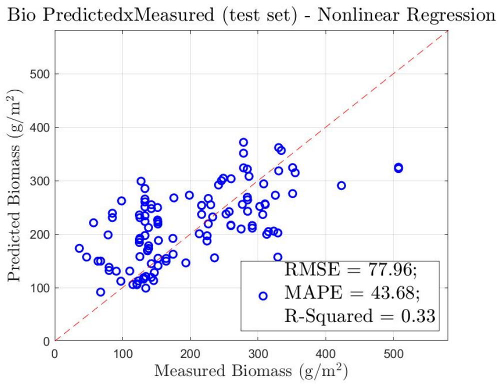

(f) G, B and GI

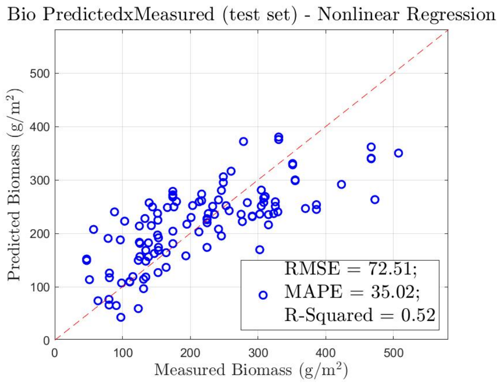

(g) R, G, B and GI

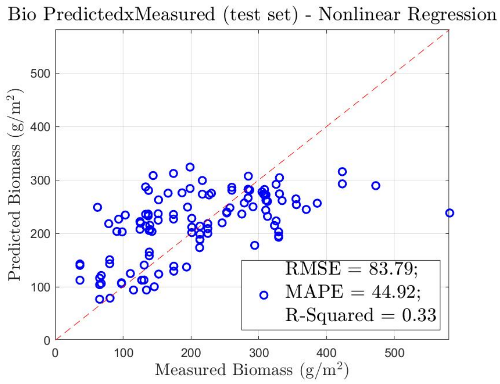

(h) RGBVI and GI

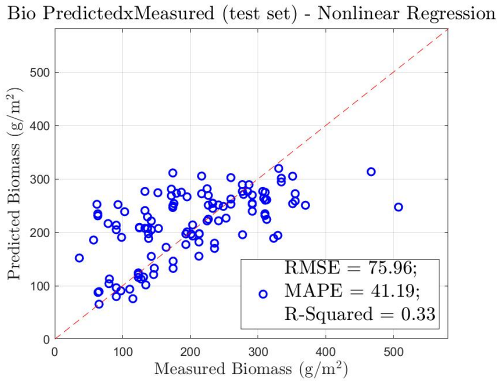

(i) GLI and GI

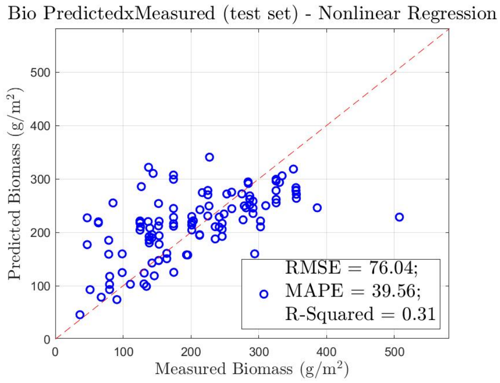

(j) VARI and GI

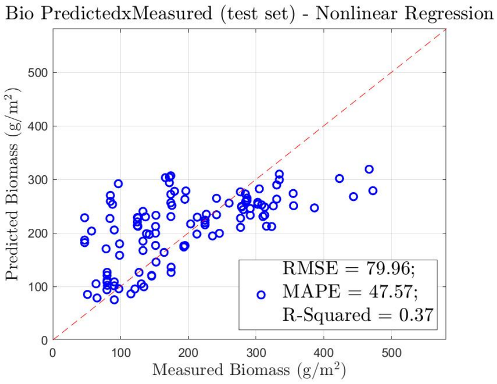

(k) NGRDI and GI

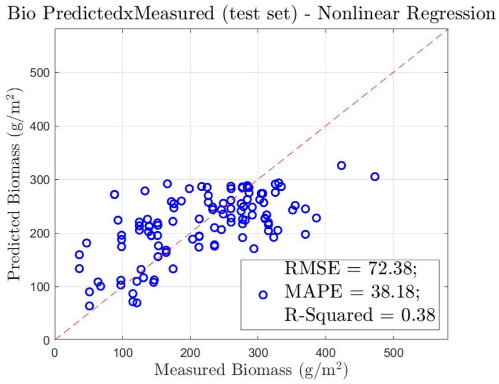

(l) ExG and GI

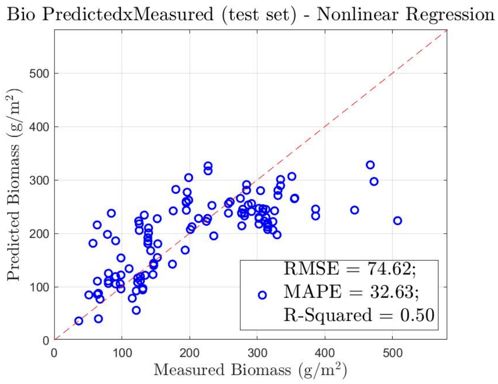

(m) ExGR and GI

Figure 4.13: Best Nonlinear Regression Performance using as inputs combinations of the RGB channels and VIs with the green intensity (GI): (a) R and GI, (b) G and GI, (c) B and GI, (d) R, G and GI, (e) R, B and GI, (f) G, B and GI, (g) R, G, B and GI, (h) RGBVI and GI, (i) GLI and GI, (j) VARI and GI, (k) NGRDI and GI, (l) ExG and GI, and (m) ExGR and GI.

Table 4.27: Results of different performance metrics for the developed Nonlinear Regression models, using as inputs combinations of the RGB channels and VIs with the green intensity (GI).

Input	Best RMSE (g/m^2)	MAPE (%)	R^2
R and GI	78.51	41.46	0.34
G and GI	81.85	52.53	0.20
B and GI	87.79	51.50	0.27
R, G and GI	79.08	35.33	0.46
R, B and GI	84.90	41.97	0.30
G, B and GI	77.96	43.68	0.33
R, G, B and GI	72.51	35.02	0.52
RGBVI and GI	83.79	44.92	0.33
GLI and GI	75.96	41.19	0.33
VARI and GI	76.04	39.56	0.31
NGRDI and GI	79.96	47.57	0.37
ExG and GI	72.38	38.18	0.38
ExGR and GI	74.62	32.63	0.50

In this case, the model using ExGR and GI as inputs have the best MAPE and using R, G, B and GI the best R^2, considering their best RMSE. However, the lowest RMSE is obtained for the nonlinear regression model with ExG and GI as inputs. Notice that this VI have not appeared until now as one of the inputs more directly associated to performance enhancements. However, it should be pointed out that the RMSE obtained with R, G, B and GI is only slightly higher (72.51 g/m^2 vs. 72.38 g/m^2).

4.2.2.5
RGB-based and SR

The next tests were done combining the RGB channels and the VIs with solar radiation (SR). The analysis of RMSE is shown in Tab. 4.28. The plots of the best results among the 30 runs performed for each inputs combination can be seen on Fig. 4.14 and the comparative results of the performance metrics for each case are shown in Tab. 4.29.

Table 4.28: Analysis of RMSE performance using Nonlinear Regression, for combinations of the RGB channels and VIs with SR.

Input	Avg RMSE (g/m^2)	Std Dev RMSE (g/m^2)	Min RMSE (g/m^2)	Max RMSE (g/m^2)
R and SR	96.08	8.65	78.54	117.79
G and SR	104.77	7.29	90.31	118.41
B and SR	99.53	8.14	83.92	121.43
R, G and SR	83.59	7.24	69.68	108.10
R, B and SR	93.70	6.61	79.57	107.92
G, B and SR	89.10	7.70	74.46	103.15
R, G, B and SR	84.27	5.80	74.32	100.74
RGBVI and SR	91.46	7.18	80.82	107.46
GLI and SR	87.77	8.28	70.30	105.76
VARI and SR	85.75	8.29	72.19	100.49
NGRDI and SR	86.20	8.60	65.24	98.69
ExG and SR	87.84	7.13	74.21	105.52
ExGR and SR	87.90	8.19	73.49	105.92

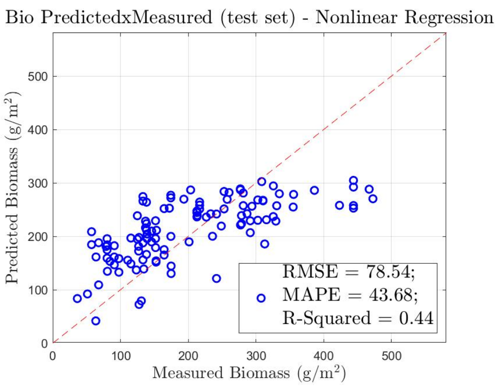

(a) Red and SR

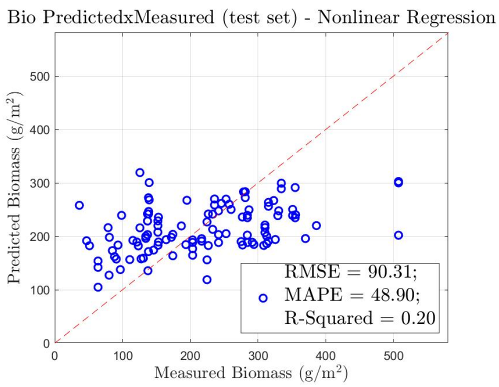

(b) Green and SR

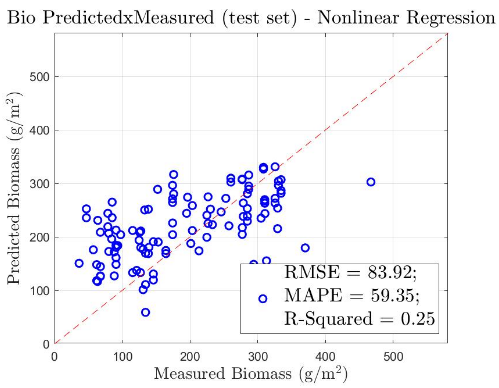

(c) Blue and SR

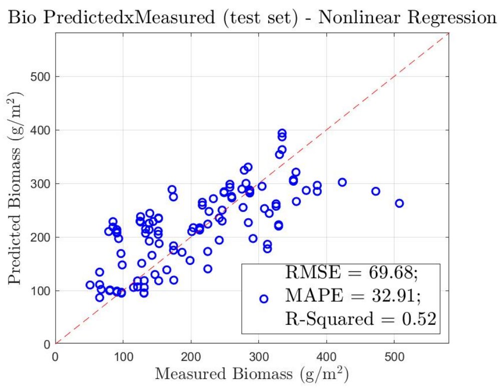

(d) R, G and SR

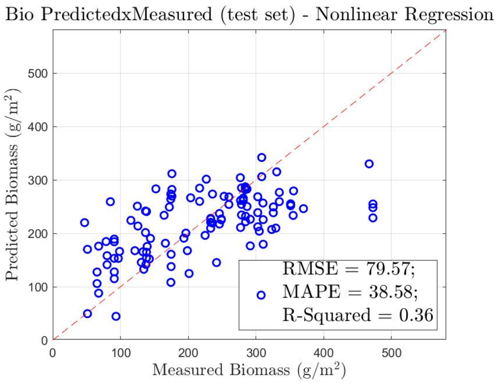

(e) R, B and SR

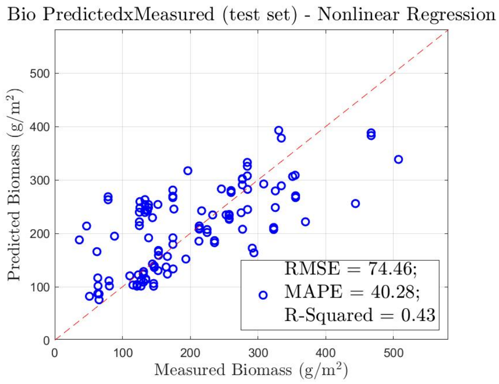

(f) G, B and SR

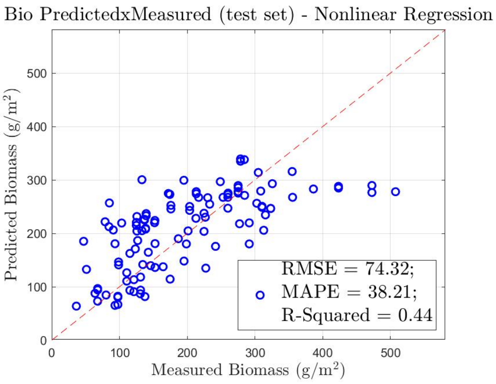

(g) R, G, B and SR

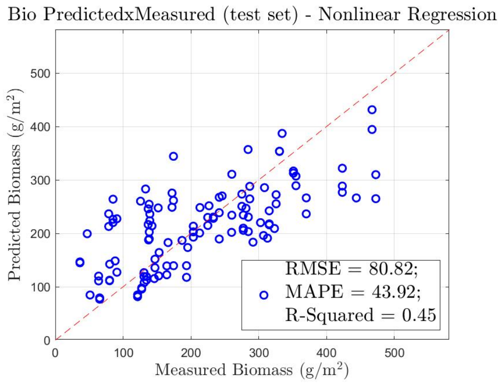

(h) RGBVI and SR

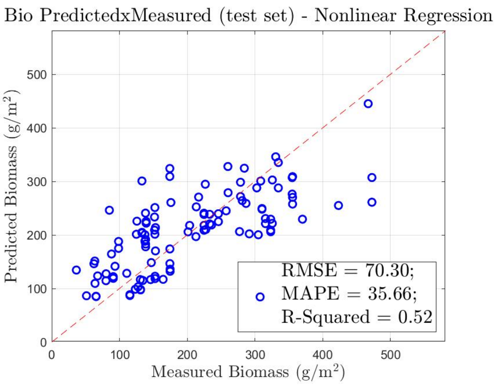

(i) GLI and SR

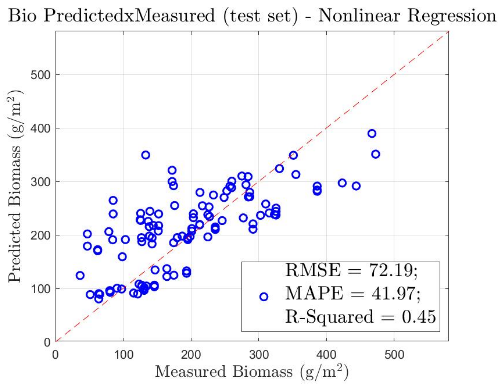

(j) VARI and SR

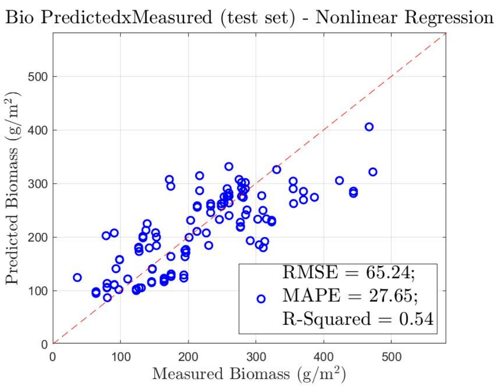

(k) NGRDI and SR

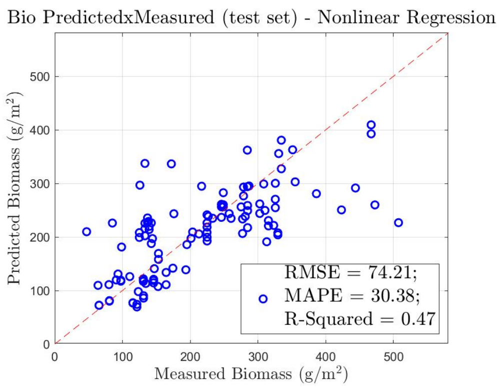

(l) ExG and SR

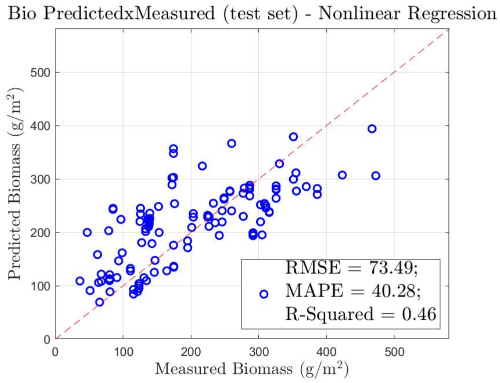

(m) ExGR and SR

Figure 4.14: Best Nonlinear Regression Performance using as inputs combinations of the RGB channels and VIs with the solar radiation (SR): (a) R and SR, (b) G and SR, (c) B and SR, (d) R, G and SR, (e) R, B and SR, (f) G, B and SR, (g) R, G, B and SR, (h) RGBVI and SR, (i) GLI and SR, (j) VARI and SR, (k) NGRDI and SR, (l) ExG and SR, and (m) ExGR and SR.

Table 4.29: Results of different performance metrics for the developed Nonlinear Regression models, using as inputs combinations of the RGB channels and VIs with the solar radiation (SR).

Input	Best RMSE (g/m^2)	MAPE (%)	R^2
R and SR	78.54	43.68	0.44
G and SR	90.31	48.90	0.20
B and SR	83.92	59.35	0.25
R, G and SR	69.68	32.91	0.52
R, B and SR	79.57	38.58	0.36
G, B and SR	74.46	40.28	0.43
R, G, B and SR	74.32	38.21	0.44
RGBVI and SR	80.82	43.92	0.45
GLI and SR	70.30	35.66	0.52
VARI and SR	72.19	41.97	0.45
NGRDI and SR	65.24	27.65	0.54
ExG and SR	74.21	30.38	0.47
ExGR and SR	73.49	40.28	0.46

The obtained results indicate that the combination of NGRDI and SR leads to the best performance, among all combinations between the SR and RGB channels or VI's. Notice that, among the results shown in Tab. 4.29, this input combination presented the lowest RMSE, lowest MAPE and highest R-Squared. Furthermore, it should be highlighted that the nonlinear model with NGRDI and SR as inputs obtained the best performance metrics, among all input's combinations analyzed along this section. This VI is a good candidate to reach better results in MLP, when simulated with the SR measurement.

4.2.3
Comparative Results

Gathering the two best results obtained for each one of the tested input's combinations, we built Tab. 4.30. Similarly to what was done in subsection 4.1.3, the selection criteria adopted to define the best results gives priority to the best RMSEs in each one of the tables presented in this section, which are: (i) Separate Inputs for the RGB-based; (ii) Separate Inputs for the features; (iii) Combination of channels; (iv) Combined Inputs between VIs and channels with PH; (v) Combined Inputs between VIs and channels with DF; (vi) Combined Inputs between VIs and channels with GI; and (vii) Combined Inputs between VIs and channels with SR. The marked results on the table show the three best RMSE values in blue and the best associated MAPE and R-Squared in red.

Table 4.30: Best results for Nonlinear Regression.

Input	Best RMSE (g/m^2)	MAPE (%)	R^2
VARI	79.77	43.18	0.36
NGRDI	80.81	43.14	0.28
ExGR	79.68	37.06	0.38
GI	96.47	63.92	-0.05
R, G and B	79.28	41.83	0.37
R, G and PH	67.27	38.64	0.50
G, B and PH	72.74	39.87	0.34
RGBVI and PH	71.73	30.70	0.44
RGBVI and DF	74.01	38.51	0.43
ExG and DF	75.04	39.33	0.39
ExGR and DF	75.06	37.29	0.45
R, G, B and GI	72.51	35.02	0.52
ExG and GI	72.38	38.18	0.38
ExGR and GI	74.62	32.63	0.50
R, G and SR	69.68	32.91	0.52
GLI and SR	70.30	35.66	0.52
NGRDI and SR	65.24	27.65	0.54

Comparing the results shown in Tab. 4.15 and Tab. 4.30, it is noticeable that ExGR, VARI, NGRDI, and combinations between the R and G channels and among all RGB channels together are contained in both best results tables, for linear and nonlinear regressions. Therefore, note that these inputs are good candidates to help the MLP that will be implemented in the next subsection to reach satisfactory results in the biomass estimation task.

On the other hand, GLI appeared only in Tab. 4.13 (best results for linear regression), and ExG and RGBVI appeared only in Tab. 4.26 (best results for nonlinear regression). All other VIs and RGB channels combinations did not appeared among the best inputs neither in linear nor nonlinear regressions.

Furthermore, the linear regression achieved better results with the RGB channels and VIs alone, and also combining them with the DF and GI features. On the other hand, the nonlinear regression achieved better results with the PH and SR features, that seems to further benefit from a model that could adjust to the nonlinearities of their relation with the estimated biomass.

Moreover, the lowest RMSE among all cases analyzed using linear and nonlinear regressions is found when combining NGRDI with the Solar Radiation as inputs of the nonlinear regression model. That case also reached the lowest MAPE and highest R-Squared, so they will be carefully analyzed as potential candidates to be used as inputs of the neural network model that will be presented in the next subsection. Besides, as expected, the plant height feature seem to contribute to the enhancement of the performance of the linear and nonlinear regressions, since the best RMSE of the linear regression is obtained by using the PH as input and the second best RMSE of the nonlinear regression is achieved with PH as input. Note that using PH and SR as inputs of the neural network is a promising idea for the studies presented in the next subsection.

Despite that, it is important to note that neither the results achieved by the nonlinear regression nor by linear regression obtained satisfactory performance metrics. Using the nonlinear regression model, the lowest RMSE (65.24 $\mathsf{g/m^2}$) is still high and the best R^2 (0.54) still doesn't guarantee a good relationship between the input and output, so this method also can not be satisfactorily used to estimate biomass on a pasture.

4.3 MLP Regression

This section presents the results and discussion about the MLP regression algorithm, firstly showing the performance metrics obtained by using the RGB channels and RGB-based VIs as inputs alone and, then, combining them with other features as plant height (PH), drone flight altitude (DF), intensity of green light (GI) and solar radiation (SR). As cited in Chapter 3, 70% of the data set was used for training, 20% for validation and 10% for test. All performance metrics were calculated based on the test set.

The methodology of the analysis performed in this section is divided in two main parts. First, each input configuration was trained with the MLP algorithm in a Layer Sweep method, varying the neurons in each hidden layer from 4 to 20 neurons, in steps of 2. Moreover, the number of epochs and early stops were evaluated according 3 different options: 5000/500, 10000/1000 and 50000/5000, respectively. So, each one of the inputs tested in this part is trained 243 times. All performance metrics and and a vector with all output values estimated by the MLP for the test set are stored. The results are summarized in tables showing the MLP configuration that reached the best RMSE for each input configuration. Furthermore, the best RMSE values and their associated MAPE and R^2 are also presented.

In the second part, for each case analyzed, the 3 input's configurations associated with the better RMSE values were selected for further analysis. The MLP configurations that reached the best RMSEs for these 3 input's configurations were trained again 30 times, always with the same configuration that guaranteed their best result. These results are shown in a table considering again the best RMSE. This was done to reinforce the statistical analysis of the regression, allowing the analysis of RMSE's standard deviation, average value, lower and upper bounds. The final comparative results show the two better results from each case.

4.3.1 Layer Sweep for Separate Inputs

This subsection represents the first part of the methodology described in Section 4.3, exclusively for the separate inputs as the RGB-based and the features of the images.

4.3.1.1
RGB-based

In this subsection, the inputs are tested separately, as it was performed in Linear and Nonlinear Regressions. The MLPs associated to each input configuration were trained 243 times, following the described Layer Sweep method. To analyze the resulting data statistically, Tab. 4.31 presents the average value, standard deviation, lower and upper bounds of the resulting RMSE, computed in the test sets.

Table 4.31: Analysis of RMSE performance for the RGB-based as separate inputs, using Layer Sweep in MLP Regression.

Input	Avg RMSE (g/m^2)	Std Dev RMSE (g/m^2)	Min RMSE (g/m^2)	Max RMSE (g/m^2)
R	103.85	12.55	70.29	142.56
G	107.58	10.61	80.36	137.98
B	104.15	11.35	74.99	136.59
RGBVI	97.54	9.83	76.83	128.50
GLI	95.56	10.62	73.86	129.24
VARI	91.05	10.42	64.12	118.35
NGRDI	92.38	10.76	63.86	124.23
ExG	96.69	9.76	72.43	120.32
ExGR	91.15	11.41	64.24	132.78

Figure 4.15 shows the regression graphs of the MLP configurations that produced the best RMSE, among the Layer Sweep results, using separate RGB-based inputs. Tab. 4.32 shows the amount of neurons in each hidden layer, the maximum of epochs and early stop related to the best RMSE obtained for each input configuration. The associated MAPE and R-Squared are also presented in the same table.

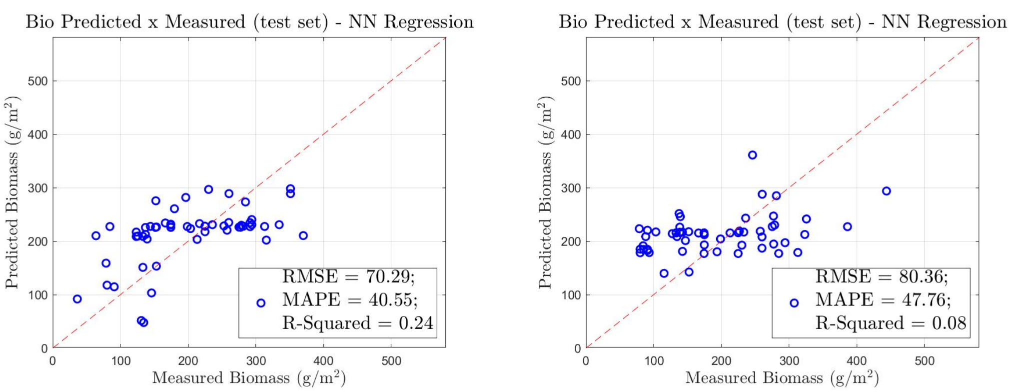

(a) Red **(b)** Green

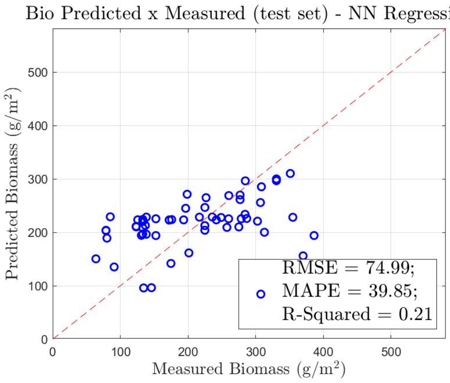

(c) Blue

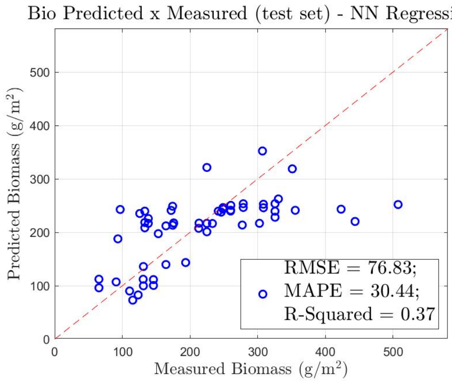

(d) RGBVI

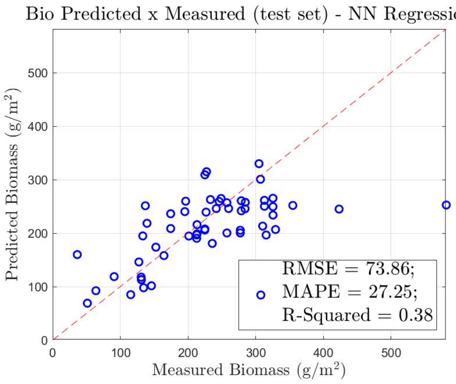

(e) GLI

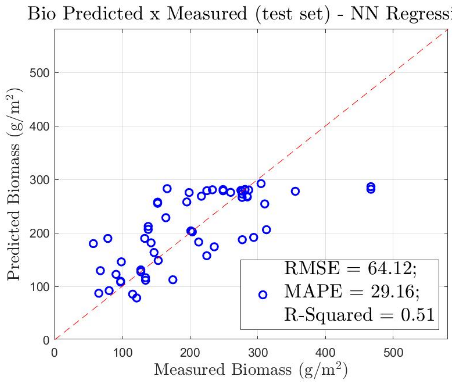

(f) VARI

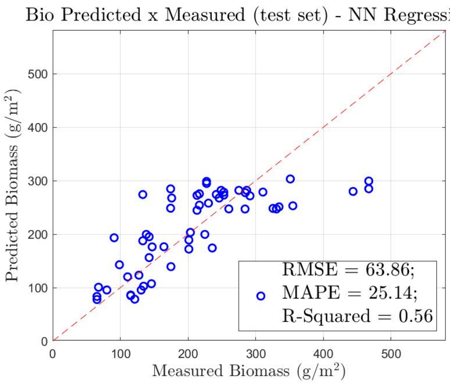

(g) NGRDI

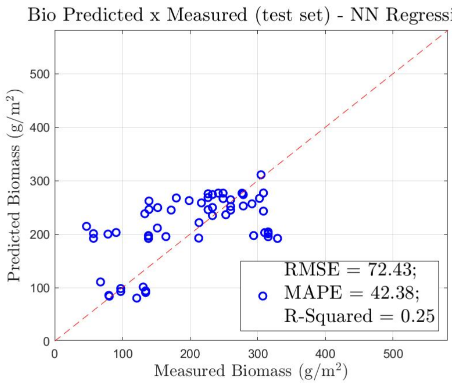

(h) ExG

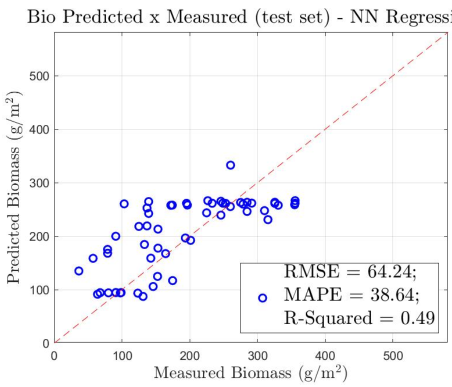

(i) ExGR

Figure 4.15: Best performance, using Layer Sweep in MLP for the RGB-based as Separate Inputs: (a) Red, (b) Green, (c) Blue, (d) RGBVI, (e) GLI, (f) NGRDI, (h) ExG, (i) ExGR.

Table 4.32: Results for the RGB-based as separate inputs using MLP Regression with Layer Sweep.

Input	#Epochs	#Early Stop	#Layer 1	#Layer 2	Best RMSE (g/m^2)	MAPE (%)	R^2
R	50000	5000	16	6	70.29	40.55	0.24
G	50000	5000	8	14	80.36	47.76	0.08
B	10000	1000	16	14	74.99	39.85	0.21
RGBVI	5000	500	16	20	76.83	30.44	0.37
GLI	10000	1000	16	18	73.86	27.25	0.38
VARI	50000	5000	10	14	64.12	29.16	0.51
NGRDI	10000	1000	10	6	63.86	25.14	0.56
ExG	50000	5000	14	4	72.43	42.38	0.25
ExGR	10000	1000	16	16	64.24	38.64	0.49

The results for the separate inputs using only RGB-based features are really similar to the Nonlinear Regression best results. They reach almost the same performance metrics. Hence, the combination of the inputs in MLP Regression will be further stressed out so that the results are boosted by the combination of right inputs. Even though, the MLPs with NGRDI, VARI and ExGR as inputs reached the best RMSEs with really close values between one to another and very different to the other RGB-based inputs analyzed.

4.3.1.2 Features

To analyze the resulting data statistically, Tab. 4.33 presents the average value, standard deviation, lower and upper bounds of the resulting RMSE, computed in the test sets.

Table 4.33: Analysis of RMSE performance for the features as separate inputs, using Layer Sweep in MLP Regression.

Input	Avg RMSE (g/m^2)	Std Dev RMSE (g/m^2)	Min RMSE (g/m^2)	Max RMSE (g/m^2)
PH	98.33	11.59	67.97	129.10
DF	114.48	11.26	85.77	153.09
GI	107.87	11.11	80.49	140.34
SR	77.87	10.67	57.32	119.05

Figure 4.16 shows the regression graphs of the MLP configurations that produced the best RMSE, among the Layer Sweep results, using separate inputs. Tab. 4.34 shows the amount of neurons in each hidden layer, the maximum of epochs and early stop related to the best RMSE obtained for each

input configuration. The associated MAPE and R-Squared are also presented in the same table.

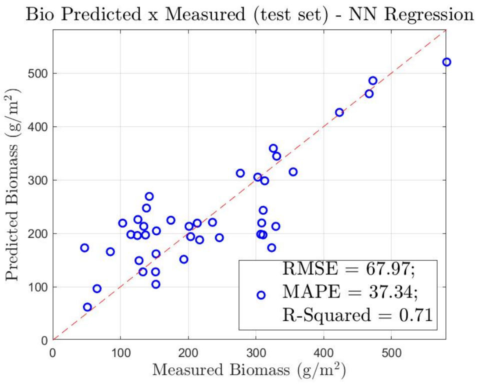

(a) PH

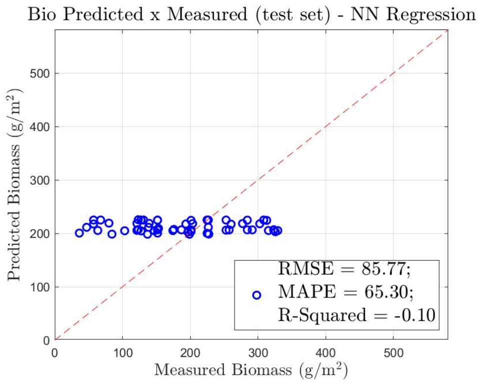

(b) DF

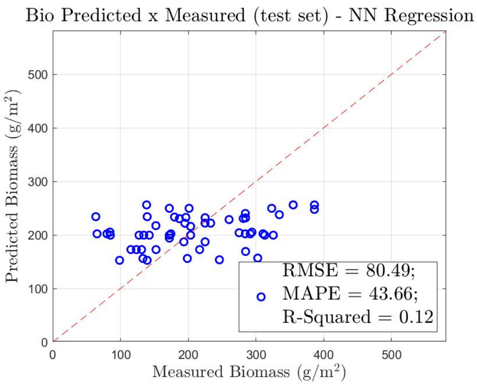

(c) GI

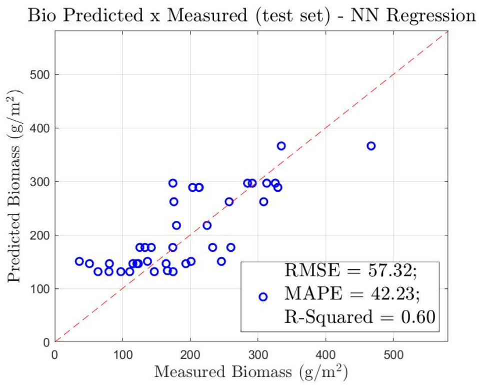

(d) SR

Figure 4.16: Best performance, using Layer Sweep in MLP for Separate Inputs: (a) PH, (b) DF, (c) GI, (d) SR.

Table 4.34: Results for the features as separate inputs, using MLP Regression with Layer Sweep.

Input	#Epochs	#Early Stop	#Layer 1	#Layer 2	Best RMSE (g/m^2)	MAPE (%)	R^2
PH	50000	5000	14	8	67.97	37.34	0.71
DF	5000	500	20	4	85.77	65.30	-0.10
GI	50000	5000	14	10	80.49	43.66	0.12
SR	5000	500	12	10	57.32	42.23	0.60

The results of the MLP regression algorithm show some surprises in relation to results that may be expected by observing the linear and nonlinear regressions. The best RMSE for separate inputs was obtained by using Solar Radiation as input. Although the results obtained by the linear and nonlinear regressions indicate that SR did not present any significant correlation with biomass when analyzed alone, it was expected that this input could boost the performance metrics as a secondary input. Another surprise is the R-Squared of the network that have plant height as input. Notice that 0.71 is greater than any other R-Squared value seen until now.

4.3.2 Layer Sweep for Combined inputs

This subsection presents the results of the MLP regression algorithm with the layer sweep, using different combinations of the RGB-based and the features as inputs aiming at analyzing how the performance metrics benefit from different kinds of information.

4.3.2.1 Combinations of R, G and B

Even with the MLP algorithm, it is noticeable that R (red), G (green) and B (blue) do not correlate so well with the outputs, when tested separately. Hereafter, they will be combined among themselves and tested to evaluate if these associations could enhance the performance metrics. The RMSE analysis is shown in Tab. 4.35. The metric results are shown in Tab. 4.36 and in Fig. 4.17.

Table 4.35: Analysis of RMSE performance for different combinations of the RGB channels, using MLP Regression with Layer Sweep.

Input	Avg RMSE (g/m^2)	Std Dev RMSE (g/m^2)	Min RMSE (g/m^2)	Max RMSE (g/m^2)
R and G	89.85	9.96	66.71	116.03
R and B	103.05	11.29	79.34	134.13
G and B	95.98	9.02	75.27	119.42
R, G and B	82.70	11.06	60.34	113.75

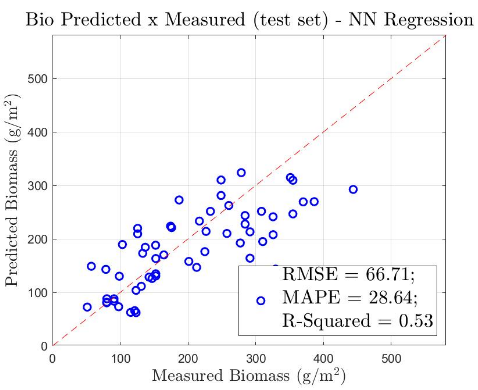

(a) R and G

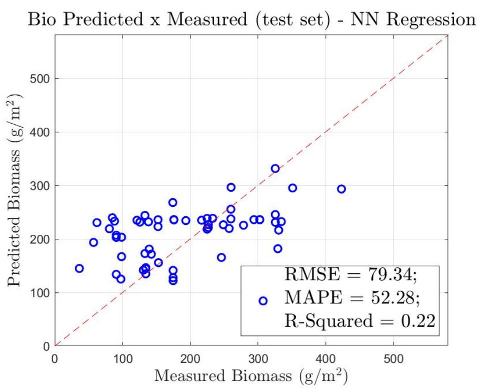

(b) R and B

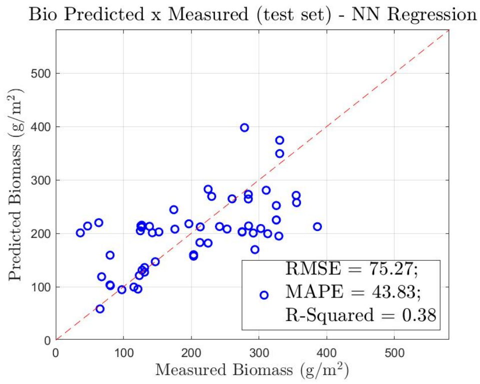

(c) G and B

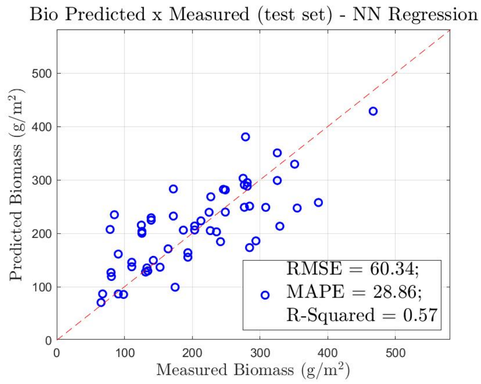

(d) R, G and B

Figure 4.17: Best performance, using MLP regression with Layer Sweep, for Combined Inputs between R, G and B: (a) R and G, (b) R and B, (c) G and B, and (d) R, G and B.

Table 4.36: Results for different combinations of the RGB channels, using MLP Regression with Layer Sweep.

Input	#Epochs	#Early Stop	#Layer 1	#Layer 2	Best RMSE (g/m^2)	MAPE (%)	R^2
R and G	10000	1000	16	6	66.71	28.64	0.53
R and B	5000	500	10	20	79.34	52.28	0.22
G and B	50000	5000	6	14	75.27	43.83	0.38
R, G and B	50000	5000	14	12	60.34	28.86	0.57

As expected, it is possible to observe in Tab. 4.36 that the lowest RMSE occurs for the MLP that uses R, G and B together as inputs. Notice that this RMSE is also the second lowest of all RMSEs obtained for separate inputs. Considering our established selection criteria, the MLPs with Solar Radiation (SR), R, G and B together and NGRDI as inputs will be the three MLPs chosen to be trained for 30 runs in subsection 4.3.3. Note that VARI will not be considered for these analysis, because the RMSE achieved by its better MLP configuration does not lay among the two best RMSEs. Besides, note that although R, G and B together reached the highest R-Squared among the cases presented in Tab. 4.36, the best one was obtained by the MLP using plant height (PH) as input, which reached the best R-Squared so far.

In the next subsections, the MLP networks using as inputs all the RGB-based VIs and the channels of pixels (separated and combined) were trained with one new input. The features used as this new input are plant height (PH), altitude of drone flight (DF), green pixel intensity (GI) and solar radiation (SR), respectively. Their RMSE statistics will be summarized in a table, presenting the average values, standard deviations, lower and upper bounds.

The MLP configuration associated with their best RMSE results will be shown in a table with their corresponding MAPE and R^2, as well as the number of epochs and early stop. Besides, we also show graphs of the measured versus the predicted biomass by the MLP networks associated with the best RMSE of each analyzed input configuration.

4.3.2.2
RGB-based and PH

Tab. 4.37 shows the RMSE statistics related to the results of the MLP regression model using as inputs the VIs and the RGB channels combined with the plant height (PH).

Table 4.37: Analysis of RMSE performance using MLP Regression with Layer Sweep, for combinations of the RGB channels and VIs with PH.

Input	Avg RMSE (g/m^2)	Std Dev RMSE (g/m^2)	Min RMSE (g/m^2)	Max RMSE (g/m^2)
R and PH	94.37	11.14	64.89	124.27
G and PH	96.88	9.33	69.38	121.51
B and PH	97.47	11.00	72.38	127.07
R, G and PH	81.02	11.59	52.43	111.11
R, B and PH	88.21	10.90	64.86	126.07
G, B and PH	81.69	11.62	46.65	113.99
R, G, B and PH	70.21	11.42	36.23	114.48
RGBVI and PH	87.80	10.97	62.27	116.30
GLI and PH	85.85	9.95	56.49	116.67
VARI and PH	74.87	11.00	44.20	111.80
NGRDI and PH	78.94	11.29	52.65	112.22
ExG and PH	86.31	10.74	60.42	118.93
ExGR and PH	78.38	9.84	57.80	110.30

Figure 4.18 shows the plots of the predicted biomass as a function of the measured biomass, considering as inputs combinations of the RGB channels and VIs with the plant height (PH) feature. The curves plot in Fig. 4.18 represent the best RMSE obtained for each input combination. On the other hand, Tab. 4.38 shows the MLP configurations associated to the best RMSE obtained for each input combination, and their respective MAPE and R-Squared.

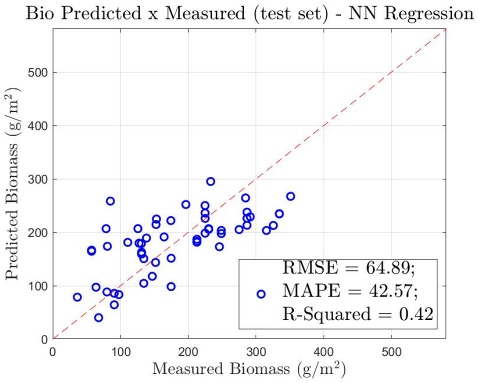

(a) Red and PH

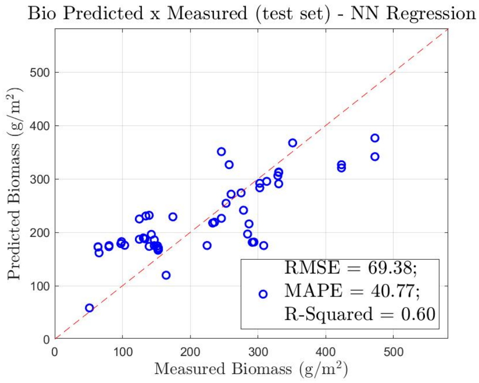

(b) Green and PH

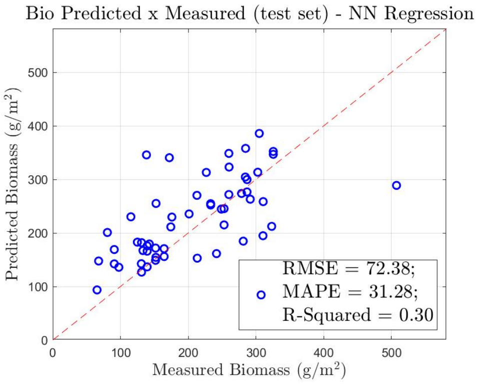

(c) Blue and PH

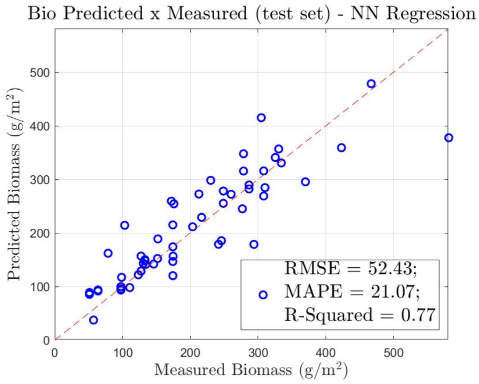

(d) R, G and PH

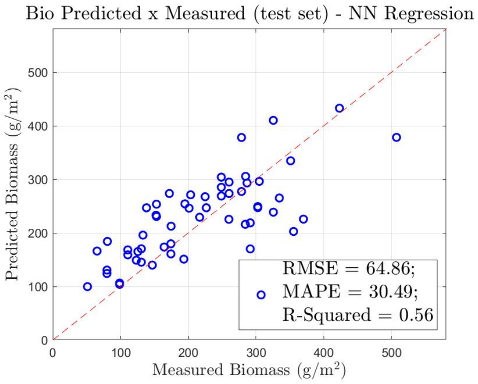

(e) R, B and PH

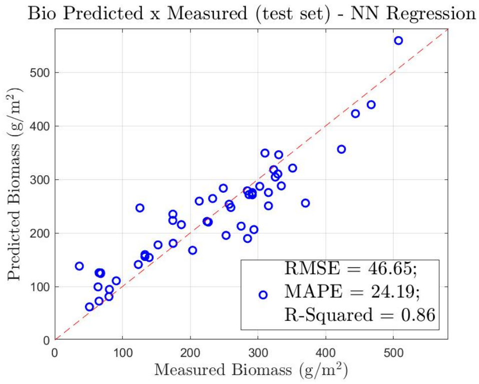

(f) G, B and PH

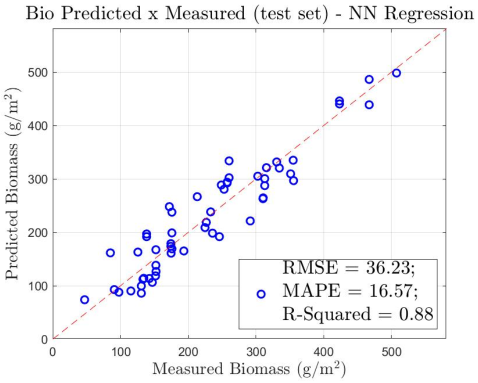

(g) R, G, B and PH

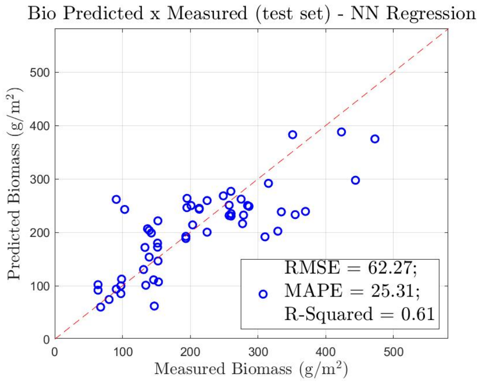

(h) RGBVI and PH

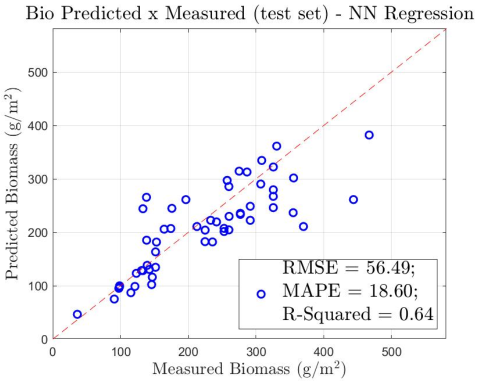

(i) GLI and PH

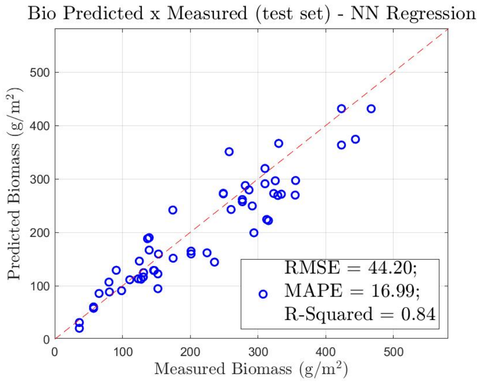

(j) VARI and PH

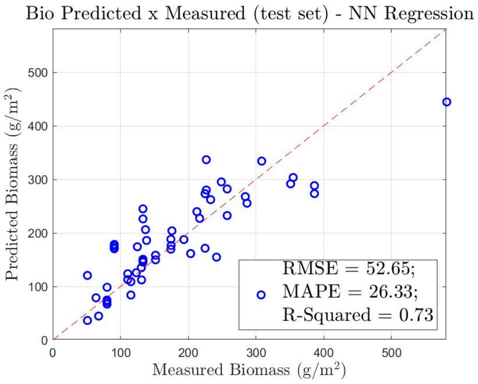

(k) NGRDI and PH

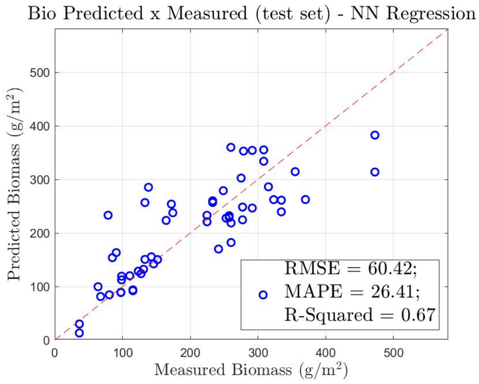

(l) ExG and PH

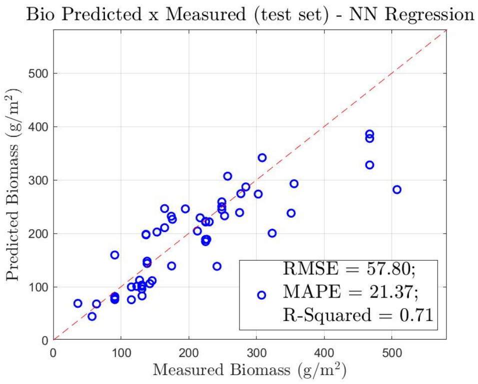

(m) ExGR and PH

Figure 4.18: Best Performance MLP with Layer Sweep, using as inputs combinations of the RGB channels and VIs with the plant height (PH): (a) R and PH, (b) G and PH, (c) B and PH, (d) R, G and PH, (e) R, B and PH, (f) G, B and PH, (g) R, G, B and PH, (h) RGBVI and PH, (i) GLI and PH, (j) VARI and PH, (k) NGRDI and PH, (l) ExG and PH, and (m) ExGR and PH.

Table 4.38: Results of different performance metrics for the MLP Regression model's associated with the best RMSEs obtained with Layer Sweep, using as inputs combinations of the RGB channels and VIs with the plant height (PH).

Input	#Epochs	#Early Stop	#Layer 1	#Layer 2	Best RMSE (g/m^2)	MAPE (%)	R^2
R and PH	10000	1000	4	20	64.89	42.57	0.42
G and PH	50000	5000	12	4	69.38	40.77	0.60
B and PH	10000	1000	10	12	72.38	31.28	0.30
R, G and PH	50000	5000	8	6	52.43	21.07	0.77
R, B and PH	10000	1000	6	20	64.86	30.49	0.56
G, B and PH	50000	5000	10	12	46.65	24.19	0.86
R, G, B and PH	50000	5000	6	12	36.23	16.57	0.88
RGBVI and PH	5000	500	4	12	62.27	25.31	0.61
GLI and PH	5000	500	12	14	56.49	18.60	0.64
VARI and PH	50000	5000	20	18	44.20	16.99	0.84
NGRDI and PH	50000	5000	18	14	52.65	26.33	0.73
ExG and PH	50000	5000	18	16	60.42	26.41	0.67
ExGR and PH	10000	1000	16	10	57.80	21.37	0.71

This configuration showed the best results so far. The smallest RMSE ever achieved (36.23 g/m^2) is obtained from the combination of R, G, B and PH as inputs of the MLP with 6 and 12 neurons in its hidden layers. This could be reached setting 50000 rounds of epochs and 5000 of early stop. Besides, this MLP configuration also leaded to the smallest MAPE (16.57 %) and highest R-Squared (0.88). This is a promising result that can be even further improved after running the algorithm 30 times with the same configuration. Besides, the MLPs configurations with R, G and B together, G and B, and VARI will also be trained again in the second part, in order to assure this performance. It is possible to notice that most of the input's combinations achieved better results than the MLPs with separate inputs and Linear or Nonlinear Regressions, considering any configuration. It is simple to conclude that the addition of the plant height to the model increases the performance significantly and, consequently, it is highly recommended to use this feature as input of the MLPs.

4.3.2.3
RGB-based and DF

The second configuration of input's combinations adds the altitude of drone flight (DF) as an input together with the VIs and RGB channel. Table 4.39 shows the RMSE statistics related to the results of the MLP regression models developed for these new sets of inputs.

Table 4.39: Analysis of RMSE performance using MLP Regression with Layer Sweep, for combinations of the RGB channels and VIs with DF.

Input	Avg RMSE (g/m^2)	Std Dev RMSE (g/m^2)	Min RMSE (g/m^2)	Max RMSE (g/m^2)
R and DF	104.30	12.76	72.35	136.41
G and DF	108.36	9.87	81.66	139.04
B and DF	105.65	11.45	75.73	135.23
R, G and DF	91.91	10.16	63.44	128.14
R, B and DF	102.96	12.42	76.78	139.39
G, B and DF	96.80	9.91	73.16	130.16
R, G, B and DF	89.51	11.84	58.60	140.16
RGBVI and DF	95.62	10.69	72.16	136.18
GLI and DF	96.10	11.08	68.60	130.92
VARI and DF	93.24	11.17	71.06	119.32
NGRDI and DF	93.02	10.93	66.27	127.71
ExG and DF	95.13	11.89	68.54	141.13
ExGR and DF	92.63	11.32	61.70	130.12

Figure 4.19 shows the plots of the predicted biomass as a function of the measured biomass, considering as inputs combinations of the RGB channels and VIs with the altitude of drone flight (DF) feature. The curves plot in Fig. 4.19 represent the best RMSE obtained for each input combination. On the other hand, Tab. 4.40 shows the MLP configurations associated to the best RMSE obtained for each input combination, and their respective MAPE and R-Squared.

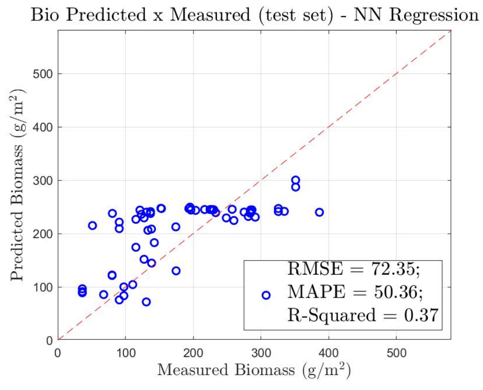

(a) Red and DF

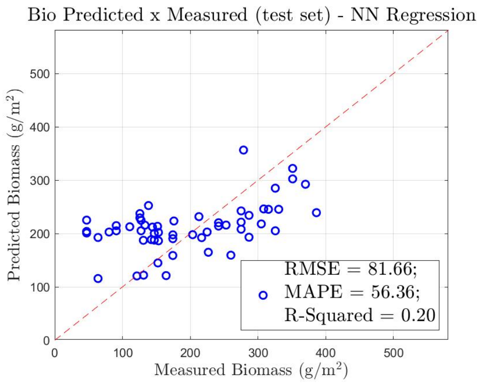

(b) Green and DF

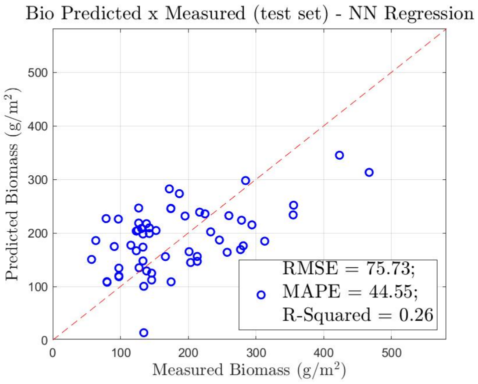

(c) Blue and DF

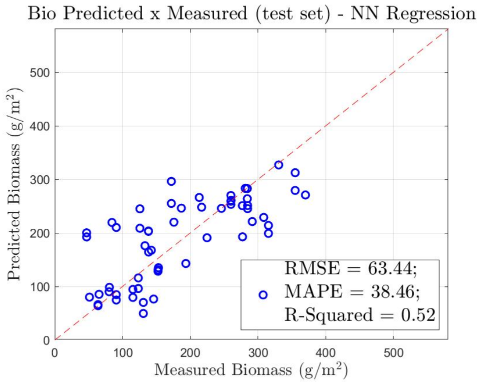

(d) R, G and DF

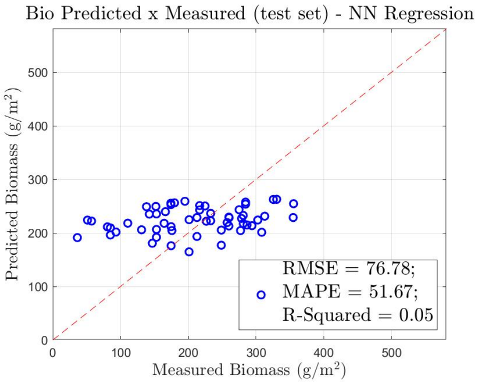

(e) R, B and DF

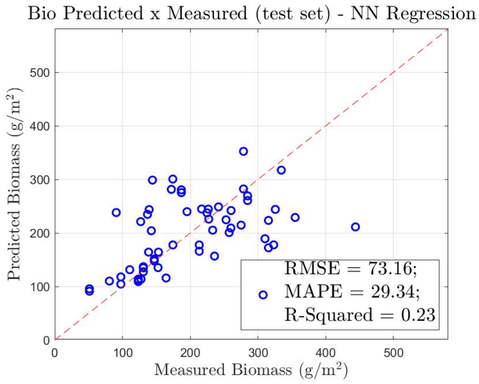

(f) G, B and DF

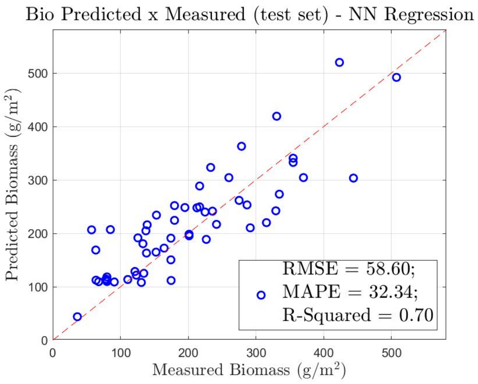

(g) R, G, B and DF

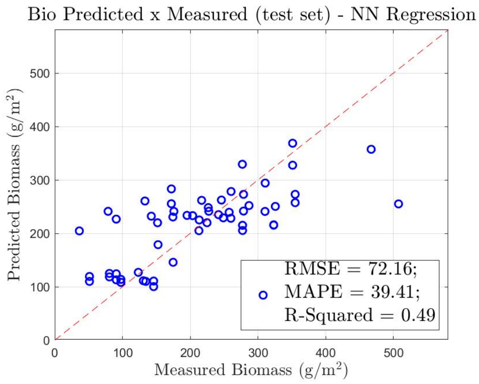

(h) RGBVI and DF

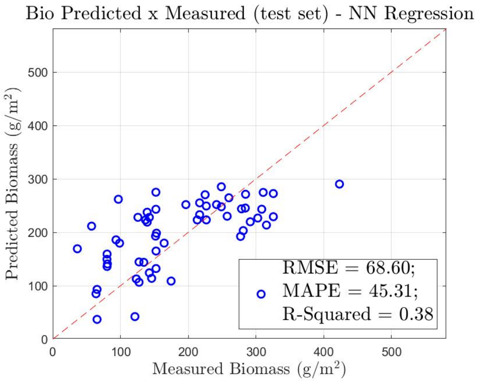

(i) GLI and DF

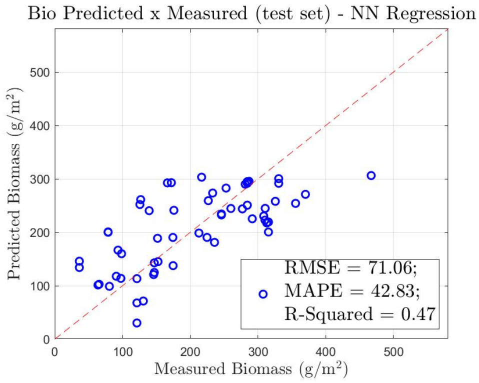

(j) VARI and DF

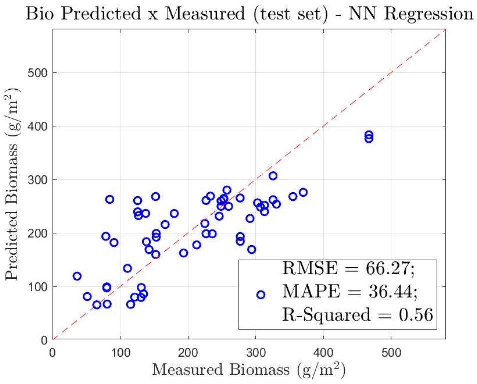

(k) NGRDI and DF

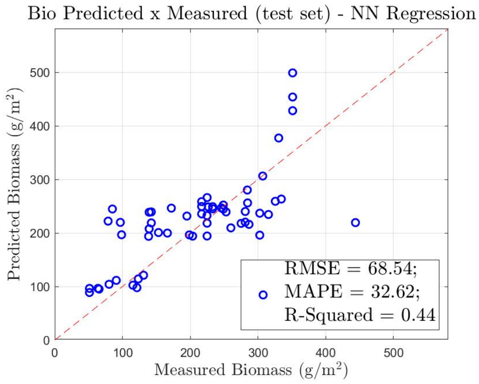

(l) ExG and DF

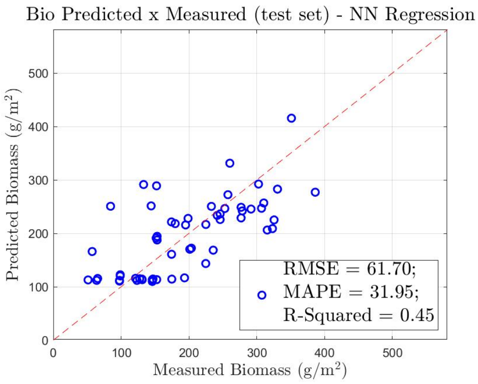

(m) ExGR and DF

Figure 4.19: Best Performance MLP with Layer Sweep, using as inputs combinations of the RGB channels and VIs with the altitude of drone flight (DF): (a) R and DF, (b) G and DF, (c) B and DF, (d) R, G and DF, (e) R, B and DF, (f) G, B and DF, (g) R, G, B and DF, (h) RGBVI and DF, (i) GLI and DF, (j) VARI and DF, (k) NGRDI and DF, (l) ExG and DF, and (m) ExGR and DF.

Table 4.40: Results of different performance metrics for the developed MLP Regression model's associated with the best RMSEs obtained with Layer Sweep, using as inputs combinations of the RGB channels and VIs with the altitude of drone flight (DF).

Input	#Epochs	#Early Stop	#Layer 1	#Layer 2	Best RMSE (g/m^2)	MAPE (%)	R^2
R and DF	50000	5000	14	10	72.35	50.36	0.37
G and DF	50000	5000	8	16	81.66	56.36	0.20
B and DF	50000	5000	8	20	75.73	44.55	0.26
R, G and DF	10000	1000	6	8	63.44	38.46	0.52
R, B and DF	10000	1000	6	4	76.78	51.67	0.05
G, B and DF	50000	5000	12	20	73.16	29.34	0.23
R, G, B and DF	50000	5000	6	8	58.60	32.34	0.70
RGBVI and DF	50000	5000	6	10	72.16	39.41	0.49
GLI and DF	50000	5000	20	12	68.60	45.31	0.38
VARI and DF	50000	5000	6	10	71.06	42.83	0.47
NGRDI and DF	5000	500	20	18	66.27	36.44	0.56
ExG and DF	10000	1000	10	4	68.54	32.62	0.44
ExGR and DF	10000	1000	6	8	61.70	31.95	0.45

The smallest RMSE achieved using DF as an input was 58.6 g/m^2, for an MLP configuration with DF and R, G and B as inputs. This configuration also reached the highest R-Squared among all MLP configurations using DF as an input. Despite being a good result comparing to the other methods (linear and nonlinear regression), it did not reach a performance improvement as relevant as using PH as input.

4.3.2.4
RGB-based and GI

The third configuration of input's combinations adds the intensity of green pixel (GI) as an input together with the VIs and RGB channels. Table 4.41 shows the RMSE statistics related to the results of the MLP regression models developed for these new sets of inputs.

Table 4.41: Analysis of RMSE performance using MLP Regression with Layer Sweep, for combinations of the RGB channels and VIs with GI.

Input	Avg RMSE (g/m^2)	Std Dev RMSE (g/m^2)	Min RMSE (g/m^2)	Max RMSE (g/m^2)
R and GI	94.12	12.24	63.98	134.76
G and GI	106.33	11.16	78.08	143.54
B and GI	96.98	11.40	70.12	127.29
R, G and GI	88.25	11.40	60.44	118.01
R, B and GI	93.77	13.40	61.41	131.72
G, B and GI	92.99	10.22	60.32	123.32
R, G, B and GI	86.80	10.73	59.53	119.71
RGBVI and GI	92.58	11.72	68.30	125.23
GLI and GI	90.81	11.13	63.04	124.30
VARI and GI	87.87	12.69	59.86	124.77
NGRDI and GI	87.34	11.26	59.08	127.86
ExG and GI	88.91	10.52	60.99	126.01
ExGR and GI	88.14	11.62	60.84	127.19

Figure 4.20 shows the plots of the predicted biomass as a function of the measured biomass, considering as inputs combinations of the RGB channels and VIs with the pixel's green intensity (GI) feature. The curves plot in Fig. 4.20 represent the best RMSE obtained for each input combination, among the 30 runs performed for each of them. On the other hand, Tab. 4.42 shows the MLP configurations associated to the best RMSE obtained for each input combination, and their respective MAPE and R-Squared.

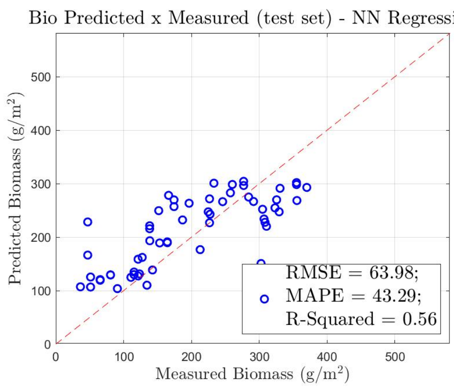

(a) Red and GI

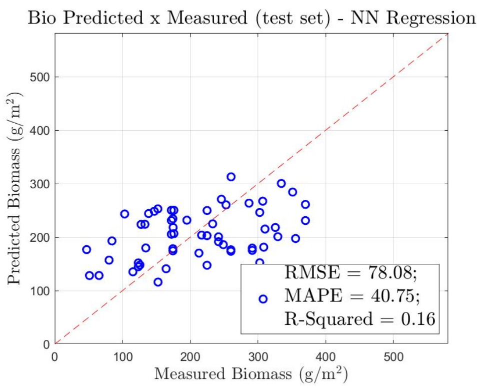

(b) Green and GI

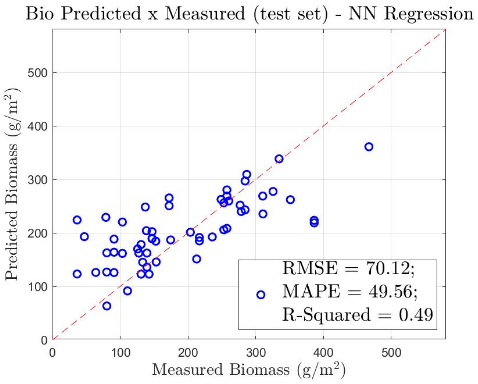

(c) Blue and GI

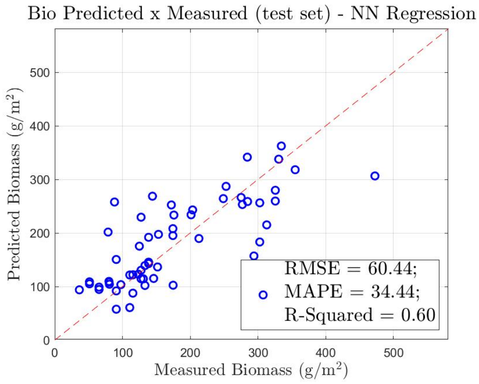

(d) R, G and GI

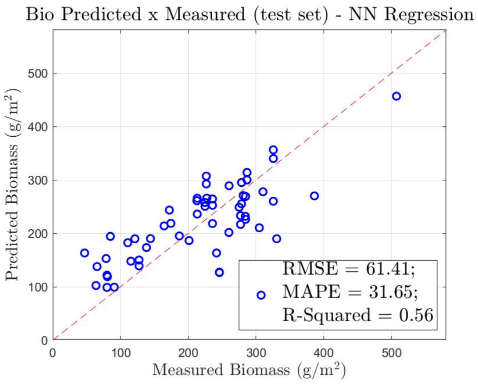

(e) R, B and GI

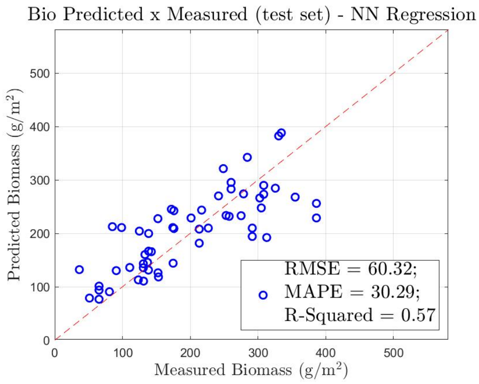

(f) G, B and GI

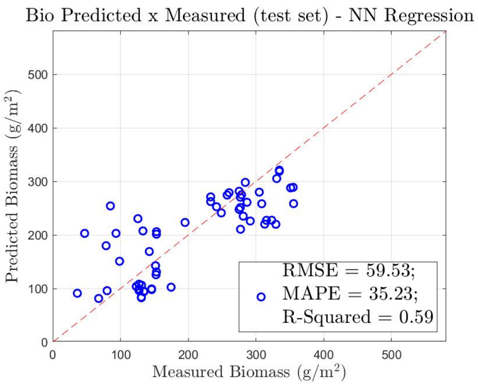

(g) R, G, B and GI

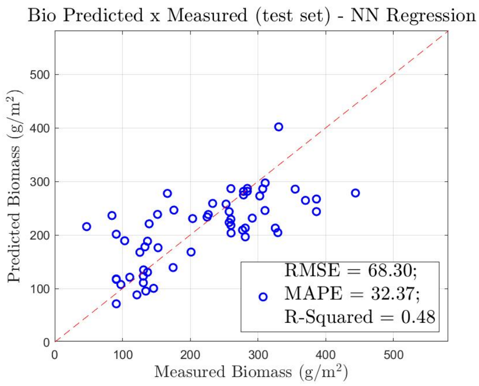

(h) RGBVI and GI

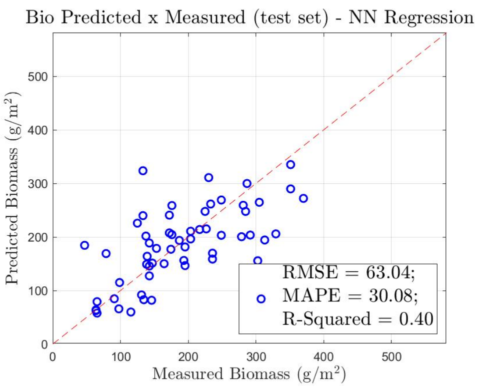

(i) GLI and GI

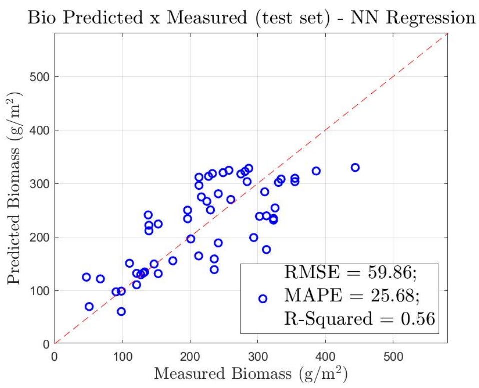

(j) VARI and GI

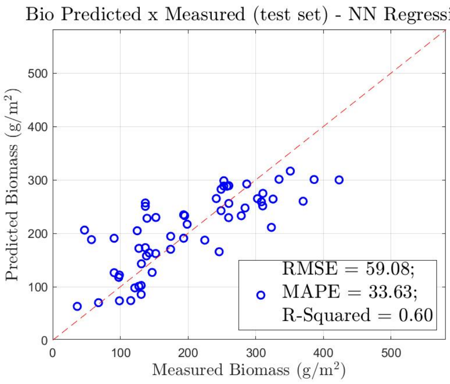

(k) NGRDI and GI

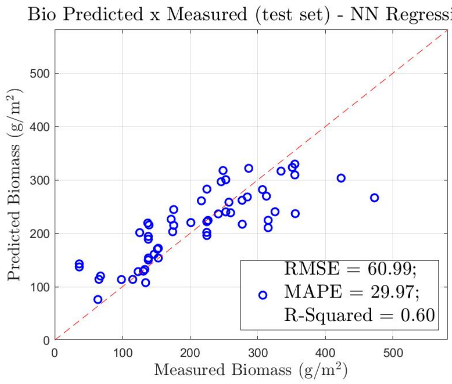

(l) ExG and GI

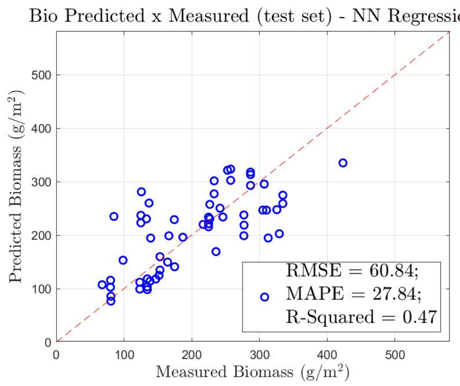

(m) ExGR and GI

Figure 4.20: Best Performance MLP with Layer Sweep, using as inputs combinations of the RGB channels and VIs with the pixel's intensity of green (GI): (a) R and GI, (b) G and GI, (c) B and GI, (d) R, G and GI, (e) R, B and GI, (f) G, B and GI, (g) R, G, B and GI, (h) RGBVI and GI, (i) GLI and GI, (j) VARI and GI, (k) NGRDI and GI, (l) ExG and GI, and (m) ExGR and GI.

The combination of the GI with the RGB channels and VIs contributed to the enhancement of the performance metrics. These results are consistent with the behavior observed up to now which the performance metrics of the MLP improves by adding new features as inputs. Among the analyzed cases using GI as input, the smallest RMSE (59.08 g/m^2) was obtained by the MLP that uses NGRDI and GI as inputs. Besides, notice that the three lowest RMSEs are very close to each other (all of them reaches about 59 g/m^2), corresponding to the MLPs using as inputs GI and (i) NGRDI, (ii) R, G and B together, and (iii) VARI. These inputs are also the ones commonly associated to the best performance metrics for the linear and nonlinear regression models. Moreover, although there are 3 configuration of inputs reaching a R-Squared of 0.6, only NGRDI is among the inputs with the lowest RMSEs.

Table 4.42: Results of different performance metrics for the developed MLP Regression model's associated with the best RMSEs obtained with Layer Sweep, using as inputs combinations of the RGB channels and VIs with the pixel's intensity of green (GI).

Input	#Epochs	#Early Stop	#Layer 1	#Layer 2	Best RMSE (g/m^2)	MAPE (%)	R^2
R and GI	50000	5000	4	6	63.98	43.29	0.56
G and GI	50000	5000	14	4	78.08	40.75	0.16
B and GI	50000	5000	18	18	70.12	49.56	0.49
R, G and GI	50000	5000	14	12	60.44	34.44	0.60
R, B and GI	50000	5000	20	8	61.41	31.65	0.56
G, B and GI	5000	500	20	18	60.32	30.29	0.57
R, G, B and GI	50000	5000	4	14	59.53	35.23	0.59
RGBVI and GI	5000	500	18	20	68.30	32.37	0.48
GLI and GI	50000	5000	6	20	63.04	30.08	0.40
VARI and GI	50000	5000	18	4	59.86	25.68	0.56
NGRDI and GI	50000	5000	18	16	59.08	33.63	0.60
ExG and GI	5000	500	12	4	60.99	29.97	0.60
ExGR and GI	5000	500	14	12	60.84	27.84	0.47

4.3.2.5
RGB-based and SR

The fourth configuration of input's combinations adds the solar radiation (SR) as an input together with the VIs and RGB channels. Table 4.43 shows the RMSE statistics related to the results of the MLP regression models developed for these new sets of inputs.

Figure 4.21 shows the plots of the predicted biomass as a function of the measured biomass, considering as inputs combinations of the RGB channels and VIs with the solar radiation (SR) feature. The curves plot in Fig. 4.21 represent the best RMSE obtained for each input combination, among the 30 runs performed for each of them. On the other hand, Tab. 4.44 shows the MLP configurations associated to the best RMSE obtained for each input combination, and their respective MAPE and R-Squared.

Table 4.43: Analysis of RMSE performance using MLP Regression with Layer Sweep, for combinations of the RGB channels and VIs with SR.

Input	Avg RMSE (g/m^2)	Std Dev RMSE (g/m^2)	Min RMSE (g/m^2)	Max RMSE (g/m^2)
R and SR	83.52	13.76	53.83	127.99
G and SR	94.06	11.24	63.80	123.05
B and SR	87.11	11.10	63.01	116.47
R, G and SR	71.42	12.86	40.56	126.88
R, B and SR	87.47	12.79	55.31	124.39
G, B and SR	72.77	9.95	48.21	103.83
R, G, B and SR	68.19	11.48	43.61	96.87
RGBVI and SR	72.61	10.33	50.12	112.13
GLI and SR	70.62	11.39	48.20	100.80
VARI and SR	66.48	12.00	43.58	108.12
NGRDI and SR	67.27	11.47	43.61	104.46
ExG and SR	71.09	11.77	41.78	106.02
ExGR and SR	67.60	12.02	42.87	115.57

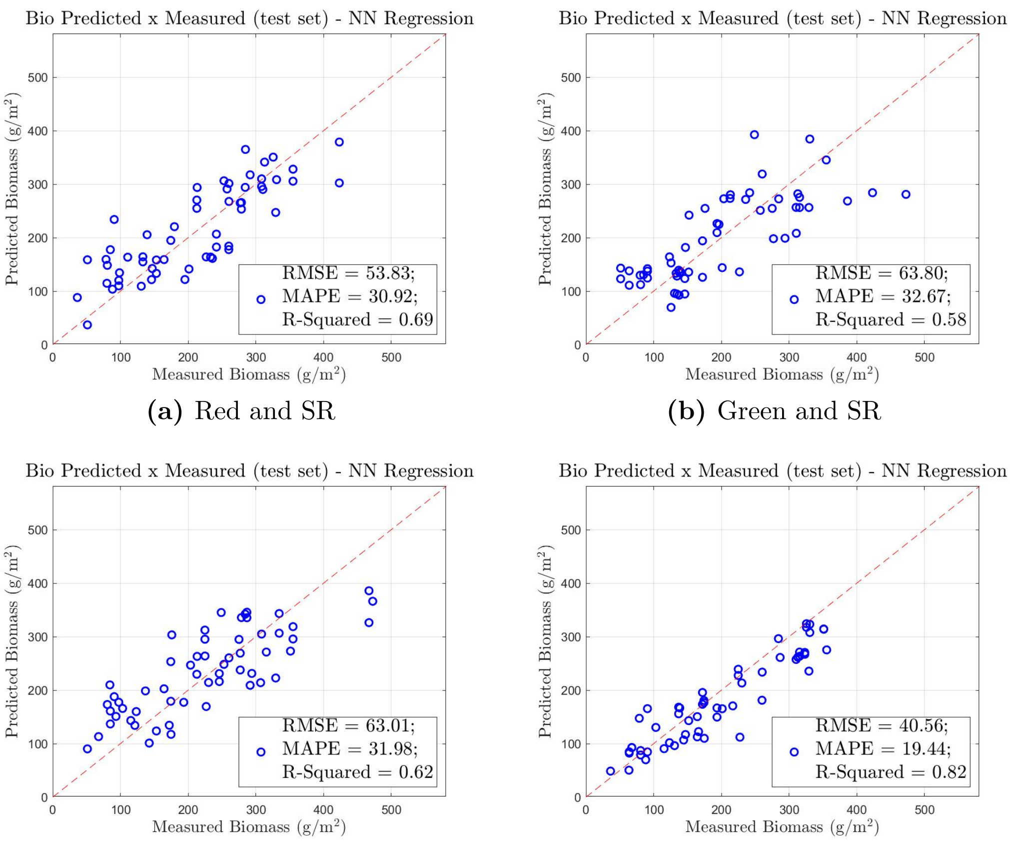

(a) Red and SR

(b) Green and SR

(c) Blue and SR

(d) R, G and SR

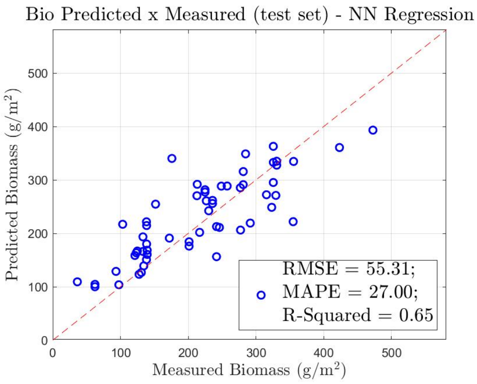

(e) R, B and SR

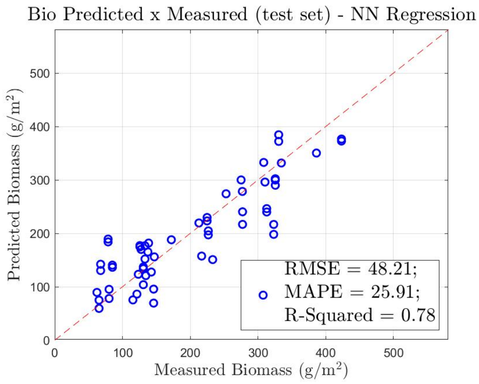

(f) G, B and SR

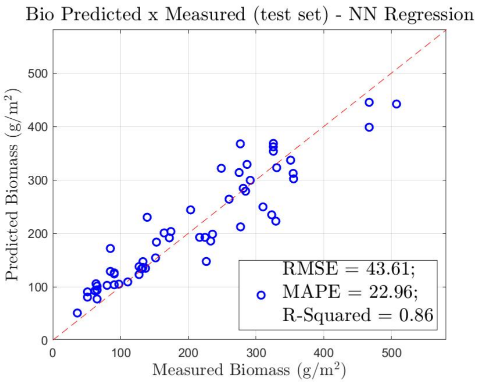

(g) R, G, B and SR

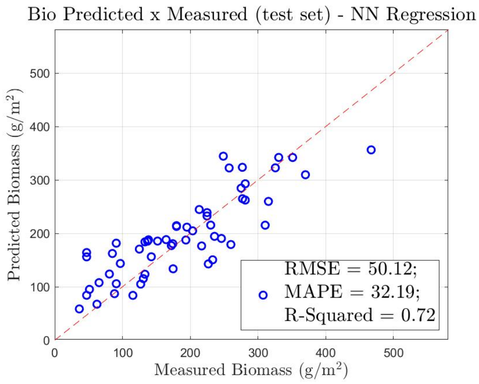

(h) RGBVI and SR

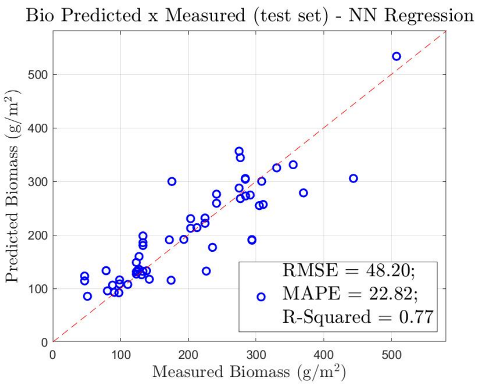

(i) GLI and PH

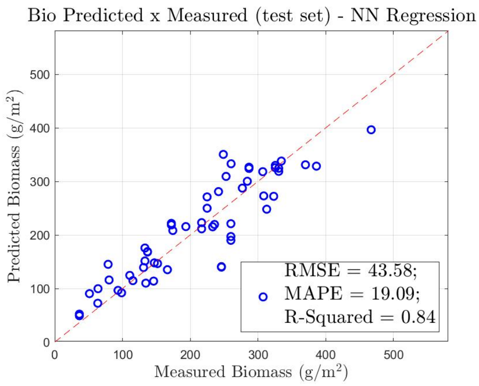

(j) VARI and PH

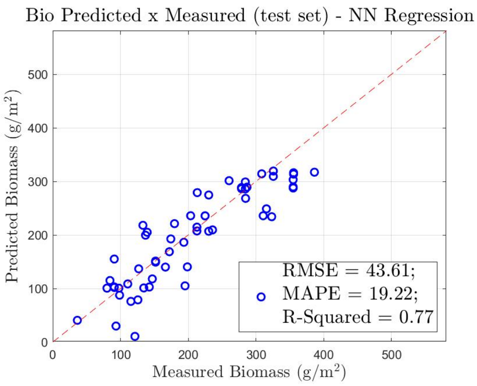

(k) NGRDI and PH

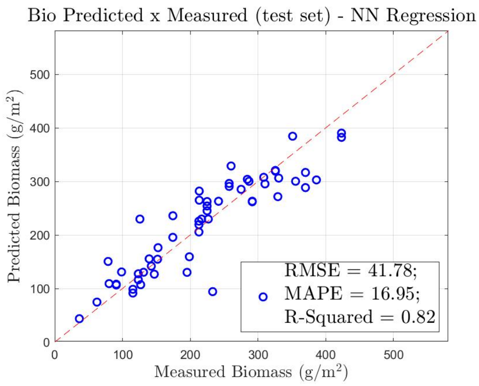

(l) ExG and PH

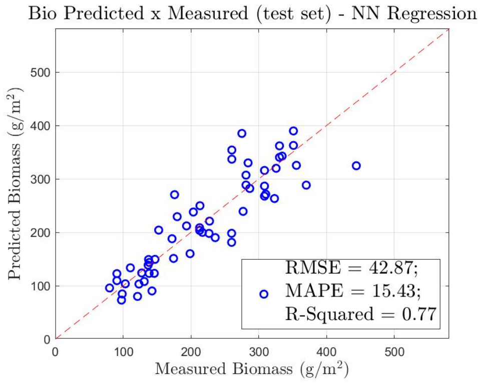

(m) ExGR and PH

Figure 4.21: Best Performance MLP with Layer Sweep, using as inputs combinations of the RGB channels and VIs with the solar radiation (SR): (a) R and SR, (b) G and SR, (c) B and SR, (d) R, G and SR, (e) R, B and SR, (f) G, B and SR, (g) R, G, B and SR, (h) RGBVI and SR, (i) GLI and SR, (j) VARI and SR, (k) NGRDI and SR, (l) ExG and SR, and (m) ExGR and SR.

Table 4.44: Results of different performance metrics for the developed MLP Regression model's associated with the best RMSEs obtained with Layer Sweep, using as inputs combinations of the RGB channels and VIs with the solar radiation (SR).

Input	#Epochs	#Early Stop	#Layer 1	#Layer 2	Best RMSE (g/m^2)	MAPE (%)	R^2
R and SR	10000	1000	10	10	53.83	30.92	0.69
G and SR	10000	1000	4	18	63.80	32.67	0.58
B and SR	10000	1000	16	8	63.01	31.98	0.62
R, G and SR	5000	500	8	20	40.56	19.44	0.82
R, B and SR	50000	5000	12	18	55.31	27.00	0.65
G, B and SR	10000	1000	18	12	48.21	25.91	0.78
R, G, B and SR	10000	1000	18	18	43.61	22.96	0.86
RGBVI and SR	5000	500	4	20	50.12	32.19	0.72
GLI and SR	10000	1000	20	6	48.20	22.82	0.77
VARI and SR	50000	5000	6	20	43.58	19.09	0.84
NGRDI and SR	50000	5000	6	16	43.61	19.22	0.77
ExG and SR	50000	5000	12	20	41.78	16.95	0.82
ExGR and SR	50000	5000	14	14	42.87	15.43	0.77

The results achieved with the MLPs by combining the RGB channels and VIs with the solar radiation (SR) are really close to the ones found with the plant height (PH). The RMSE values of the three best MLP configurations using SR as an input are comprised in the range from 40 to 43 g/m^2, being slightly worst than the best RMSE achieved with the PH as input. Among the analyzed MLPs with SR, the three lowest RMSE were obtained by combining SR with (i) R and G, (ii) ExG and (iii) ExGR. Besides, notice that the maximum R-Squared is 0.86 using R, G, B and SR, which is also really close to the best R-Squared found with PH (0.88). Moreover, it is worth to point out that the MAPE achieved with ExGR and SR is the lowest one ever achieved (15.43%).

4.3.3 Statistical analysis of the best MLP configurations

This subsection describes the results obtained by the MLP algorithm after running 30 times the best configurations for the three best input's combinations of each case studied in the Layer Sweep subsection. The best results were based in the top 3 smallest RMSE values from the separate inputs analysis and from the combined inputs, which are: (i) PH with VIs or RGB channels; (ii) DF with VIs or RGB channels; (iii) GI with VIs or RGB channels; and (iv) SR with VIs or RGB channels. Hence, they totalize 15 simulations, as there are 3 different configurations of inputs for 5 groups. Table 4.45 shows the inputs which were further analyzed in this section by running them for 30 times, respecting the original configuration described.

Table 4.45: Configurations of the MLP Regression used for the 30 runs analysis.

Input	#Epochs	#Early Stop	#Layer 1	#Layer 2
NGRDI	10000	1000	10	6
SR	5000	500	12	10
R, G and B	50000	5000	14	12
G, B and PH	50000	5000	10	12
R, G, B and PH	50000	5000	6	12
VARI and PH	50000	5000	20	18
R, G and DF	10000	1000	6	8
R, G, B and DF	50000	5000	6	8
ExGR, DF	10000	1000	6	8
R, G, B and GI	50000	5000	4	14
VARI and GI	50000	5000	18	4
NGRDI and GI	50000	5000	18	16
R, G and SR	5000	500	8	20
ExG and SR	50000	5000	12	20
ExGR and SR	50000	5000	14	14

Table 4.46 shows the average value, standard deviation, lower and upper bounds of RMSE, considering the results from the 30 runs executed for each one of the input's configurations analyzed.

Table 4.46: Analysis of RMSE performance using MLP Regression, after running 30 times each configuration.

Input	Avg RMSE (g/m^2)	Std Dev RMSE (g/m^2)	Min RMSE (g/m^2)	Max RMSE (g/m^2)
NGRDI	87.81	11.95	66.87	119.67
SR	76.43	7.15	62.93	93.47
R, G and B	84.07	12.74	60.63	116.22
G, B and PH	80.81	10.30	65.79	101.05
R, G, B and PH	63.52	11.93	41.95	98.14
VARI and PH	69.89	9.82	53.13	90.90
R, G and DF	94.34	11.86	72.34	119.72
R, G, B and DF	83.45	10.52	61.01	114.17
ExGR and DF	90.47	14.37	72.20	119.61
R, G, B and GI	85.05	12.89	64.59	118.83
VARI and GI	91.29	11.41	74.47	120.68
NGRDI and GI	83.85	8.15	68.95	108.70
R, G and SR	72.93	9.48	56.54	93.51
ExG and SR	69.30	12.69	50.88	101.31
ExGR and SR	61.95	9.25	51.14	84.26

Figure 4.22 shows the relationship between the measured and predicted biomass, in g/m^2,for the data contained in the test set. Notice that these plots considered the MLP configuration associated with the best RMSE obtained among the 30 runs performed for each case presented in Tab. 4.46.

It is possible to notice that the majority of results shown in Fig. 4.22, even though showing points close to the desired red dashed line, do have a better performance for the low to medium values of biomass than for high values. As mentioned in 2.3, this behavior is probably due to the data set which has much more examples of low and medium values of biomass than of high values (see Fig. 2.13), so that the MLP prioritizes learning low and medium values of biomass. Note that only 9% of the data set are associated to biomass greater than 350 g/m^2. Despite this fact, some of the combinations of inputs, as R, G, B and PH, VARI and PH, ExGR and PH, can fit well for the amount of biomass over the threshold of 350 g/m^2, since the best result, after 30 runs, shows high values in the test set.

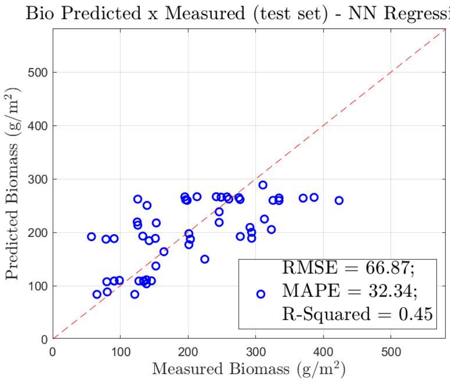

(a) NGRDI

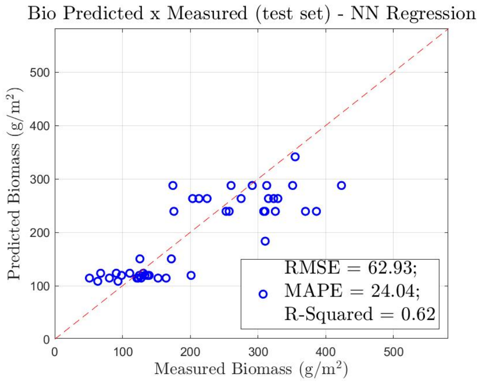

(b) SR

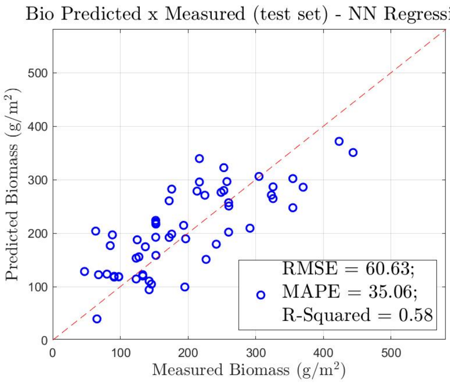

(c) R, G and B

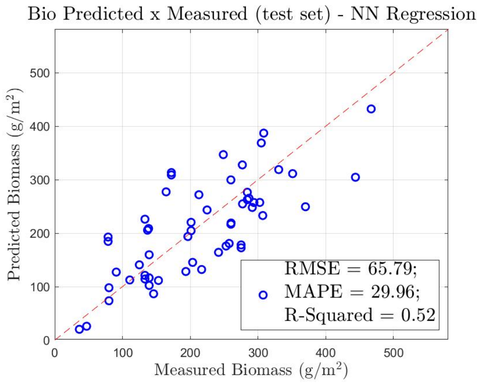

(d) G, B and PH

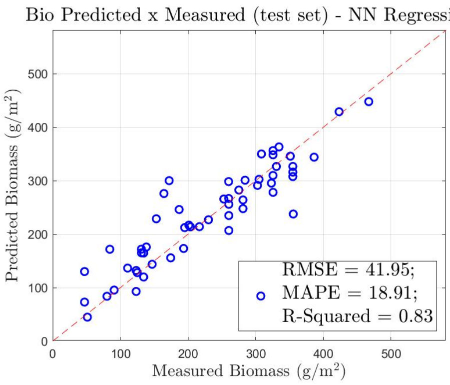

(e) R, G, B and PH

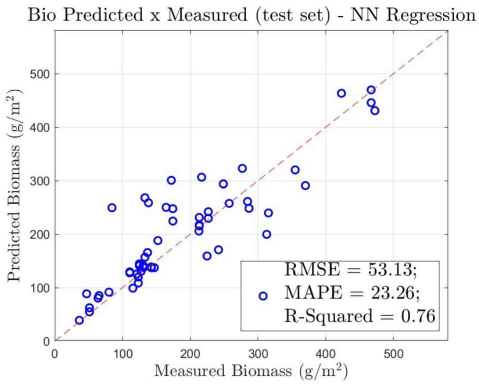

(f) VARI and PH

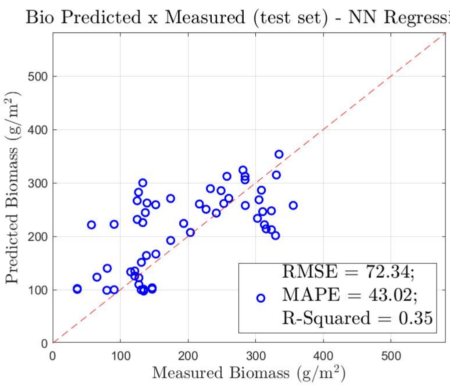

(g) R, G and DF

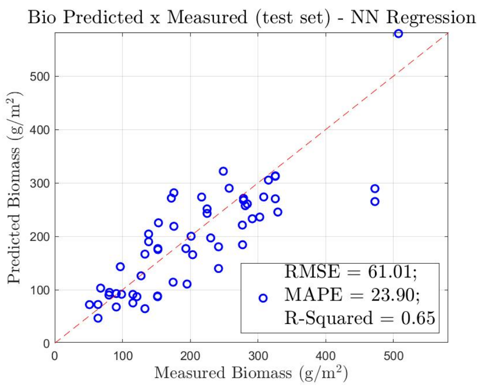

(h) R, G, B and DF

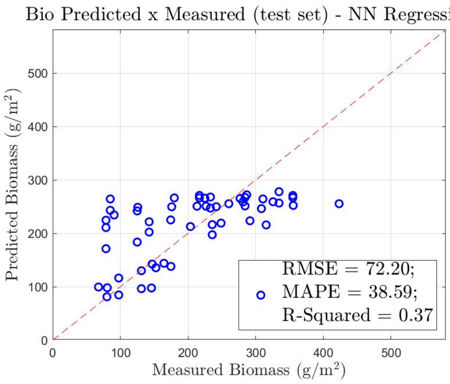

(i) ExGR and DF

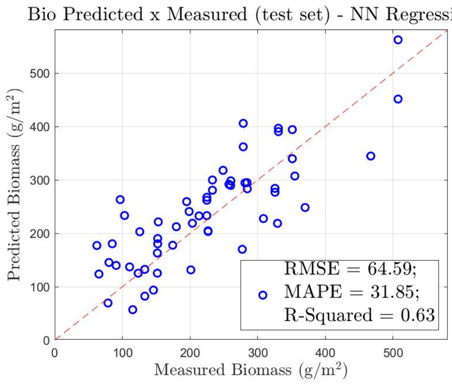

(j) R, G, B and GI

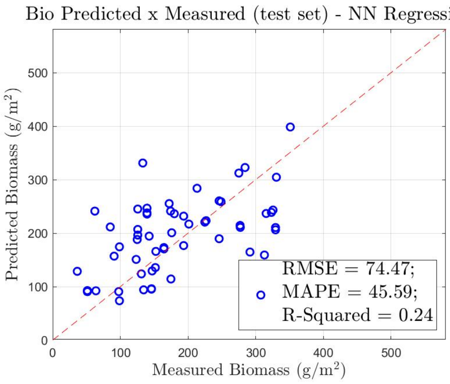

(k) VARI and GI

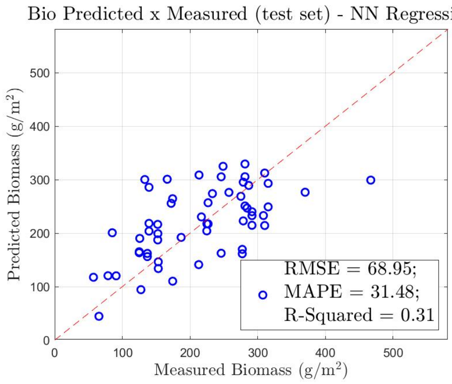

(l) NGRDI and GI

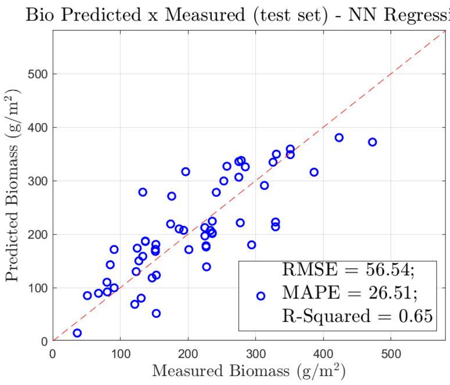

(m) ExGR and PH

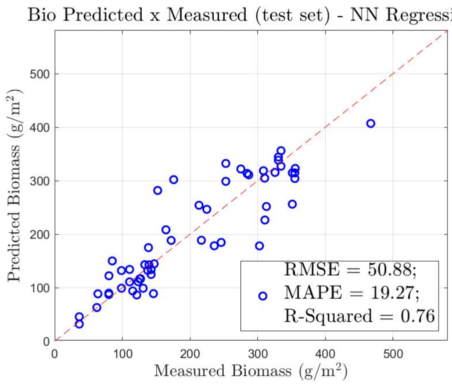

(n) ExG and PH

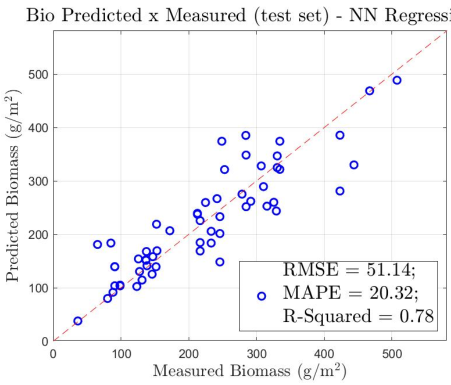

(o) ExGR and PH

Figure 4.22: Best Performance MLP after 30 runs for each of the best cases identified in the Layer Sweep subsection, using as inputs: (a) NGRDI, (b) SR, (c) R, G and B, (d) G, B and PH, (e) R, G, B and PH, (f) VARI and PH, (g) R, G and DF, (h) R, G, B and DF, (i) ExGR and DF, (j) R, G, B and GI, (k) VARI and GI, (l) NGRDI and GI, (m) R, G and SR, (n) ExG and SR, (o) ExGR and SR.

Table 4.47 presents the best RMSE obtained among the 30 runs performed to each configuration. The MAPE and R^2 associated to the best RMSE achieved by each configuration are also presented.

Table 4.47: Results of different performance metrics for the developed MLP Regression model's associated with the best RMSEs, considering the results from the 30 runs executed for each one of the input's configurations analyzed.

Input	Best RMSE ($\mathsf{g/m^2}$)	MAPE (%)	R^2
NGRDI	66.87	32.34	0.45
SR	62.93	24.04	0.62
R, G and B	60.63	35.06	0.58
G, B and PH	65.79	29.96	0.52
R, G, B and PH	41.95	18.91	0.83
VARI and PH	53.13	23.26	0.76
R, G and DF	72.34	43.02	0.35
R, G, B and DF	61.01	23.90	0.65
ExGR, DF	72.20	38.59	0.37
R, G, B and GI	64.59	31.85	0.63
VARI and GI	74.47	45.59	0.24
NGRDI and GI	68.95	31.48	0.31
R, G and SR	56.54	26.51	0.65
ExG and SR	50.88	19.27	0.76
ExGR and SR	51.14	20.32	0.78

As already expected, the best results among the 30 runs performed to each of the selected configurations from the Layer Sweep subsection are the ones obtained by the MLPs using plant height (PH) and solar radiation (SR) combined with VIs or RGB channels as inputs. R, G, B and PH presented the best RMSE of all, with 41.95 $\mathsf{g/m^2}$, and also the best MAPE (18.91%) and R-Squared (0.83). The combination of solar radiation (SR) with ExG and ExGR leaded to the second and third best results in terms of RMSE, respectively. It is important to notice that there were different number of epochs/early stops for the configurations, as the early stop can prevent overfitting. Moreover, another important issue is that even after running the same configuration in Layer Sweep for 30 times, the best RMSE did not reach the one obtained in the previous section. There, the best RMSE was also from R, G, B and PH, but it reached 36.23 $\mathsf{g/m^2}$. This may have occurred due to the random selection of training and test sets in Layer Sweep for this configuration. Notice that each configuration was evaluated only once in the last subsection, so that the values presented here are more reliable, statistically speaking, as they were repeatedly trained for 30 times.

4.4 Stacking Regression

In this section, it was developed a stacking regression algorithm, based on Multi-Layer Perceptron (MLP), using as inputs the outputs of the best Linear Regression, Nonlinear Regression and MLP Regression models developed in the previous sections. Figure 3.3 shows the block diagram of the stacking regression model and Tab. 4.48 presents the configurations of the regression algorithms connected to the inputs of the stacking model.

Table 4.48: Algorithms used as inputs of the Stacking model.

Method	Input	Best RMSE (g/m^2)	Configuration
Linear Regression	R, G, B and PH	68.96	(i)
Nonlinear Regression	NGRDI and SR	65.24	(ii)
MLP Regression	R, G, B and PH	41.95	(iii)

(i) The best fit for the Linear Regression was set by Eq. (4-1):

$$\begin{aligned} y_L &= \beta_0 + \beta_1 x_1 + \beta_2 x_2 + \beta_3 x_3 + \beta_4 x_4 \\ y_L &= 0.44 + 0.01\, x_{PH} - 0.90\, x_R + 0.66\, x_G + 0.04\, x_B \end{aligned} \tag{4-1}$$

(ii) The best fit for the Nonlinear Regression was set by Eq. (4-2), following the equation defined for two variables in Eq. (3-4):

$$\begin{aligned} y_{NL} &= \alpha_0 + \alpha_1 x_1^2 + \alpha_2 x_2^2 + \alpha_3 x_1 x_2 + \alpha_4 x_1 + \alpha_5 x_2 \\ y_{NL} &= 0.07 + 0.34\, x_{SR}^2 + 0.47\, x_{NGRDI}^2 + 0.83\, x_{SR}\, x_{NGRDI} + \\ &\quad 0.06\, x_{SR} + 0.35\, x_{NGRDI} \end{aligned} \tag{4-2}$$

(iii) The best fit for the neural network, using MLP Regression, was set by the following configuration:

- Number of Epochs: 50000
- Number of Early Stops: 5000
- Neurons on Layer 1: 6
- Neurons on Layer 2: 12

Therefore, the outputs of these three models were used as inputs of a new MLP algorithm aiming at estimating biomass more accurately than the models alone. First, the network was trained with a Layer Sweep in order to identify the best configuration for both hidden layers, varying the number of neurons from 4 to 20 in steps of 2. Furthermore, the following combinations of maximum number of epochs and early stop were analyzed: (i) 5000/500, (ii) 10000/1000 and (iii) 50000/5000. MLPs using all possible combinations of these parameters were trained and tested. Hence, 243 runs were executed.

Then, for statistical analysis of the best configurations, the top three best stacking models, in terms of RMSE, obtained in the Layer Sweep step were chosen to be trained again for 30 runs, aiming at evaluating the liability of the results.

4.4.1 Layer Sweep

This subsection shows the results obtained from the Layer Sweep in Stacking Ensemble, focusing on minimizing their RMSEs. Table 4.49 shows the whole analysis of RMSE, including average value, standard deviation, lower and upper bounds computed considering the results obtained from all configurations.

Table 4.49: Analysis of RMSE performance using Stacking Ensemble Regression, after Layer Sweep.

Avg RMSE (g/m^2)	Std Dev RMSE (g/m^2)	Min RMSE (g/m^2)	Max RMSE (g/m^2)
49.70	7.04	33.26	78.23

Figure 4.23 presents the plots of predicted biomass versus measured biomass for the three configurations that reached the lowest RMSE values, defined after running the entire Layer Sweep.

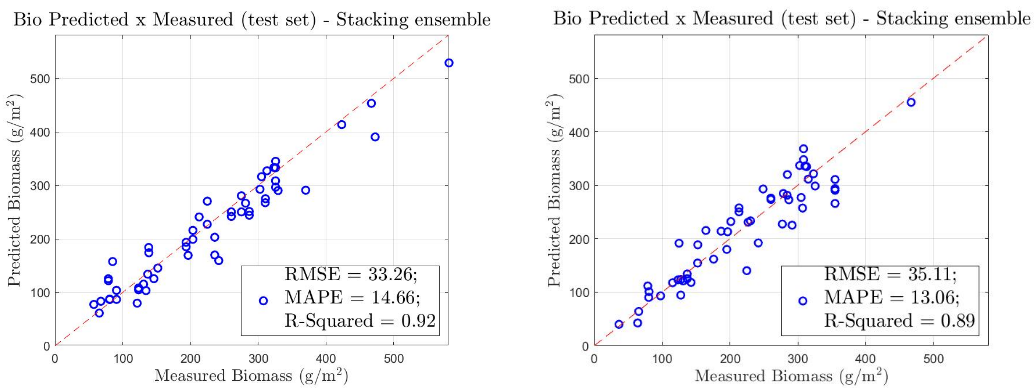

(a) First best RMSE **(b)** Second best RMSE

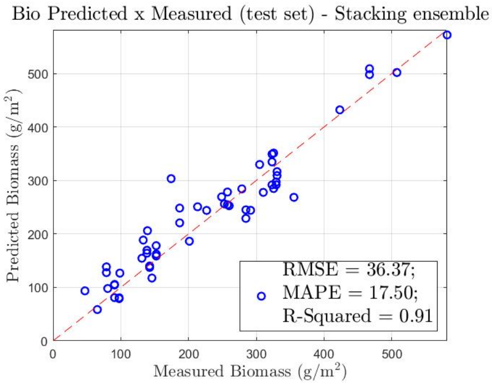

(c) Third best RMSE

Figure 4.23: Performance of the 3 Best Stacking Ensemble models with Layer Sweep, using as inputs the outputs of the Linear, Nonlinear and MLP Regressions.

Yet, Table 4.50 lists the first, second and third best configurations of the MLPs developed for the Stacking model, together with their respective RMSE, MAPE and R-Squared.

Table 4.50: Top 3 developed Stacking Ensemble Regression models, considering the RMSEs obtained with Layer Sweep.

Position	#Epochs	#Early Stop	#Layer 1	#Layer 2	Best RMSE (g/m^2)	MAPE (%)	R^2
1^{st}	5000	500	8	10	33.26	14.66	0.92
2^{nd}	50000	5000	16	20	35.11	13.06	0.89
3^{rd}	5000	500	12	6	36.37	17.50	0.91

Beforehand, it is noticeable that all three results are better than the ones presented by any of the regression models (including the MLP) developed in previous sections, in all performance metrics. So, we can conclude that the proposed Stacking Ensemble method can improve considerably the regression results.

Besides, note that the best configuration was set to use up to 5000 epochs and 500 early stops while the second best uses up to 50000/5000. Therefore, the total number of epochs not necessarily guarantee a better result, because the number of early stops prevent the neural network to overfit, favoring the network generalization.

4.4.2 Statistical analysis of the best configurations for Stacking

Here, all of the three best configurations identified in subsection 4.4.1 (see Tab. 4.50) are trained again for 30 times in a row to guarantee the reliability of the achieved results. Table 4.51 resumes the configuration of the varied hyperparameters that were selected to be trained in this subsection.

Table 4.51: Configurations of the 3 best results in Layer Sweep.

Config.	#Epochs	#Early Stop	#Layer 1	#Layer 2
1	5000	500	8	10
2	50000	5000	16	20
3	5000	500	12	6

Table 4.52 shows the average value, standard deviation, lower and upper bounds of RMSE, considering the results from the 30 runs executed for each one of the analyzed configurations.

Table 4.52: Analysis of 3 best RMSE performance using Stacking Ensemble Regressions, after running 30 times each configuration.

Config.	Avg RMSE (g/m^2)	Std Dev RMSE (g/m^2)	Min RMSE (g/m^2)	Max RMSE (g/m^2)
1	51.01	6.87	31.76	63.53
2	47.94	4.53	37.89	55.53
3	49.36	6.36	35.76	62.11

Figure 4.24 shows the plot of predicted biomass versus measured biomass associated with the best RMSE obtained among the 30 runs of each one of the analyzed configurations.

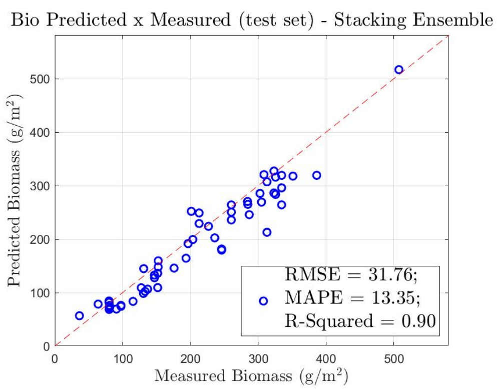

(a) First best RMSE

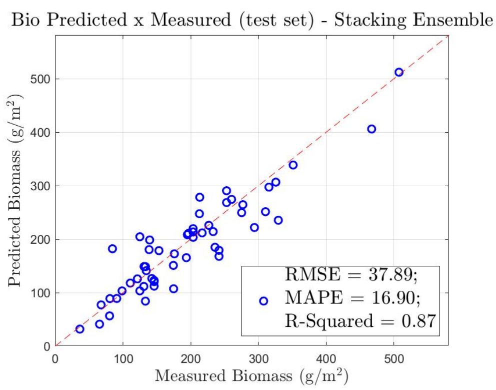

(b) Second best RMSE

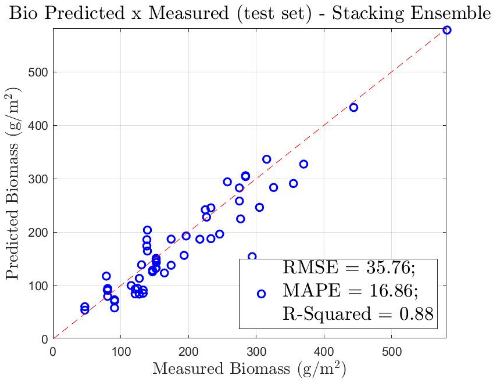

(c) Third best RMSE

Figure 4.24: Best Performance Stacking Ensemble models among the 30 runs executed for each of the 3 best cases identified in the Layer Sweep subsection.

Table 4.53 presents the performance metrics computed for each one of the top three configurations identified in the Layer Sweep subsection. Notice that the results shown in Table 4.53 are related to the best RMSE obtained by each configuration after 30 runs.

Table 4.53: Results of different performance metrics for the developed Stacking ensemble Regression model's associated with the best RMSEs, considering the results from the 30 runs executed for each one of the 3 selected configurations.

Config.	Best RMSE (g/m^2)	MAPE (%)	R^2
1	31.76	13.35	0.90
2	37.89	16.90	0.87
3	35.76	16.86	0.88

The obtained results indicate that the first configuration reaches again the lowest RMSE value, which is even smaller than the obtained in subsection 4.4.1. MAPE also decreased, but the R-Squared was slightly worst than before. Nevertheless, it is noteworthy that all metrics showed better performance using the stacking model than using the MLP alone with VIs, RGB channels and other features as inputs (see Subsection 4.3.3). Moreover, contrary to expected, the third configuration overcame the second one in every way, but the first one is still the best ever reached in this analysis and defined as the final metric for the work.

A RMSE value of 31.76 g/m^2 can be considered good enough for the desired task of estimating biomass on pastures. Besides, the best stacking model reached a MAPE of 13.35% and R-Squared of 0.9, that indicate a low percentage error and high R-Squared.

4.5 Comparative results

This section summarizes the best results obtained by each one of the developed regression methods, described along this chapter. Table 4.54 shows the top 3 linear, nonlinear and MLP regressions, among all tested configurations. Furthermore, the stacking ensemble implemented using the best configuration of each one of the regression methods had only its best result shown in Tab. 4.54, because it has the same inputs for all tests.

Table 4.54: Best results of the Analyzed Regression Methods.

Regression Method	Input	Best RMSE (g/m^2)	MAPE (%)	R^2
Linear	R, G, B and PH	68.96	35.02	0.51
	ExGR and GI	71.01	36.96	0.40
	GLI and SR	70.75	37.61	0.56
Nonlinear	R, G and PH	67.27	38.64	0.50
	R, G and SR	69.68	32.91	0.52
	NGRDI and SR	65.24	27.65	0.54
MLP	R, G, B and PH	41.95	18.91	0.83
	ExG and SR	50.88	19.27	0.76
	ExGR and SR	51.14	20.32	0.78
Stacking		31.76	13.35	0.90

It is noticeable that, among the raw RGB-based input combinations, the best results are obtained by combining R, G and B with PH, for linear and MLP regressions, and R and G with PH or SR in nonlinear regressions. Besides, among all tested VIs, the best results are achieved by using ExGR or GLI, in the linear regression, NGRDI in the nonlinear regression, and ExG or ExGR in the MLP. Moreover, the best results using VIs as inputs are usually obtained by combining them with the SR feature. The only exception, among the cases shown in Tab. 4.54, occurs for the combination of ExGR and GI, in the linear regression. We can conclude that SR and PH features significantly contribute to the biomass estimation.

Another important conclusion evidenced by this comparative study is that the performance metrics are improved when the complexity of the model increases. Table 4.54 shows that the best results are obtained by the stacking ensemble, followed by the MLP, nonlinear and linear regressions, respectively. Notice that the information obtained by the RGB camera used in this work do not deliver many details as multi spectral images or other high tech resources, so that estimating the output (biomass) from the available inputs are not an easy task. However, the results indicate that a good performance can be achieved by increasing the model's complexity. The results also bring important understandings on the relationship between the inputs and the measured biomass (output). The best result was achieved by the stacking ensemble, using the information provided by the best linear, nonlinear and MLP models. It reached an RMSE of 31.76 $\mathsf{g/m^2}$, MAPE of 13.35% and R^2 of 0.9. This result indicate a good correlation from the input with the measured output and it is suitable for the application of biomass estimation in livestock farm fields.

5
Conclusion and Future Work

In this work, we have proposed an intelligent biomass estimation algorithm based on neural networks, using a MLP for regression. We have computed a number of RGB-based VIs from UAV Imagery, that were used together with other features as plant height (PH), altitude of the drone flight (DF), intensity of green on the histogram (GI) and Solar Radiation (SR) to determine the biomass amount of a given region of interest. The MLP regression was compared with linear and nonlinear regression methods also applied to the biomass estimation task, using the same inputs, aiming at minimizing the RMSE. Other performance metrics were calculated as well. So, the accuracy of the designed estimators were evaluated using RMSE and it was related to other key performance metrics such as R^2 and MAPE.

Comparing the linear and nonlinear regression with the neural network, we can verify that the results from simple regressions do not allow a good accuracy in the biomass estimation task, by using RGB-based inputs or even their combinations with the other features. Among the results achieved by using linear and nonlinear regressions, the best performance metrics obtained were: RMSE = 70.75 $\mathsf{g/m^2}$, MAPE = 37.61% and R-Squared = 0.56.

On the other hand, the results obtained with the neural network were significantly better. The use of R, G and B channels combined with PH as inputs of the MLP led to the better biomass estimation results, among all analyzed MLP input's configurations, as it reached a RMSE of 41.95 g/m^2, a MAPE of 18.91% and a R-Squared of 0.83. Afterwards, aiming at improving even further the performance metrics a Stacking Ensemble method was developed, based on using the output of the best configuration of each one of the three other regression methods as inputs to another neural network model. This topology confirmed our expectations reaching a RMSE of 31.76 g/m^2, MAPE of 13.35% and R-Squared of 0.9.

Our proposed biomass estimation algorithm provides satisfactory results when compared with recently published works: (i) a CNN-based regression approach based on RGB Imagery [17], with a MAPE of 12.98 and an R-Squared of 0.88 ; and (ii) a linear regression approach using multi-spectral sensors to compute other vegetation indices [22], with an R-Squared of 0.65. These works use either a more complex regression method or more expensive resources, it seems advantageous to implement the estimation of green biomass in the field using the methodology proposed in our work in order to obtain even better results using a low cost system, in terms of computational cost and technology resources.

As shown in Tab. 4.54, it is worth to mention that all regression methods reached good performances by combining the SR feature with the investigated VIs, with emphasis on ExGR and NGRDI. The best RMSE obtained with nonlinear regressions was achieved by using NGRDI and SR as inputs. The second best RMSE obtained with linear regression was achieved by using GLI and SR as inputs, while the second best RMSE obtained with MLP regression was achieved by using ExG and SR as inputs. However, the best RMSEs obtained by linear and MLP regressions were achieved by using all R, G and B channels combined with PH as inputs. The nonlinear regression reached better results using a VI as input, that is computed as predefined combination of the raw RGB channels, than by using the raw RGB channels separately. In this case, a predefined combination of the colors, as it is performed with a VI, is better evaluated by less complex equations and less coefficients in nonlinear regression.

It is important to note that the addition of the PH and SR data as inputs improved the performance metrics remarkably, in all analyzed regression methods. Hence, these features are essential to be acquired in order to estimate the biomass accurately.

Regarding the other two features used as inputs, altitude of drone flight (DF) and green pixel intensity (GI), it is noticeable that they do not contribute to enhancement of the performance metrics as much as PH and SR. Only in linear regression, the model using GI assumed the third best RMSE, but it did not achieve performance metrics that allow its use for biomass estimation.

The results obtained by the MLPs using all raw RGB channels as inputs show that we can have even better performance in estimation than by using the VIs, as the RGB channels provide more useful information to the neural network that can solve by itself the right weights for each of the channels, instead of connecting a predefined VI to network's input. Thus, they can be considered more promising in delivering better results with a neural network than any other VI.

The developed regression models estimate the biomass inside 1 squared meter, so that if the image captured by the drone is dived in a matrix, with each element measuring 1 squared meter, we can conclude that the entire field's total biomass can be inferred by summing the biomass computed by each element of the matrix. As an example, Figure 5.1 shows an image captured by the camera at 30 meters high, depicting the field divided in 713 (23 x 31) elements (complete squares) measuring 1 square meter each. The best

Stacking Ensemble regression model was used to estimate the biomass of the matrix element highlighted in yellow, in Figure 5.1. The estimated biomass for this specific spot was 176.27 $\mathsf{kg/m^2}$, while its target biomass density is 175.85 $\mathsf{kg/m^2}$. Hypothetically, if all the spots are estimated with the same biomass 176.27 $\mathsf{kg/m^2}$, a field of 713 $\mathsf{m^2}$ have approximately 125.68 ton of green biomass. On the other hand, assuming that all spots have the same biomass, the real total biomass of this field would be 125.38 ton. The difference between the real and estimated biomass is 300 kg (less than 1% of the total biomass), which can be considered a small error. In a real case, each spot has a different density, which should be separately processed by the proposed computational method, hence the total biomass calculated for the farmer's field is the sum of those spots' density.

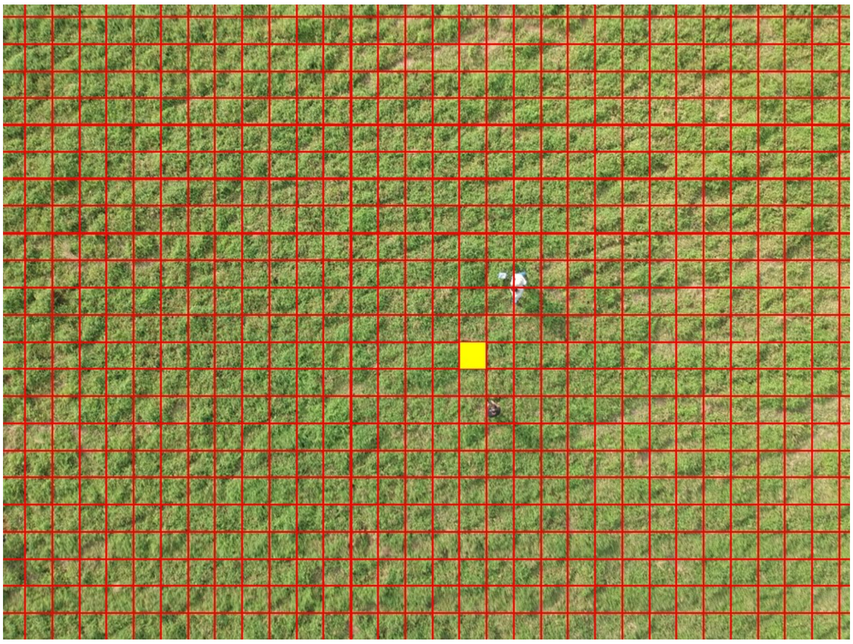

Figure 5.1: Field divided in different spots, of 1 squared meter each.

We conclude that the proposed methodology may become a feasible solution for plant biomass estimation toward sustainable and efficient herd management, considering the combination of different features as inputs of the models proposed in this work.

5.1 Future Works

As a suggestion for future works, other sensors could be embedded in the drone to measure direct information from the ground as the height of the grass, intensity of light and non visible wavelengths. They can be measured with specific sensors, such as three-dimensional image-based [45] like LiDARs (Light

Detection And Ranging), multi or hyper spectral cameras, spectrometers, ultrasounds and thermal cameras. It is important to point out that a sensor capable of measuring the height of the grass during the drone flight over the field is crucial for this work, as the main goal is to eliminate the necessity of the farmer to walk through the field to perform any measurement. The data set used in this experimental study is composed by plant height measurements collected in the field with a proper ruler. However, in the final system this will no longer be needed, because the PH information will be measured by an optical sensor with a good resolution embedded in the drone. Moreover, the results obtained by our regression methods reinforce the importance of using plant height as an input, which considerably increases the performance of the models.

The combination of different features, mainly PH and SR, as inputs of the models is a promising idea that should be further investigated. This could lead to even better results with the MLP regression and, consequently, with the stacking ensemble. A future perspective for this work also considers additional analysis over the combination of several VIs and channels on the network's input aiming at no longer needing plant height information, as the removal of the optical sensor can reduce project's cost even more.

With the addition of new measurements and new images, the data set can grow sufficiently to allow testing more complex regression methods, considering available pre-trained networks or, if necessary, a new one from scratch, with the study of different Deep Learning Networks. Nonetheless, it is necessary to mention that this work covered all seasons of the year with a set of images collected each month, for over almost one year (10 months). Hence, this means that the main information of seasonality was captured in this study and it reached good performance metrics using shallow neural networks and even simple fitting methods.

Furthermore, other important future analysis for this work is to perform a more in-depth test relating the inputs with only the legume biomass, rather than the overall amount of legume and grass. This idea can be implemented using all the present resources as inputs or adding others with different kind of information. Also, it would be important to analyze other regression methods which could be more suitable for this kind of differentiation in the image. The first step of estimating the total biomass in order to have an estimate of the total biomass was completed in this work, as the final RMSE can be considerably low enough. Hence, the second step of estimating the legume biomass separately is an important future work to obtain the correct amount of the herd in the field and the fixed nitrogen in the soil, as seen in Sec. 1.1.

6
Bibliography

[1] FEDERICO, G. *Feeding the World: An Economic History of Agriculture, 1800-2000*. [S.l.]: Princeton University Press, 2010. Cited in page 21.

[2] BODDEY, R. M. et al. Brazilian agriculture: The transition to sustainability. *Journal of Crop Production*, Taylor & Francis, v. 9, n. 1-2, p. 593–621, 2003. Cited in page 21.

[3] Secretaria de Política Agrícola. *Agropecuária Brasileira em Números*. [S.l.]: Ministério da Agricultura, Pecuária e Abastecimento, 2018. Cited in page 21.

[4] SILVA, C. Thaiana Rueda da et al. Yield component responses of the brachiaria brizantha forage grass to soil water availability in the brazilian cerrado. *Agriculture*, v. 10, n. 1, 2020. Cited in page 21.

[5] STEINFELD, H. et al. *Livestock's Long Shadow: Environmental Issues and Options*. [S.l.]: Food and Agriculture Organization of the United Nations, 2006. v. 24. Cited in page 21.

[6] ANDRADE, C. M. et al. Productivity, utilization efficiency and sward targets for mixed pastures of marandugrass, forage peanut and tropical kudzu. *Revista Brasileira de Zootecnia*, v. 41, p. 512–520, 03 2012. Cited in page 21.

[7] BODDEY, R. M. et al. Forage legumes in grass pastures in tropical brazil and likely impacts on greenhouse gas emissions: A review. *Grass and Forage Science*, v. 75, n. 4, p. 357–371, 2020. Cited in page 21.

[8] KANKARE, V. et al. Individual tree biomass estimation using terrestrial laser scanning. *ISPRS Journal of Photogrammetry and Remote Sensing*, v. 75, p. 64–75, 2013. Cited 2 times in pages 22 and 24.

[9] FAO. *Impact of animal nutrition on animal welfare*. [S.l.]: FAO Headquarters, 2011. Cited in page 22.

[10] MAHONY, R.; BEARD, R.; KUMAR, V. Modeling and control of aerial robots. p. 1307–1334, 01 2016. Cited in page 23.

[11] BRYSON, M. et al. Airborne vision-based mapping and classification of large farmland environments. *J. Field Robotics*, v. 27, p. 632–655, 09 2010. Cited in page 23.

[12] CORKE, P. *Robotics, Vision and Control - Fundamental Algorithms in MATLAB®*. [S.l.: s.n.], 2011. v. 73. 78-85 p. Cited in page 23.

[13] RURAL, S. S. N. de A. Agricultura de precisão: operação de drones/. In: *Coleção SENAR*. [S.l.: s.n.], 2018. v. 249, p. 84p. Cited in page 23.

[14] YOUNG, S.; KAYACAN, E.; PESCHEL, J. Design and field evaluation of a ground robot for high-throughput phenotyping of energy sorghum. *Precision Agriculture*, v. 20, 08 2019. Cited in page 23.

[15] JONES, R. The relation of animal and pasture production to stocking rate on legume based and nitrogen fertilized subtropical pastures. In: *Proceedings of the Australian Society of Animal Production*. [S.l.: s.n.], 1974. p. 340–343. Cited in page 24.

[16] LEDGARD, S. F.; STEELE, K. W. Biological nitrogen fixation in mixed legume/grass pastures. *Plant and Soil*, v. 141, p. 137–153, 2004. Cited in page 24.

[17] CASTRO, W. et al. Deep learning applied to phenotyping of biomass in forages with uav-based rgb imagery. *Sensors*, v. 20, n. 17, 2020. Cited 3 times in pages 24, 33, and 134.

[18] BARNETSON, J.; PHINN, S.; SCARTH, P. Estimating plant pasture biomass and quality from uav imaging across queensland's rangelands. *AgriEngineering*, v. 2, n. 4, p. 523–543, 2020. Cited 2 times in pages 24 and 25.

[19] CLEMENTINI, C. et al. Long-term grass biomass estimation of pastures from satellite data. *Remote Sensing*, v. 12, n. 13, 2020. Cited in page 24.

[20] REIS, A. et al. Monitoring pasture aboveground biomass and canopy height in an integrated crop–livestock system using textural information from planetscope imagery. *Remote Sensing*, v. 12, p. 2534, 08 2020. Cited in page 24.

[21] WIGLEY, K. et al. Photogrammetry for assessment of pasture biomass. *Journal of New Zealand Grasslands*, v. 81, p. 33–40, 10 2019. Cited in page 24.

[22] LUSSEM, U. et al. Evaluation of rgb-based vegetation indices from uav imagery to estimate forage yield in grassland. *ISPRS - International Archives of the Photogrammetry, Remote Sensing and Spatial Information Sciences*, XLII-3, p. 1215–1219, 04 2018. Cited 3 times in pages 24, 25, and 134.

[23] CHEN, Y. et al. Estimating pasture biomass using sentinel-2 imagery and machine learning. *Remote Sensing*, v. 13, n. 4, 2021. ISSN 2072-4292. Cited in page 24.

[24] LU, N. et al. Improved estimation of aboveground biomass in wheat from rgb imagery and point cloud data acquired with a low-cost unmanned aerial vehicle system. *Plant Methods*, v. 15, 02 2019. Cited in page 24.

[25] OZCELIK, R. et al. Artificial neural network models: An alternative approach for reliable aboveground pine tree biomass prediction. *Forest Science*, v. 63, p. 291–302, 06 2017. Cited in page 24.

[26] ZHENG, H. et al. Evaluation of rgb, color-infrared and multispectral images acquired from unmanned aerial systems for the estimation of nitrogen accumulation in rice. *Remote Sensing*, v. 10, p. 824, 05 2018. Cited in page 24.

[27] SANTOS, G.; ROSALEN, D.; FARIA, R. Use of active optical sensor in the characteristics analysis of the fertigated brachiaria with treated sewage. *Engenharia Agrícola*, v. 37, p. 1213–1221, 12 2017. Cited in page 24.

[28] GAHROUEI, O. R. et al. Crop biomass estimation using multi regression analysis and neural networks from multitemporal l-band polarimetric synthetic aperture radar data. *International Journal of Remote Sensing*, v. 40, p. 1–19, 03 2019. Cited in page 24.

[29] BENDIG, J. et al. Combining uav-based plant height from crop surface models, visible, and near infrared vegetation indices for biomass monitoring in barley. *International Journal of Applied Earth Observation and Geoinformation*, v. 39, p. 79–87, 03 2015. Cited 6 times in pages 25, 35, 39, 40, 48, and 54.

[30] LOUHAICHI, M.; BORMAN, M.; JOHNSON, D. Spatially located platform and aerial photography for documentation of grazing impacts on wheat. *Geocarto International*, v. 16, 04 2001. Cited 2 times in pages 25 and 39.

[31] GITELSON, A. et al. Novel algorithms for remote estimation of vegetation fraction. *Remote Sensing of Environment*, v. 80, p. 76–87, 04 2002. Cited 2 times in pages 25 and 39.

[32] TUCKER, C. J. Red and photographic infrared linear combinations for monitoring vegetation. *Remote Sensing of Environment*, v. 8, n. 2, p. 127–150, 1979. Cited 2 times in pages 25 and 39.

[33] WOEBBECKE, D. et al. Color indices for weed identification under various soil, residue, and lighting conditions. *Transactions of the ASABE*, American

Society of Agricultural and Biological Engineers, v. 38, n. 1, p. 259–269, jan. 1995. Cited 2 times in pages 25 and 39.

[34] MEYER, G.; NETO, J. C. Verification of color vegetation indices for automated crop imaging applications. *Computers and Electronics in Agriculture*, v. 63, p. 282–293, 10 2008. Cited 2 times in pages 25 and 39.

[35] COPEL. *Manual de Travessia sob Linhas de Transmissão - Projeto de Redes de Distribuição*. CED/CNPO, 1996. Disponível em: <https://www.copel.com/hpcopel/root/pagcopel2.nsf/0/44A585CD2B6B6C2C0325751900605E31/>. Cited in page 30.

[36] SPARK User Manual v1.6. [S.l.]: DJI, 2017. Cited in page 32.

[37] CHEN, Y. et al. Estimating pasture biomass using sentinel-2 imagery and machine learning. *Remote Sensing*, v. 13, n. 4, p. 603, 2021. Cited in page 36.

[38] ROUSE J. W., J. et al. Monitoring Vegetation Systems in the Great Plains with Erts. In: *NASA Special Publication*. [S.l.: s.n.], 1974. v. 351, p. 309. Cited in page 38.

[39] JUSTICE, C. et al. An overview of modis land data processing and product status. *Remote Sensing of Environment*, v. 83, n. 1, p. 3–15, 2002. Cited in page 38.

[40] OYELAMI, S. et al. A pyranometer for solar radiation measurement-review. v. 3, p. 61–68, 12 2020. Cited in page 43.

[41] HAYKIN, S.; HAYKIN, S.; HAYKIN, S. *Neural Networks: A Comprehensive Foundation*. [S.l.]: Prentice Hall, 1999. (International edition). ISBN 9780132733502. Cited in page 50.

[42] RAMACHANDRAN, P.; ZOPH, B.; LE, Q. V. *Searching for Activation Functions*. 2017. Cited in page 51.

[43] MENDES-MOREIRA, J. a. et al. Ensemble approaches for regression: A survey. *ACM Comput. Surv.*, Association for Computing Machinery, New York, NY, USA, v. 45, n. 1, 2012. Cited in page 52.

[44] KWAK, S. G.; KIM, J. H. Central limit theorem: the cornerstone of modern statistics. *Korean journal of anesthesiology*, The Korean Society of Anesthesiologists, v. 70, n. 2, 2017. Cited in page 54.

[45] LATI, R. N.; MANEVICH, A.; FILIN, S. Three-dimensional image-based modelling of linear features for plant biomass estimation. *International Journal*

of Remote Sensing, Taylor & Francis, v. 34, n. 17, p. 6135–6151, 2013. Cited in page 136.